

8-2023

A Computational Kinetics Model To Quantify Radiation Induced Chemical Products Of Atmospheric Gas Mixtures

Patrick Ables

Follow this and additional works at: <https://aquila.usm.edu/dissertations>



Part of the [Biological and Chemical Physics Commons](#)

Recommended Citation

Ables, Patrick, "A Computational Kinetics Model To Quantify Radiation Induced Chemical Products Of Atmospheric Gas Mixtures" (2023). *Dissertations*. 2138.

<https://aquila.usm.edu/dissertations/2138>

This Dissertation is brought to you for free and open access by The Aquila Digital Community. It has been accepted for inclusion in Dissertations by an authorized administrator of The Aquila Digital Community. For more information, please contact aquilastaff@usm.edu.

A COMPUTATIONAL KINETICS MODEL TO QUANTIFY RADIATION INDUCED
CHEMICAL PRODUCTS OF ATMOSPHERIC GAS MIXTURES

by

Patrick Ross Ables

A Dissertation
Submitted to the Graduate School,
the College of Arts and Sciences
and the School of Mathematics and Natural Sciences
at The University of Southern Mississippi
in Partial Fulfillment of the Requirements
for the Degree of Doctor of Philosophy

Approved by:

Dr. Christopher B. Winstead, Committee Chair
Dr. Khin Maung Maung
Dr. Michael D. Vera
Dr. Jeremy Scott

August 2023

COPYRIGHT BY

Patrick Ross Ables

2023

Published by the Graduate School



THE UNIVERSITY OF
SOUTHERN
MISSISSIPPI®

ABSTRACT

This research is focused on the development of a computational model which will calculate the effects of radiation on the chemical composition of the atmosphere. The approach utilizes the open-source chemical kinetics toolkit Cantera to model the creation of radiation-induced reactant species within irradiated air mixtures. Chemical solutions are iteratively stepped toward chemical equilibrium within a ‘constantly stirred’ (homogeneous) reactor of fixed volume. Three different radiation chemistry models are implemented in several different pulsed and continuous radiation schemes. The first model includes the mechanisms and rates of a pulse radiation model from the literature to test the validity of the new approach by comparison. The second uses identical mechanisms with the latest accepted rates to explore the change in induced chemical product yields in both schemes. The third model implements an extensive list of reactions and rates found within atmospheric chemistry literature and is an attempt to posit an updated radiation chemistry model that fits both pulsed and continuous radiation models and experimental data from the literature.

Measurements of radiation-induced ozone within continuously irradiated air mixtures demonstrated a need for a more accurate representation of the energy deposition distribution specific to the radioactive source. The volume in the space above the source is partitioned into a grid of independent voxels, and an energy deposition rate at each location is calculated. The average dose rate along the optical path of the spectroscopy-based model validation experiment is calculated from the voxel data. This method offers the flexibility necessary to easily correlate precomputed solutions with experimental measurements made through any part of the irradiated air mixture.

Several computational solutions are computed for dry 80/20 nitrogen/oxygen gas mixtures at various pressures with a gaseous mix of reactants introduced at different rates corresponding to a range of dose rates. Yields produced by the new approach in the pulse radiation scheme are found to be in good agreement with experimental results within the literature. Spectroscopy measurements of radiation-induced ozone show a strong correlation with computational results of the posited model in the continuous radiation scheme at the average dose rate of the optical measurements.

ACKNOWLEDGMENTS

I would like to thank Sidney Gautrau for providing the datasets collected in his work to measure the ozone concentration induced in air by continuous irradiation and from his GEANT4 model which determined the spatial distribution of the energy deposited by the radiation source used in his experiments. I would like to thank Dr. Tyler Reese for our weekly discussions throughout the commencement of this work and for his contribution to the editorial process of this paper. I would also like to thank my committee members Drs. Christopher Winstead, Khin Maung, Michael Vera, and Jeremy Scott for their support and guidance in the preparation of this dissertation.

DEDICATION

I would like to dedicate this dissertation to my parents, Ross and Pam Ables.

Without their years of encouragement and support, I would not be where I am today.

TABLE OF CONTENTS

ABSTRACT	ii
ACKNOWLEDGMENTS	iv
DEDICATION	v
LIST OF TABLES	x
LIST OF ILLUSTRATIONS	xi
LIST OF ABBREVIATIONS	xiii
CHAPTER I – INTRODUCTION	1
CHAPTER II – CHEMICAL KINETICS	3
2.1 Collision Theory	4
2.2 Primary Drivers of Atmospheric Chemistry	6
2.2.1 Oxygen Compounds	8
2.2.2 Nitrogen Compounds	10
2.2.2.1 Nitrous Oxide	10
2.2.2.2 Nitrogen Oxides	11
2.2.2.3 Reactive Odd Nitrogen Oxides	12
2.2.3 Catalytic Cycles	13
CHAPTER III – RADIATION CHEMISTRY	15
3.1 Ionizing Radiation	16
3.1.1 Alpha Particles	17

3.1.2 Beta Particles	17
3.1.3 Gamma Rays	18
3.2 Previous Work	18
3.2.1 Pulsed Radiation	19
3.2.2 Continuous Radiation.....	23
CHAPTER IV – COMPUTATIONAL MODEL	27
4.1 Preliminary Calculations.....	27
4.1.1 Electron Impact Cross-sections.....	28
4.1.2 g-value Calculations.....	30
4.1.3 Source Modelling.....	31
4.2 Chemical Kinetics Toolkit	34
4.2.1 Mechanism File.....	35
4.2.2 Solution Objects.....	36
4.2.3 Reactors.....	36
4.2.4 Gas Reservoirs	37
4.2.5 Flow Controllers	38
4.2.5.1 Mass Flow Controller	38
4.2.5.2 Pressure Controller.....	38
4.2.6 Reactor Network	39
4.3 Radiation Chemistry Model.....	39

CHAPTER V – MODEL RESULTS	44
5.1 Pulse Radiation Scheme.....	45
5.1.1 WB Figure 4 Comparison	47
5.1.2 WB Figure 5 Comparison	52
5.2 Gautrau Modelled Source	54
5.3 Continuous Exposure Scheme	57
5.4 Cycled Exposure Scheme	65
CHAPTER VI – DISCUSSION.....	68
CHAPTER VII – CONCLUSIONS	72
7.1 Future Work Toward Model Improvement.....	72
7.1.1 Possible Diffusion Approach	73
7.2 Final Thoughts	75
APPENDIX A – Willis and Boyd Reaction List	76
APPENDIX B – Posited Model Reaction List.....	78
APPENDIX C – Permissions	82
APPENDIX D – Source Code.....	93
D.1 user_set_parameters.py	93
D.2 functionContainer.py.....	97
D.3 simRad.py	103
D.4 Data for Building CTI Files	107

D.4.1 Species Data.....	107
D.4.2 CTIfile Willis.cti	120
D.4.3 CTIfile Willis_update.cti	123
D.4.4 WorkingThermo.v6.cti.....	126
REFERENCES	134

LIST OF TABLES

Table 2.1 Primary Reaction Types.....	6
Table 3.1 Moss et al. – Dominant Species Generated in Humid Air.....	25
Table 4.1 G-Values for Radiolysis Fragments.....	31
Table 4.2 Model Initialization Input Values	40
Table 5.1 Continuous – Posited Model: Top Products at Beam Height	64
Table 5.2 Continuous – Posited Model: Top Products at Max Dose Rate	64
Table A.1 Ion-Molecule Reactions for Irradiated N ₂ –O ₂ Mixtures	76
Table A.2 Neutral-Neutral Reactions for Irradiated N ₂ –O ₂ Mixtures	77
Table B.1 Neutral-Neutral Reactions for Irradiated N ₂ –O ₂ Mixtures.....	78
Table B.2 Ion-Molecule Reactions for Irradiated N ₂ –O ₂ Mixtures	80

LIST OF ILLUSTRATIONS

Figure 2.1 Layers of Earth’s Atmosphere.....	7
Figure 3.1 Willis and Boyd: Calculated Concentrations of Ionic and Neutral Species	22
Figure 3.2 Willis and Boyd: O ₃ and NO ₂ Yields vs. Dose Rate at 700 Torr	23
Figure 3.3 Moss et al. – Dominant Molecular Species Created in Humid Air by Irradiation with a 113 Ci ⁶⁰ Co Source.....	26
Figure 4.1 Neutral and Ionic Species Production by Electron Collision with N ₂	29
Figure 4.2 Neutral and Ionic Species Production by Electron Collision with O ₂	29
Figure 4.3 Energy Deposition of GEANT4 Modelled ²¹⁰ Po Source	33
Figure 4.4 Bragg Curve Comparison	34
Figure 4.5 Visual Representation of the Cantera Model Structure.....	43
Figure 5.1 WB Reproduction: Neutral and Ionic Species.....	48
Figure 5.2 WB Reproduction – No N ₄ ⁺ Ions: Neutral and Ionic Species	49
Figure 5.3 WB Reproduction – Updated Rates: Neutral and Ionic Species	50
Figure 5.4 WB Reproduction – Updated Rates, WB 11 & 12: Neutral and Ionic Species	50
Figure 5.5 Pulse – Posited Model: Neutral and Ionic Species	51
Figure 5.6 Pulse – O ₃ Yields vs. Dose Rate at 700 Torr.....	53
Figure 5.7 Pulse – NO ₂ Yields vs. Dose Rate at 700 Torr.....	54
Figure 5.8 Gautrau: Modelled Dose Rate Distribution.....	55
Figure 5.9 Gautrau: Dose Rate Along Vertical Plane of Beam Path	56
Figure 5.10 Gautrau: Average Dose Rate v. Distance Above Experimental Sources	56
Figure 5.11 Continuous – WB Mechanisms: O ₃ vs. Time vs. Dose Rate.....	59
Figure 5.12 Continuous – WB Mechanisms, Updated Rates: O ₃ vs. Time vs. Dose Rate	60

Figure 5.13 Continuous – Posited Model: O ₃ vs. Time vs. Dose Rate	60
Figure 5.14 Continuous – Posited Model, Reaction 88 Off: O ₃ vs. Time vs. Dose Rate .	61
Figure 5.15 Continuous – Posited Model: NO vs. Time vs. Dose Rate	63
Figure 5.16 Continuous – Posited Model: NO ₂ vs. Time vs. Dose Rate	63
Figure 5.17 Continuous – Posited Model: N ₂ O vs. Time vs. Dose Rate	64
Figure 5.18 Cycled – WB Mechanisms: O ₃ vs. Time vs. Dose Rate.....	66
Figure 5.19 Cycled – WB Mechanisms, Updated Rates: O ₃ vs. Time vs. Dose Rate	66
Figure 5.20 Cycled – Posited Model: O ₃ vs. Time vs. Dose Rate	67

LIST OF ABBREVIATIONS

<i>CFC</i>	chlorofluorocarbon
<i>CRDS</i>	cavity ring down spectroscopy
<i>CSDA</i>	continuous slowing down approximation
<i>DIAL</i>	differential absorption lidar
<i>FWHM</i>	full width half max
<i>IR</i>	infrared
<i>JPL</i>	Jet Propulsion Laboratories
<i>mCi</i>	millicurie
<i>mm</i>	<i>millimeter</i>
<i>ODE</i>	ordinary differential equation
<i>ppb</i>	parts per billion
<i>ppt</i>	parts per trillion
<i>RH</i>	relative humidity
<i>STP</i>	standard temperature and pressure
<i>USM</i>	The University of Southern Mississippi
<i>UV</i>	ultraviolet
<i>WB</i>	Willis and Boyd

CHAPTER I – INTRODUCTION

This research explores the utilization of a kinetics model to calculate number densities associated with chemical products formed in the presence of atmospheric radiolysis fragmentation. The model calculates the molar fraction of each fragmentary product per unit of kinetic energy absorbed by a unitary airmass. Starting with a pre-irradiated steady-state, the time-evolution of each species concentration is recorded as a continuous stream of radiolysis fragments are introduced and a new steady-state is approached. This model improves upon one produced by Willis and Boyd¹ (WB) by taking advantage of an open-sourced, python based chemical kinetics toolkit as opposed to an inhouse FORTRAN based differential solver. In addition, decades of atmospheric chemistry research have led to much higher confidence levels for reaction mechanisms and their respective rates. A computational model for radiation chemistry will help to determine whether the amount of radiation absorbed by an airmass can be determined indirectly by measuring the effective concentrations of nitrogen and oxygen compounds within. Relative number densities between select chemical products may correlate well with energy deposition rates. Through continued improvement of the kinetics-based radiation chemistry model, detection schemes can potentially be designed to measure radioactivity from a safe distance. The maturation of this research would be especially useful in areas where radioactivity is too high even for lead shielding or in territory where personnel are unable to travel. Three different radiation chemistry models are implemented. The first includes the mechanisms and rates of the original WB model to test the validity of the new approach. The second uses those same mechanisms with the latest accepted reaction rates to explore how yields of induced chemical products change.

The third model is an attempt to posit an updated and more comprehensive radiation chemistry model that implements 104 reactions and rates found in the atmospheric chemistry literature.

CHAPTER II – CHEMICAL KINETICS

Chemical kinetics is the study of the rates at which chemical reactions occur.² In atmospheric chemistry, it is concerned with understanding the rates at which gases and particles in the atmosphere react with each other and with other substances in the atmosphere. These reactions play a key role in determining the concentrations and distributions of various gases and particles in the atmosphere, as well as the overall chemical composition of the atmosphere.

Reaction rates can be influenced by factors such as temperature, pressure, and the presence of catalysts.² For example, the rate of a chemical reaction may increase with higher temperatures, as the increased thermal energy can help to overcome the energy barriers that often exist for chemical reactions to occur. Similarly, the rate of a chemical reaction may be influenced by the pressure of the gases involved in the reaction, as higher pressures can increase the chances of collisions between reactant molecules.

Another important aspect of chemical kinetics in atmospheric chemistry is the study of chemical equilibrium, which refers to the state at which the rates of the forward and reverse reactions are equal. This can occur when the concentrations of the reactants and products in a reaction are in a specific ratio. Understanding chemical equilibrium can help to predict the direction in which a chemical reaction will proceed under different conditions, as well as the concentrations of reactants and products that will be present at equilibrium.

Overall, the study of chemical kinetics in atmospheric chemistry is important for understanding the processes that control the concentrations and distributions of gases and

particles in the atmosphere and in systems containing atmospheric gases as well as the chemical reactions that contribute to the formation and removal of pollutants and other substances.

2.1 Collision Theory

Molecular collision theory is based on the idea that for a reaction to occur, the reactant molecules must collide with one another with sufficient energy and in a way that allows them to react.² The theory allows chemists to predict the rate at which a particular reaction will occur, given certain variables such as the concentration of the reactants and the temperature at which the reaction takes place. The theory is based on the concept of the "collision complex," which is a transient state that occurs when two molecules collide. If the collision complex has enough energy and the right orientation, the molecules will react and form the products of the reaction. If the collision complex does not have enough energy or occurs in the wrong orientation, the molecules will simply bounce off each other, and no reaction will occur. This theory does not account for the Coulomb forces through which real molecules interact over distances larger than the sum of their hard sphere radii.

The rate at which a reaction occurs is directly proportional to the number of successful collisions that take place per unit time.² Factors that affect the rate of a reaction include the concentration of the reactants, the temperature, the presence of a catalyst, and the surface area of the reactants. Increasing the concentration of the reactants or the temperature will increase the number of collisions and therefore the rate of the reaction. The presence of a catalyst also increases the rate of a reaction by

providing an alternative pathway for the reactants to follow, which may have a lower activation energy and be more favorable for the reaction to occur.

Molecular collision theory is an important concept in chemistry because it helps chemists understand how different factors affect the rate of a reaction and how to control the rate of a reaction to optimize the yield of a desired product. Radiation chemistry studies use the theory to model chemical changes effected by reactants which were produced from bombarding the gas mixture with radiation.³ The forward rate constant, k_f , gives the temperature dependence of the rate constant and makes explicit the temperature dependence of the pre-exponential factor. It is expressed in the form of a modified Arrhenius equation shown below, where the collision frequency, A , is determined experimentally rather than from theory.

$$k_f = AT^b e^{-\frac{E_a}{RT}}$$

where, $A \equiv$ collision frequency factor

$T \equiv$ temperature

$b \equiv$ temperature exponent

$E_a \equiv$ activation energy

$R \equiv$ gas constant

The lifetime of the initial collision complex for reactions involving three bodies relies on the number of vibrational modes it has.² For instance, when two free oxygen atoms collide, all energy is focused into the single vibrational mode of the newly produced O_2^\ddagger complex. To remove the surplus energy and prevent the bond from breaking, a tertiary impact must take place within one vibratory period. Consequently, the rate coefficient for the creation of O_2 is small for the $O + O + M$ reaction. In contrast, the

combination of two methyl radicals, $CH_3 + CH_3$, results in the formation of the $C_2H_6^\dagger$ complex, which has 18 different vibrational modes in which to distribute the excess energy. Therefore, $C_2H_6^\dagger$ has a comparatively long lifetime since thousands of vibrations will take place before the extra energy can be channeled into the particular bond that breaks. As a result, the rate coefficient for the formation of C_2H_6 is large for the $CH_3 + CH_3 + M$ reaction. Table 2.1 shows a few common reaction types considered by kinetics models.

Reaction Type	Examples	Expression	Rate
First-order	<i>Radioactive Decay</i>	$A \rightarrow B + C$	$\frac{d[A]}{dt} = -k[A]$
	<i>Photodissociation</i>	$A + h\nu \rightarrow B + C$	
	<i>Thermal Decomposition</i>	$A + M \rightarrow B + C + M$	
Second-order	–	$A + B \rightarrow C + D$	$\frac{d[A]}{dt} = -k[A][B]$
Third-order	–	$A + B + M \rightarrow AB + M$	$\frac{d[A]}{dt} = -k[A][B][M]$

Table 2.1 *Primary Reaction Types*

2.2 Primary Drivers of Atmospheric Chemistry

Chemical reactions between various atmospheric gases, as well as environmental influences like sunlight, temperature, and the presence of solid or liquid particles in the air, are the primary drivers of atmospheric chemistry.² Photolysis from sunlight creates vibrationally or electronically excited chemical species that either quench or react with other species through collision or dissociate into their component parts from surplus vibrational energy. Numerous conditions, such as the existence of specific gases or

compounds, the intensity and wavelength of sunlight, and the temperature and humidity of the air, can influence atmospheric chemical processes. For instance, the formation of nitrogen oxides (NO_x) from the reaction of nitrogen and oxygen-based gases in the air is impacted by the presence of heat, sunlight, as well as other gases like hydrocarbons and carbon monoxide. The driving forces behind atmospheric chemistry might also come from outside sources. Airborne particles like dust, smoke, or sea salt can act as catalysts for chemical reactions, and alterations in temperature and humidity can have an impact on how quickly reactions take place. The chemical makeup of the atmosphere is ultimately determined by the intricate interactions between these different forces. Figure 2.1 describes the temperature, pressure, and altitude for each layer of the atmosphere and is included for reference when needed.

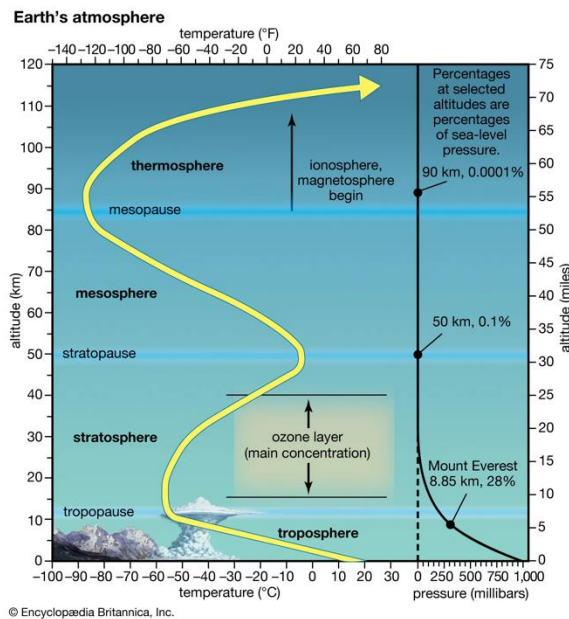


Figure 2.1 *Layers of Earth's Atmosphere*

Image obtained from Encyclopædia Britannica⁴

Seinfeld² outlines the complex mechanisms that drive Earth's atmospheric chemistry. He classifies major atmospheric species based on chemical composition: sulfur-containing, nitrogen-containing, carbon-containing, and halogen-containing compounds. Except for water and hydrogen peroxide, compounds of the form H_xO_y are not given a category because they are radicals; however, these compounds play a significant role in atmospheric chemistry. Since this paper will focus on dry N_2/O_2 mixtures, only reactions and reaction sequences that include nitrogen and oxygen compounds are described in the following sections.

2.2.1 Oxygen Compounds

The first electronically excited state of the oxygen atom, $O(^1D)$, is one of the more significant excited species in atmospheric chemistry because it reacts with the essentially inert species H_2O and N_2O .² Two hydroxyl radicals, OH , are produced from the reaction between $O(^1D)$ and H_2O . The interaction between $O(^1D)$ and N_2O yields two NO molecules and is the main source of NO in the stratosphere. As the primary producer of these two molecules, $O(^1D)$ is a crucial component of the atmospheric chemical system. An abundance of $O(^1D)$ is created in the upper atmosphere (~80 km) by O_2 photolysis, the majority of which is quenched by collision with O_2 or N_2 . In the lower stratosphere and troposphere, it is produced from the photodissociation of ozone by solar radiation of wavelengths above 290 nm.²

Ozone (O_3) is another major oxygen species to consider and is essential to shielding life on Earth from the negative effects of ultraviolet (UV) radiation from the sun. The absorption of the shorter wave UV radiation causes O_2 in the stratosphere to

dissociate into individual oxygen atoms. Those free atoms can then react with other oxygen molecules to form O_3 . This continuous process is called the ozone-oxygen cycle. The ozone-oxygen cycle is a delicate balance, and many factors affect the creation and destruction rates of O_3 . The presence of certain chemicals in the atmosphere, such as chlorofluorocarbons (CFCs) and halons, can break down O_3 molecules through a process known as catalytic destruction and is one of the primary ways to upset this equilibrium. O_3 production is dominated by the single oxygen atom dependent reaction,

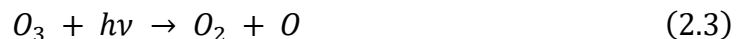


where O_2 and O react with a third collision partner (M) to produce O_3 . The third body is required to carry away the excess energy before the collision complex dissociates.

O_3 has been studied for many years, and its generation in the upper atmosphere has been researched extensively. Solar UV light with wavelengths less than 242 nm split apart O_2 in the upper atmosphere to produce free oxygen atoms.² The photolysis driven reaction is:



where $h\nu$ is the energy of the UV photon. O_3 can then be produced from reaction (2.1) once there are free oxygen atoms available. O_3 is a very strong optical absorber of wavelengths between 240 and 320 nm. The reaction below depicts this photolysis-driven pathway, whereby O_3 absorbs the energy of the photon causing it to dissociate into O_2 and O .



Equation (2.3) is responsible for the diminishment of this wavelength band of the solar spectrum in the lower atmosphere. It is also an indication of the significant amounts of O_3 in the upper atmosphere. Although less likely within the atmosphere, O_3 can react with a O to produce two O_2 molecules by the equation below.



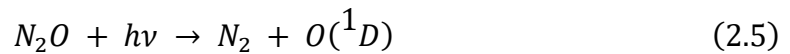
2.2.2 Nitrogen Compounds

The triple bond of the nitrogen molecule (N_2) is strong, making it essentially inert. Because it is so stable, it plays no role in the chemistry of the troposphere or stratosphere.² The key nitrogen compounds in the atmosphere are nitrous oxide (N_2O), nitric oxide (NO), nitrogen dioxide (NO_2), nitric acid (HNO_3), and ammonia (NH_3). Nearly all N_2O is emitted by natural sources, primarily from bacteria in the soil. NO comes from both natural and human generated sources. NO_2 is produced in limited quantities from combustion processes but is also produced in the atmosphere by the oxidation of NO . Other nitrogen oxides, such as NO_3 and N_2O_5 , exist in comparatively low concentrations but have an influential role in atmospheric chemistry. HNO_3 is produced in the atmosphere by an OH and NO_2 oxidation reaction. NH_3 is released predominantly by natural sources, such as bacterial processes in the soil and decomposition of organic matter.

2.2.2.1 Nitrous Oxide

N_2O is inert in the troposphere. The lifetime of N_2O is estimated to be 120 years; because of this, N_2O concentrations throughout the troposphere are roughly uniform. Ice core records show number densities were around 276 ppb in the preindustrial age, but

have since risen by 15%, near 315 ppb in 2000.² Bacterial action in soil and modern fertilizers appear to be the primary sources for atmospheric N_2O . The only known atmospheric source is through the NH_3 oxidation pathway. Its main destruction mechanism is photodissociation in the stratosphere, shown in (2.5) and representing about 90% of its destruction. Reaction with excited oxygen atoms, $O(^1D)$, is responsible for the remaining 10% and yields either two NO molecules, (2.6a), or N_2 and O_2 , (2.6b). 58% of this reaction proceeds through (2.6a) which is the main source of NO_x in the stratosphere.²

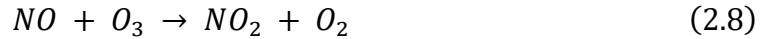


Although $O(^1D)$ is produced by the photodissociation of N_2O , the primary source in the stratosphere is the photodissociation of O_3 .²

2.2.2.2 Nitrogen Oxides

NO_x refers to the combined concentration of NO and NO_2 which are among the most important molecules in atmospheric chemistry. These concentrations, along with the O_3 concentration, remain stable during the day. Due to industrial activities and the burning of hydrocarbons the concentration of NO_x has increased over the last century.⁵ NO_x can also be produced in the air by natural processes like lightning that break down N_2 and O_2 . NO is highly reactive due to an unpaired electron. It is transient and susceptible to numerous processes, including reactions with other atmospheric gases such as O_3 and OH . Wet and dry depositional processes also remove NO from the atmosphere where it is absorbed by plants and other surfaces on the Earth.

The amount of sunlight, which turns NO_2 into NO , and the amount of O_3 , which combines with NO to create NO_2 , both influence the NO to NO_2 ratio.

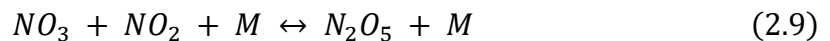


2.2.2.3 Reactive Odd Nitrogen Oxides

Reactive nitrogen oxides (NO_y) refer to combinations of the two NO_x oxides and any compound produced by NO_x . These include nitric acid (HNO_3), nitrous acid ($HONO$), the nitrate radical (NO_3), dinitrogen pentoxide (N_2O_5), peroxyntiric acid (HNO_4), among others. The total NO_y concentration is indicative of the total oxidized nitrogen in the atmosphere and is much steadier than the concentration of each constituent species.⁶ The concentration of each NO_y species relative to the total indicates the degree of interconversion between the species. NO_3 plays a significant part in the chemistry of the troposphere, particularly at night when its concentration can reach up to 300 ppt in the boundary layer.² There are many different NO_2 oxidation pathways to NO_3 when water vapor is present, but dry air only allows a reaction with O_3 .

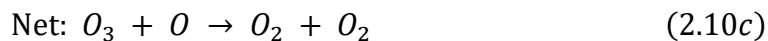
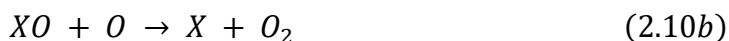


NO_2 and NO_3 concentrations play a role in O_3 creation and destruction rates by enabling additional catalytic cycles. Both are relatively unreactive molecules within the atmosphere; therefore, background levels can increase when cycles involving NO_x are disturbed. There is one direct reaction mechanism available in dry air, the combination of NO_2 and NO_3 into N_2O_5 ,

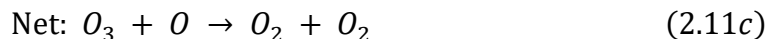


2.2.3 Catalytic Cycles

Sydney Chapman proposed equations (2.2), (2.3), and (2.4) in 1930 to describe how O_3 is created and destroyed in the upper atmosphere.² This set of reactions is referred to as the Chapman mechanism and was the leading conceptual model until the 1960s. Observations of the upper atmosphere at that time revealed that O_3 levels were half what was calculated by Chapman proving that there were O_3 destruction pathways the Chapman mechanism did not consider. The missing destruction mechanisms were found by Crutzen⁷ (1970) and Johnston⁸ (1971) after they identified the function of nitrogen oxides in the stratosphere. These additions to the Chapman mechanism are described by the following catalytic cycle:

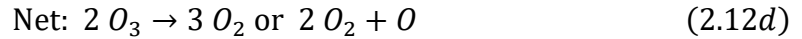
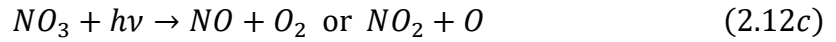


where X may be NO , H , OH , Cl , or Br and serves as the cycle catalyst. The cycle results in the reaction of ozone and atomic oxygen generating two oxygen molecules. The catalyzing species is consumed in the first reaction but is reproduced when the cycle completes. Below is the catalytic cycle involving NO in the upper atmosphere:



The net result is the conversion of two odd oxygen species (O_3 , O) to two even oxygen species (O_2 , O_2).

In the lower stratosphere where O_3 is more prevalent, and when sunlight is available, another NO catalytic cycle exists:



where NO_3 is the nitrate radical. Equation (2.12c) has two possible reactions that represent a conclusion of the cycle destroying O_3 with the first product, being eight times less likely than the second, resulting in the complete conversion of odd oxygen to even oxygen. Although not the most likely result of this catalytic cycle, it still occurs in an appreciable magnitude. One more NO catalytic cycle results in the destruction of O_3 into an even oxygen molecule and an odd oxygen atom. This cycle is referred to as a null cycle because odd oxygen is not destroyed.



CHAPTER III – RADIATION CHEMISTRY

Radiation chemistry is a subfield of nuclear chemistry that deals with the interaction of ionizing radiation with matter, specifically with the chemical changes that occur as a result of such interactions.⁹ It involves the study of the physical and chemical processes that occur when ionizing radiation (such as alpha particles, beta particles, gamma rays, and X-rays) interacts with atoms, molecules, and materials. In radiation chemistry, the interaction of ionizing radiation with matter that changes its composition is known as radiolysis and can result in the production of radicals, which can then participate in chemical reactions. The study of these reactions and their products provides insights into the mechanisms of radiation-induced chemical processes. The field is closely related to photochemistry which can be studied when reactants are stimulated to a distinct state by the influence of nearly monochromatic light to trigger one molecule at a time and ensure that the ensuing reactions take place uniformly throughout the volume. In contrast, a single high-energy charged particle or photon results in a huge number of excited and ionized molecules close to its emission source. The likelihood of the subsequent reactions is higher among neighbors on the same track than among reactive species on other tracks. Due to the separation of identical elements on the particle track, this results in tiny spherical areas, or spurs, holding the activated reactants.

The primary effects of radiolysis include the dissociation, excitation, and/or ionization of molecules by alpha, beta, and gamma ray emissions. The impact from one of these high energy particles causes successive cascades of lower energy secondary electrons until the charged particles thermalize to energies below the threshold necessary to produce electronic transitions within the atoms or molecules of the irradiated

medium.¹⁰ Its study differs from standard atmospheric chemistry primarily due to its localized effect in contrast to solar driven photolysis where the system is large and oscillates between two equilibrium points throughout the day. Radiation chemistry studies must consider a localized source of ionizing radiation and an infinite reservoir into which chemical products can diffuse. The radiation source's decay-particle energy and radioactivity effectively create a chemical equilibrium gradient within the enclosed volume that changes with the inverse square of the radial distance. A robust radiation chemistry model could calculate the concentration of each chemical species relative to a range of energy deposition rates. It might then be possible to arrange that data to match the distinctive depositional profile of all known decay particles moving through air. Deeper analysis of radiation-induced species concentrations might yield a method for calculating the radioactivity of an emission source. It may also be possible to determine the dose rate gradient of a volume from species distributions to help identify an unknown source type.

3.1 Ionizing Radiation

The chemical effects of radiation on N_2/O_2 mixtures utilizing various types of ionizing radiation, including alpha, beta, and gamma rays, have been the subject of research for decades.^{1,9,11-29} Radioactivity should induce chemical reactions and catalytic cycles similar to those induced by cosmic and solar radiation in the upper atmosphere. Chemical equilibrium within a large enough volume enclosing a radioactive source is best described as a gradient with its maximum deviation from background centered on the source. The activity of a particular radioactive source only scales the production rates for excited and fragmentary species produced directly from bombardment. Internal forces

then radially diffuse the modified concentrations of each product into the surrounding volume. The more reactive a chemical species is, the less distance it will travel before a reaction pathway is encountered. Therefore, depending on its diffusion rate, chemical reactivity, and distance from the emitter, the distribution of each species over a large volume is a spherically symmetric equilibrium gradient.

3.1.1 Alpha Particles

Alpha particles are a type of ionizing radiation that consists of two protons and two neutrons bound together.³⁰ They are essentially highly energetic helium nuclei ejected from a specific class of radioactive elements by the nuclear decay process and carry a +2 elementary charge. Their relatively large mass means alphas have the lowest velocities. The +2 elementary charge gives them the strongest Coulomb force. These properties increase the potential for interaction within a medium and makes alpha radiation more effective at ionizing atoms or molecules as a function of depth than other forms of ionizing radiation. Penetration has a negative correlation to ionization potential; therefore, alpha particles have the least penetration into a medium. In fact, alpha particles can sometimes be stopped by a single sheet of paper or a few centimeters of air. As a result, alpha particle radiation chemistry is generally more limited to the surface of materials.

3.1.2 Beta Particles

Beta particles are high-energy electrons or positrons ejected from a specific class of radioactive materials by nuclear decay processes.³⁰ Electrons carry a -1 elementary charge while positrons carry a +1. The weaker Coulomb force and smaller mass allows a beta particle to travel much farther than an alpha of the same energy. The penetration

depth is more dependent on material density but can reach about 30 cm through air at one atmosphere or a few millimeters into aluminum. With higher penetration efficiency, it follows that the ionization potential of beta particles is lower than that of alphas making betas less effective per unit distance at ionizing atoms or molecules comparatively; however, they can still induce significant chemical changes in materials.

3.1.3 Gamma Rays

Gamma rays are high-energy photons emitted by nuclear decay processes.³⁰ They are highly energetic, massless particles that carry no charge. The lack of charge means they experience no Coulomb force. Being massless, gamma rays travel at the speed of light. Thus, the penetration depth of gamma rays can be much deeper than alpha and beta particles, possibly infinite. There is a large variance in the kinetic energy of gamma rays between different gamma sources. Scientists quantify their penetration by the thickness required for a specific substance to stop half of the initial radiation intensity, or “half value layer.” In general, gamma rays can penetrate solid materials anywhere from several centimeters to several meters thick, depending on the gamma ray energy and the material density. The ionization potential of gamma rays is the lowest of the three types discussed.

3.2 Previous Work

Radiation chemistry has been studied since Roentgen¹¹ first discovered the chemical action of ionizing radiation in 1896.²⁷ Two years later, Marie and Pierre Curie¹² published one of the first papers on the subject with their discovery of radium.²⁷ In the years that followed, scientists observed many of the chemical effects of ionizing radiation, from ozone production in oxygen to the discoloration of paper; The early history of this research in France is summarized by Ferradini and Bensasson.^{23,27} The

term radiolysis was coined after the phenomenon was thought to be analogous with electrolysis.²⁷ In 1961, Lind¹⁴ defined radiation chemistry as the science of chemical effects brought about by the absorption of ionizing radiation in matter primarily due to electronic processes, separating it from radiochemistry which is driven by nuclear transformations.²⁷

Called the godfather of radiation chemistry, Burton¹³ was the first to introduce the unit G for radiation chemical action, defining it as “the number of molecules formed or destroyed by the absorption of 100 eV of ionizing radiation.”²⁷ The unit G was intended to refer to a purely experimental number. Currently, G is used for experimental measurements while g refers to theoretical primary yields.²⁷ Within air mixtures, radiation chemistry studies show an increase in ozone and nitrogen oxide numbers over natural background levels.^{1,17,19,28,29}

3.2.1 Pulsed Radiation

Many pulsed radiation experiments have been carried out since the mid 20th century to study the effects of radiolysis and quantify resultant chemical products. WB¹⁹ first published a pulsed radiation kinetics model in 1970 based on the WR16 FORTRAN code produced by Schmidt in a 1966 AEC Research and Development report titled *A Computer Program for the Kinetic Treatment of Radiation-Induced Simultaneous Chemical Reactions*.¹⁶

The authors acknowledge the need for transition probabilities, differential oscillator strengths or equivalent information, for the prediction of various states and the necessity for detailed knowledge of the secondary electron energy spectrum, otherwise known as a degradation spectrum, specific to the sample. Realistic estimates on the

reliability of continuous slowing down approximation (CSDA) calculations were difficult to make at the time. Having no access to a reliable degradation spectrum, noting its dependence on state and experimental variables, a different technique was proposed and utilized.

The simplified method used relative cross-sections for 100 eV electrons to calculate production rates for several processes based on the average energy required to form an ion pair, W . The yield of each process was calculated as follows.

$$G(\text{process}) = \frac{\sigma_{\text{process}}}{\sigma_{\text{total ionization}}} \times \frac{100 \text{ eV}}{W}$$

A fixed electron energy was chosen instead of attempting to integrate an assumed degradation spectrum. The explanation for the use of 100 eV electron energy cross-sections is to give weight to forbidden processes, and the assertion is made that relative cross-sections for major processes do not change much above that energy. Where cross-section data for major ionic processes was unavailable, standard 70 eV mass spectral abundances were used to calculate yields. In these cases, yields of neutral processes were derived from radiation chemistry mechanisms.

$$G(\text{process}) = \frac{\text{Abundance}_{\text{process}}}{\sum \text{Abundance}} \times \frac{100 \text{ eV}}{W}$$

The model published in 1970 used chemical reaction rates to calculate production numbers for oxygen and nitrogen compounds but lacked more sophisticated thermodynamic data for the species involved. Gas phase radiolysis yield data and available electron impact cross-sections were used to derive excitation mechanisms and to discuss the role of excited states in the radiation chemistry of O_2 , N_2 , N_2O , CO , CO_2 , H_2S , H_2O , and NH_3 .

In-house pulsed radiation experiments were performed to validate the kinetics model. A Febetron 705 was used to measure ozone production within nitrogen/oxygen mixtures for a period of 10 seconds after a 60ns beta pulse was generated.¹ Trials with increasing pulse energies were conducted to compare with the computational model. Experimental precision is suggested to be within less than 4% due to the very consistent dose per pulse generated by the Febetron. Experiments with air pressures above 400 Torr measured O_3 yields to be $G(O_3) = 10.3 \pm 0.5$ molecules per 100 eV.

The WB model computed the ionic and neutral yields induced by a beta pulse in dry air at 830 Torr. As seen in Figure 3.1, the model tracked the concentration of fragmentary reactants N , N_2^+ , O , O_2^+ , and electrons, and predicted a correlative change in N_2^+ ions as electrons are stripped during the beta pulse. This is followed by an exponential increase in O_2^- and electrons slightly out of phase with the pulse attributable to the capture of thermalized electrons. Immediately after the pulse, atomic oxygen is the most abundant neutral species, but its numbers reduce rapidly as O_3 becomes predominant. N is the second most abundant neutral species after the pulse, and its numbers decay at a smaller exponential rate compared to O . Primary products with the longest residence times were calculated to be NO , NO_2 , and O_3 . NO quickly reaches equilibrium over a few hundred microseconds and is the second most prominent species as the computation concludes. There is an increase in NO_2 once more reactive species have either reacted away or reached a relatively stable equilibrium.

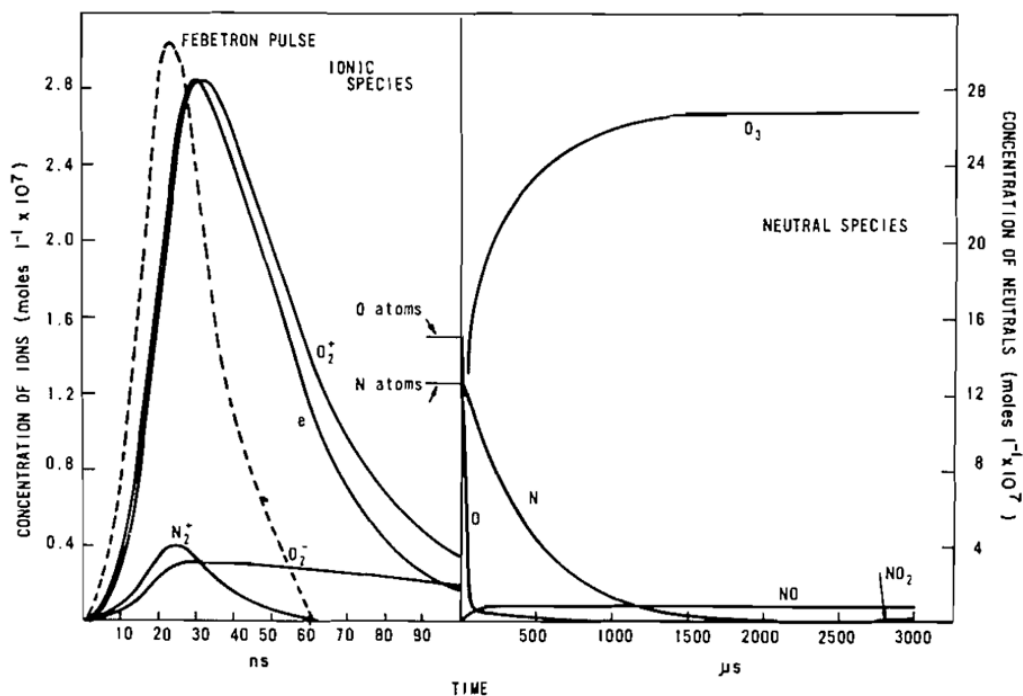


Figure 3.1 Willis and Boyd: *Calculated Concentrations of Ionic and Neutral Species*

Figure 4 reproduced from Willis and Boyd¹. “Calculated concentrations of ionic and neutral species during and after a Febetron pulse in air at 830 Torr: total dose, $1.06 \times 10^{19} \text{ eV g}^{-1}$; Febetron pulse intensity can be taken from the ordinate axis with units $0.5 \times 10^{-26} \text{ eV L}^{-1} \text{ s}^{-1}$, i.e. peak intensity $6.2 \times 10^{26} \text{ eV L}^{-1} \text{ s}^{-1}$.” Licensed for reproduction, see APPENDIX C.

Figure 3.2 shows the calculated yields of O_3 and NO_2 in air at 700 Torr as a function of dose rate compared against experimental measurements using constant pulse lengths. Both experimental and computed results show no linear correlation between O_3 and NO_2 yields and dose rate. At low dose rates it is suggested that all N_2^+ ions transfer their charges with O_2 which is then neutralized by O_2^- and yield oxygen atoms. These and all initially formed oxygen atoms will yield O_3 . The nitrogen atoms will react with O_2 to give NO and O . These oxygen atoms will also yield O_3 which reacts with NO to form NO_2 producing no net O_3 through the $N + O_2$ pathway. As the dose rate is increased,

more reactions compete for nitrogen atoms, and the NO_2 yield decreases. The direct neutralization of N_2^+ , which yields nitrogen atoms, will compete against its charge transfer reaction with O_2 . Simultaneously, less O_3 is produced by the atomic nitrogen pathway due to an increase in all atomic combination reactions.

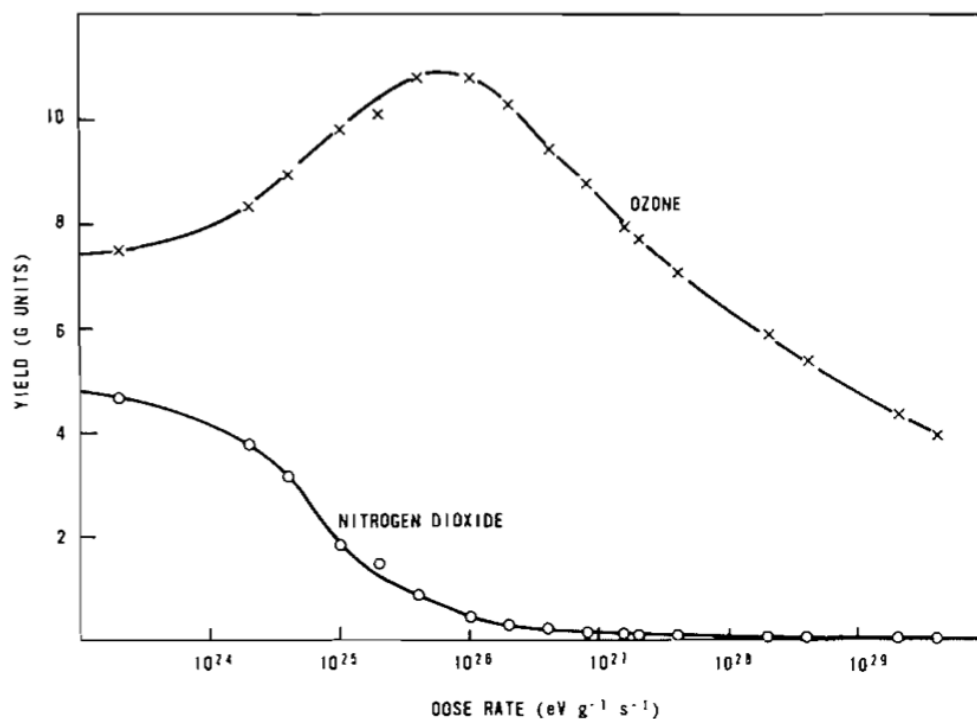


Figure 3.2 Willis and Boyd: O_3 and NO_2 Yields vs. Dose Rate at 700 Torr

Figure 5 reproduced from Willis and Boyd¹. "Calculated yields of ozone and nitrogen dioxide in single pulse irradiations of air at 700 Torr." Licensed for reproduction, see APPENDIX C.

3.2.2 Continuous Radiation

Moss et al.²⁴ were the first to publish a continuous exposure radiation chemistry model to calculate the time-evolution of suspected radiation-induced chemical products.

Moss et al. investigated the possibility of increasing the detection range for ionizing radiation from moderately intense sources by measuring the chemical effects induced in air near the source and suggests using optical techniques to remotely detect new molecular species formed. Due to the low attenuation of infrared radiation by air, they suggest the infrared absorption band of these potential signal molecules might allow long range detection of the radiation-induced chemical products at large distances using differential absorption lidar (DIAL).

Moss et al. used an in-house gas-phase chemical kinetics code to run the air chemistry computation. The computation included 49 different chemical species containing H, C, N, and O and 1849 different related reactions. Photochemical reactions were included with rates corresponding to normal sunlight at sea level. The model did not include diffusion in or out of the irradiated volume or any surface reactions that might occur with the walls of a container. The specific chemical species and reactions used were not included in the publication. Moss et al. claims the 113 curie ^{60}Co gamma source used in the experiment produced 1.05×10^9 ion pairs per cm^3 per second at 20 cm distance from source. Scaling by the energy per ion pair and air density gives a dose rate of approximately $3 \times 10^{13} \text{ eV} \cdot \text{g}^{-1} \cdot \text{s}^{-1}$. The computational model used this value as the effective average dose rate, but the actual dose rate is said to have varied as r^{-2} within the unshielded volume of the experiment. A 100% relative humidity (RH) air mixture at one atmosphere and 300 K was modelled to match experiment. After 10^4 seconds, they calculated the dominant species generated in humid air. These values are shown in Table 3.1. The computed time-evolution of the chemical composition produced

by their model is shown for reference in Figure 3.3. Moss et al. concludes that of these five indicator species, four are strong oxidizers and two are strong acids; therefore, N_2O is most likely to survive long-term, being the least reactive. Although the natural background concentration of N_2O is relatively large, elevated production numbers for higher dose rates or longer times might indicate a radiation source is present.

O_3	500 ppb
N_2O	400 ppb
HNO_3	300 ppb
HO_2NO_2	200 ppb
NO_2	50 ppb

Table 3.1 Moss et al. – Dominant Species Generated in Humid Air

Dominant chemical species produced by an in-house kinetics model after 10^4 seconds (2.77 hours). The model included 49 different chemical species and 1849 different reactions. A 113 curie ^{60}Co source was used to irradiate one atmosphere of air at 300 K and 100% RH to validate the computational model.

Moss et al. also lacked the experimental capacity to validate their computational results. They attempted to measure the molar fractions by measuring the optical absorptions with UV and IR spectrometers. O_3 was measured by a hand-held ozone monitor with an estimated sensitivity of 50 ppb. These techniques were not sensitive enough to measure the small changes in concentration that were present. The measured absorption responses for the molecular species concentrations were lower than the values predicted by model calculations. Discrepancies are attributed to diffusion of gases within the volume and surface reactions during experiment. Another difficulty is the assumed effective average dose rate over the irradiated volume implemented in the model. Because no useful reference citations or computational details were disclosed in the

publication, it is impossible to independently verify its accuracy. Comparisons between Moss et al. and other continuous exposure radiation chemistry research can only be made against their reported model results.

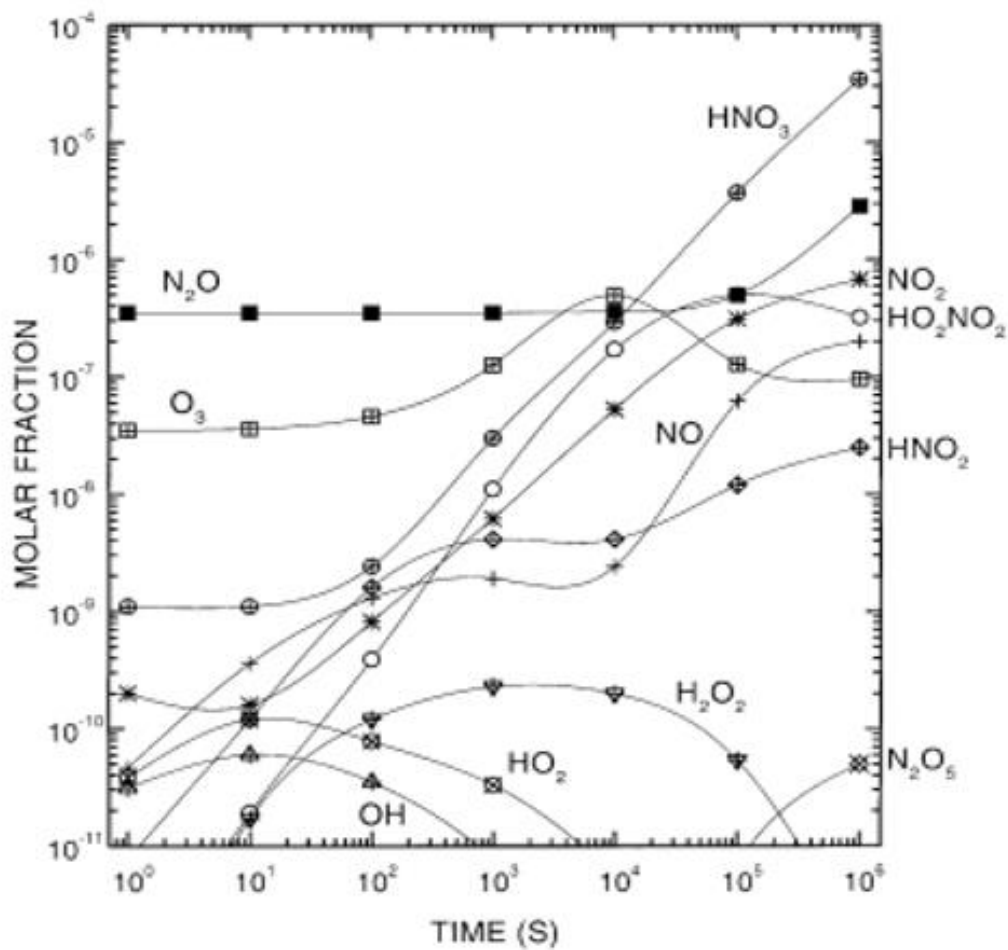


Figure 3.3 Moss et al. – Dominant Molecular Species Created in Humid Air by Irradiation with a 113 Ci ^{60}Co Source

Figure 1 from Moss et al.²⁴ Time evolution of the major chemical species produced by an in-house kinetics model. The model included 49 different chemical species and 1849 unique reactions. It was designed to simulate the effects a 113 curie ^{60}Co source has on a 100% RH air mixture. Licensed for reproduction, see APPENDIX C.

CHAPTER IV – COMPUTATIONAL MODEL

Designing a radiation chemistry model begins by characterizing the radiation source and identifying the fragmentary species produced. The energy of the ejected decay-particle is specific to the source material. It also dictates the maximum distance the particle can travel through air before the energy is completely transferred to the volume by a series of collisions. These collisions can fragment, excite, and/or ionize the collision partners resulting in cascades of secondary electrons. The temporal evolution of the secondary electron energy distribution produced by a steady state source shows that the production of high energy electrons remains constant while the number of low energy electrons increases exponentially.³¹ Secondary electron distributions and ionization cross sections for atmospheric gases were produced by Green and Sawada³² in 1972. Konovalov³³ and Konovalov and Son³⁴ have done detailed work calculating secondary electron spectra computationally. More recent work determining electron impact production cross sections for N_2 and O_2 fragments have been done by Tabata et al,³⁵ Itikawa and Yukikazu,^{36,37} and Tian and Vidal.³⁸ These cross sections can be used to calculate the number of each fragmentary species as a function of the kinetic energy absorbed by the medium. To model a constant depositional rate, each fragmentary species must be introduced into the volume at a rate defined by some average g-value. In addition, the model must be sophisticated enough to remove the parent molecules from the system at the same rate to maintain the mass balance.

4.1 Preliminary Calculations

As mentioned in the previous chapter, a g-value is the theoretical yield of a chemical species produced as a result of bombarding the absorbing medium with

energetic particles. It expresses the number of particles produced per 100 eV of energy absorbed. For a radiation chemistry model of dry N_2/O_2 mixtures, only g-values for the most predominant induced species, N_2^+ , N^+ , N , O_2^+ , O^+ , O , and electrons, are needed. Collisional processes involving species other than N_2 and O_2 do not occur for single short pulses and are relatively small for lower dose continuous models.

4.1.1 Electron Impact Cross-sections

Physical experiments or computer simulations may be necessary to calculate the ionization cross sections for unique gas mixtures. Electron-impact production cross sections for N_2 and O_2 by Tabata et al.³⁵ and Tian and Vidal³⁸ are shown in Figure 4.1 and Figure 4.2, respectively. These species production cross-sections were created through electron impact experiments designed to measure the average yield of each species over a range of collisional energies. The statistical data could be used to correlate collisional energy values with the probability that a specific ion is produced. A secondary electron energy distribution is then necessary to precisely calculate the weighted average g-value of each species.

Konovalov³³ calculated the degradation spectra of electrons in N_2 , O_2 , and air accounting for elementary processes of electron collisions with N_2 and O_2 . For 78% nitrogen, 22% oxygen mixtures at 1 atm and 290 K, he predicts approximately 50% of electron energy contributes to N_2 ionization, 30% to N_2 electronic excitation, 10% to O_2 ionization, and 10% to O_2 electronic excitation. The total energy contribution to the vibrational excitation of N_2 grows as primary electronic energy is distributed throughout the medium. As secondary electron numbers increase, the fraction of electrons with the energy to ionize is reduced.

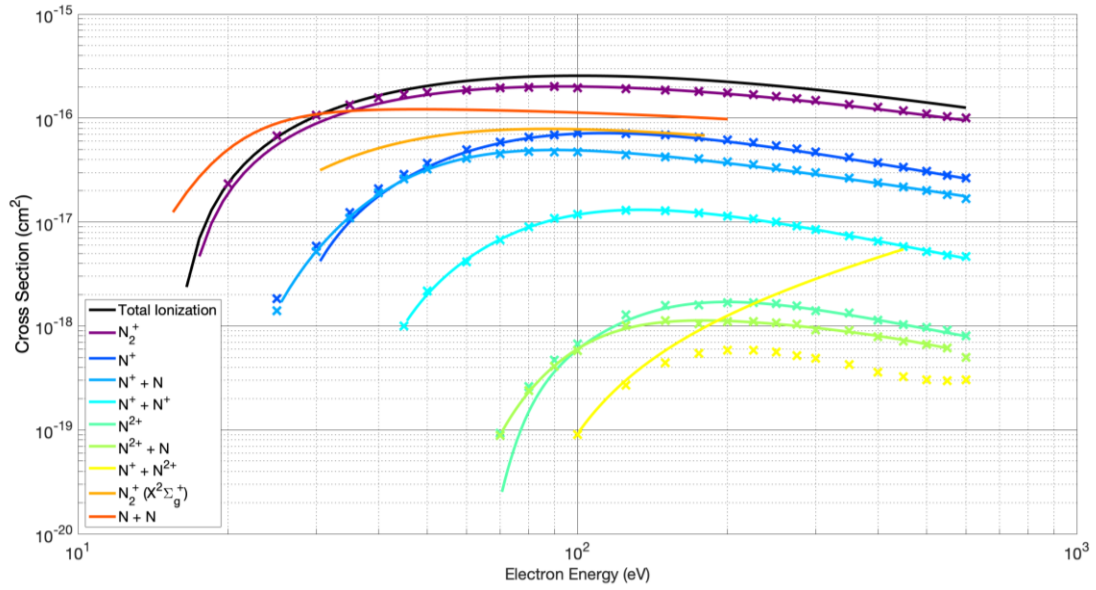


Figure 4.1 *Neutral and Ionic Species Production by Electron Collision with N₂*

Solid lines represent the calculated cross-sections from Tabata et al. fit equations. Markers represent Tian and Vidal cross sections.

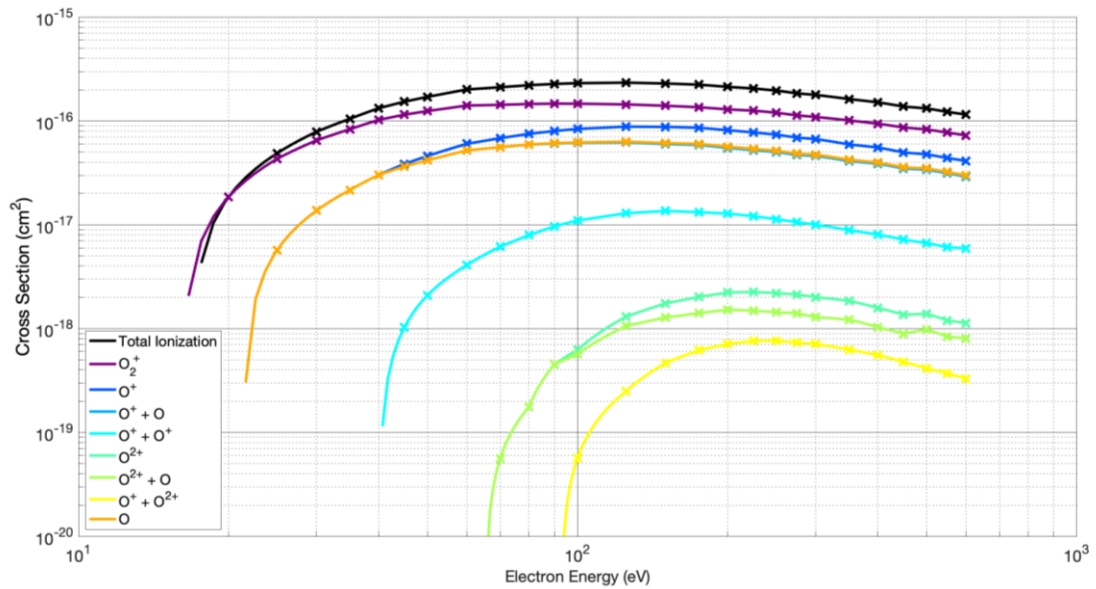


Figure 4.2 *Neutral and Ionic Species Production by Electron Collision with O₂*

Solid lines represent interpolated cross sections from Tian and Vidal data. Markers represent Tian and Vidal data.

4.1.2 g-value Calculations

The production cross section for each neutral and ionic species is scaled by the total ionization cross section at each collisional energy value. This gives the probability that a collision of energy, E , will yield a particular fragmentary species. The average energy required to produce an electron-ion pair, W , within a homogeneous gas has been shown by many authors to depend on the energy of the incident particle.^{22,39} For consistency, W values for N_2 and O_2 used in the following calculation are those chosen by WB.¹

As discussed in section 3.2.1, scaling the ion and neutral production fractions by the average energy per ion pair, g-values can be expressed as a function of collisional energy with units particles per 100 eV.

For ions

$$G_i(E) = \frac{\sigma_i(E)}{\sigma_{TI}(E)} \left(\frac{100}{W} \right) = \frac{\text{ion pairs}}{100 \text{ eV}}$$

For neutrals

$$G_n(E) = \frac{\sigma_n(E)}{\sigma_{TI}(E) + \sigma_n(E)} \left(\frac{100}{W} \right) = \frac{\text{neutrals}}{100 \text{ eV}}$$

$$\text{where } W \equiv \begin{cases} 34.7 \text{ for } N_2 \\ 30.6 \text{ for } O_2 \end{cases}$$

$\sigma_{TI} \equiv$ total ionization cross-section

$\sigma_n \equiv$ neutral production cross-section

$\sigma_i \equiv$ ion production cross-section

$E \equiv$ collisional energy

The g -values as defined above are in terms of collisional energy, E . For discrete collisional energy bins, the probabilities must be scaled by the fraction of energy within the corresponding energy bin of a discretized secondary electron energy distribution. For consistency and to narrow the scope of this work, experimentally determined G -values implemented by WB¹, shown in Table 4.1, are implemented in all Cantera based models presented.

Species	G-value
N_2^+	2.9
N^+	0.14
N	6.0
O_2^+	3.3
O^+	0.1
O	6.1

Table 4.1 *G-Values for Radiolysis Fragments*

G -values implemented by WB¹ and by all Cantera based models presented. Units are molecules per 100 eV.

4.1.3 Source Modelling

Each radioactive element's decay particle has a unique energy deposition profile which can be fully represented along a single radial dimension. The CSDA gives a very close approximation to the average path length of a charged particle passing through a medium before it is slowed to rest.⁴⁰ It assumes energy loss rate is equal to the total stopping power ($-dE/dx$). Other energy-loss fluctuations are neglected. The CSDA range can be calculated by integrating the reciprocal of the total stopping power with respect to energy. Stopping power and range data for electrons, protons, and alpha particles can be obtained from NIST using its online ESTAR, PSTAR, and ASTAR

programs, respectively.⁴¹ A radial energy deposition distribution is produced from the stopping power data. With some effort, a computational program can be written to create spherically symmetric distributions by rotating the radial vector through angles of θ and φ . The total energy deposited within the bounds of each voxel of space can then be determined.

When source geometry is more complex, software such as GEANT4 can be used to simulate emitters of all types. GEANT4⁴²⁻⁴⁴ is a radiation transport and energy-tracking toolkit developed by CERN. To demonstrate, the geometry of a radioactive source used in experiment was modelled by Gautrau⁴⁵ using a CADD file obtained from the source manufacturer. The volume around the source was discretized into a 10 cm cubic grid of one million 1 mm^3 voxels. One million ^{210}Po alpha particles and their secondary electrons were tracked as they interacted with 1 atmosphere of dry air until all particles fell below a specified lower energy threshold. The total energy deposited within each voxel was recorded to a list indexed by its three cartesian coordinates. The depositional distribution data was then scaled so that the total energy was equal to the total energy per second expected from a 5 mCi ^{210}Po source. The total energy deposition rate of the source was calculated as follows:

$$E_{Total} = 5 \text{ mCi} \left(\frac{3.7 \times 10^7 \text{ decays} \cdot \text{s}^{-1}}{1 \text{ mCi}} \right) (5.3 \times 10^6 \text{ eV} \cdot \text{decay}^{-1})$$

$$= 9.805 \times 10^{14} \text{ eV} \cdot \text{s}^{-1}$$

The dose rate distribution is calculated by further scaling the deposited energy within each 1 mm^3 voxel by its enclosed mass, 1.2×10^{-6} grams. A slice through the center of the dose rate distribution is shown in Figure 4.3. Figure 4.4 is a plot of

the Bragg curve for a ^{210}Po alpha particle shown by the energy loss/deposition rate as a function of the distance through air. It was produced using stopping power data from ASTAR and results from three different GEANT4 physics models to show how well the two approaches agree.

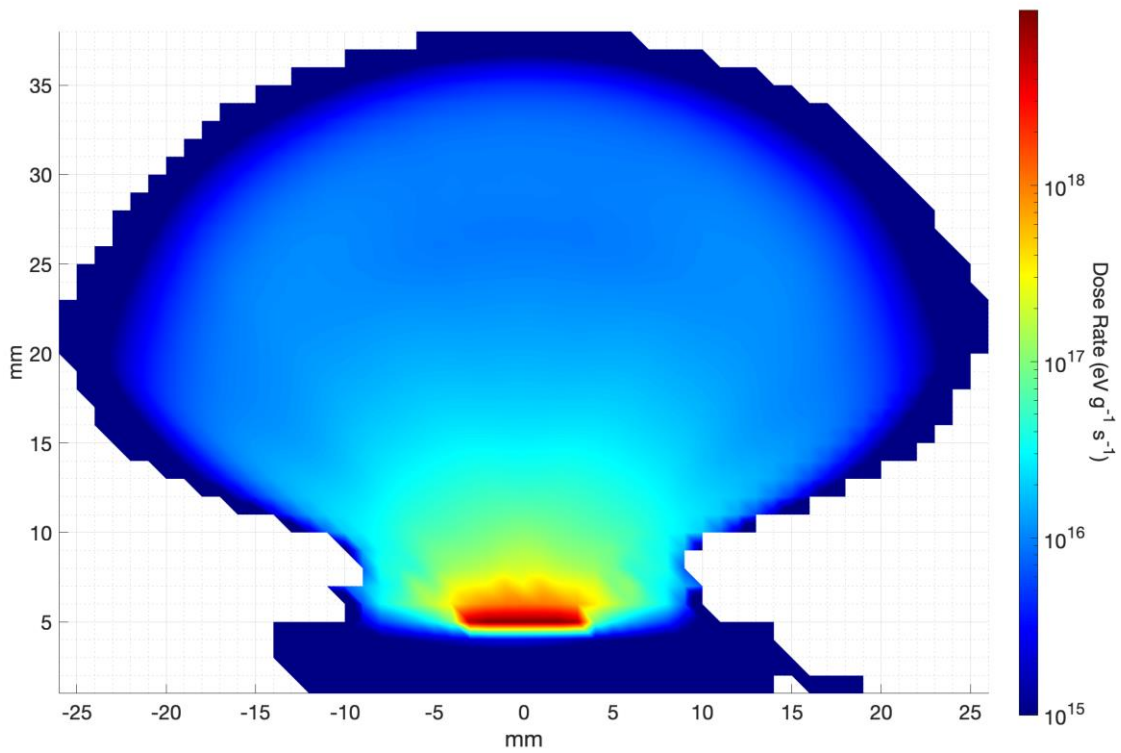


Figure 4.3 *Energy Deposition of GEANT4 Modelled ^{210}Po Source*

Created from a slice of Gautrau's unpublished GEANT4 model tracking energy deposition into each 1 mm^3 voxel of space from a ^{210}Po antistatic device irradiating one atmosphere of dry air.⁴⁵

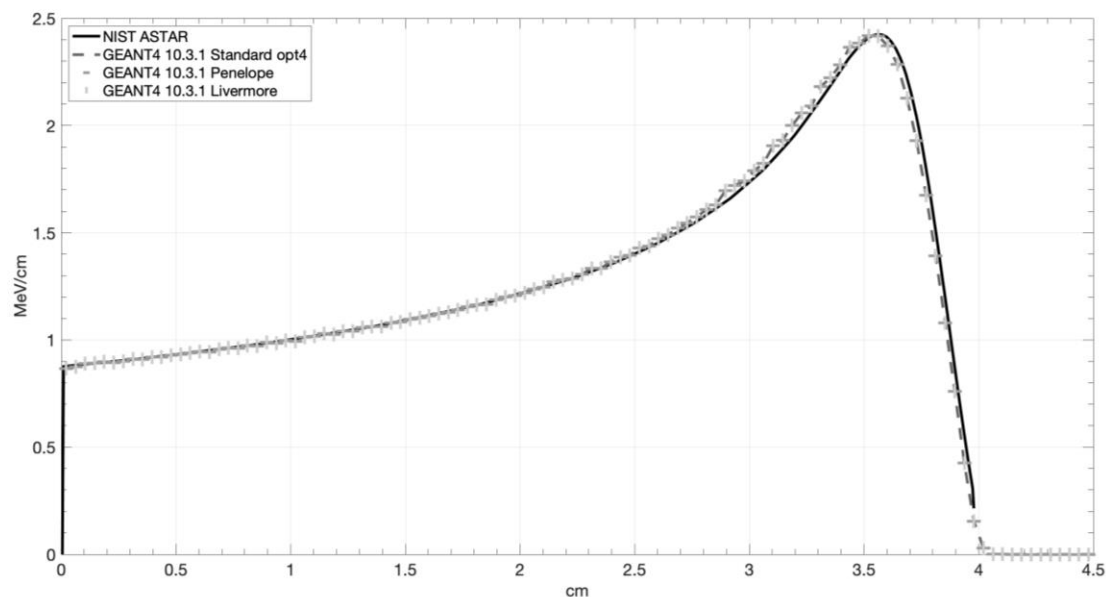


Figure 4.4 *Bragg Curve Comparison*

Energy loss rate of a ^{210}Po alpha particle moving through air as a function of penetration depth. The averaged values from a GEANT4 model are shown next to values from NIST's ASTAR tool.⁴⁶ Three different physics models were used to simulate and track one million alpha particles penetrating an air mixture and suffering collisional losses. Energy loss and location data for each collision is recorded until the particle energy becomes negligibly small. The collisional-energy-loss data is binned by its spatial coordinates and the average energy deposited into each bin is calculated. GEANT4 model data were provided by Gautrau⁴⁵ and have not yet been published.

4.2 Chemical Kinetics Toolkit

There are many chemical kinetics toolkits available, both propriety and open-source, the most well-known being Chemkin⁴⁷ and Cantera⁴⁸, respectively. The functionality of many open-source projects now rivals or surpasses that of propriety software. To increase the reach of this work, the open-source software Cantera was chosen as the computational basis for this radiation chemistry model. Cantera is a chemical kinetics, thermodynamics, and transport process modelling toolkit developed at the California Institute of Technology. It utilizes external libraries such as NumPy⁴⁹ and

SUNDIALS (Suite of Nonlinear and Differential/Algebraic equation Solvers)⁵⁰ which are called internally by class-inherited methods. From user program entry points to the internal computational flow, the toolkit structure is described in detail within Cantera's online documentation; therefore, the scope of this section will be limited to classes and functions implemented by the proposed radiation chemistry model. A Python script is used to instantiate specific Cantera classes to build the model. The primary components of this model include a mechanism file, g-value calculation function, solution objects, several reactor types, mass flow devices, a reactor network object, and an iterative loop to record internal state variables while stepping the computation through time.

4.2.1 Mechanism File

The mechanism file defines all molecular species to include, heat capacity data for each species, and all stoichiometric neutral and ionic reactions and their corresponding rates to utilize. Optionally, a matter phase can be defined and then loaded by Cantera when called by name. Thermodynamic data can be obtained from the NASA *ThermoBuild*⁵¹ tool for most compounds by selecting all applicable elements on the tool's periodic table. The output from this tool describes the thermodynamic properties of each chemical species with a nine-coefficient polynomial parameterization (determined by NASA) that Cantera uses for its internal heat capacity calculations.

NIST⁵² provides an online chemical kinetics database for neutral reactions. A reaction search is executed by entering one or more reactant species into the designated fields. A list of all reactions involving those reactants is returned which simplifies the process of identifying those reaction mechanisms relative to atmospheric chemistry. Anicich with Jet Propulsion Laboratories (JPL) reviewed literature from 1965 through

1991 and published recommendations of reaction rate coefficients and product distributions for bimolecular positive ion-molecule reactions of significance in planetary atmospheres. Anicich⁵³ and Boyarchuk⁵⁴ provided a source for most ionic reactions, with additional data provided by Torr and Torr⁵⁵, Ferguson et al.⁵⁶, Shuman et al.⁵⁷, and Verronen et al.⁵⁸

A reaction list composed of all available nitrogen and oxygen compounds was aggregated and combined with NASA's thermodynamic data to build a mechanism file consistent with Chemkin's CTI format. (See APPENDIX D)

4.2.2 Solution Objects

A basic Cantera model is initialized by building a solution object from the *Solution* class. Instances can be created to represent any gas, liquid, or solid mixture. The thermodynamic state is defined by two intensive properties, such as temperature and pressure, and the relative quantities of each species to include. The quantity of each species may be specified as molar or mass fractions. The *Transport* argument can be set to 'None', 'Mix', 'Multi', or 'default' and is used to calculate diffusion coefficients expressed in different formats if transport data for each species is supplied. The *Solution* class enables a single object to compute the thermodynamic, kinetic, and transport properties of a solution.

4.2.3 Reactors

A reactor object defines a reactor of zero spatial dimension which holds a homogeneous, constantly stirred gas mixture. By default, they are closed (no inlets or outlets), have fixed volume, and have adiabatic, chemically inert walls. The thermodynamic state of a *Reactor* object changes with time following reaction rates

specified in the mechanism file. Unidirectional *FlowDevice* or movable, heat-conductive *Wall* instances may be attached to connect multiple reactors. The *Reactor* class also serves as the base class for three special reactor types that can be instantiated.

The *IdealGasReactor* class creates a homogeneous, constant volume, zero-dimensional *Reactor* instance where the governing thermodynamic equations are based on the ideal gas equation of state.

The *ConstPressureReactor* class creates a homogeneous, constant pressure, zero-dimensional reactor object. The volume of the reactor adjusts over time as necessary to maintain constant pressure.

The *IdealGasConstPressureReactor* class creates a homogeneous, constant pressure, zero-dimensional reactor object for ideal gas mixtures. The volume of the reactor changes as needed to keep the pressure constant. This reactor type is a combination of the previous two.

4.2.4 Gas Reservoirs

A reservoir is a special instance of the *Reactor* class having infinite volume and maintaining a fixed thermodynamic state. The initial values of the temperature, pressure, and chemical composition are held constant over time. Reaction mechanisms are disabled within the reservoir, and the contents are considered perfectly mixed homogeneous solutions. Reservoir objects are created from the *Reservoir* class by passing a *Solution* instance to the *contents* argument.

4.2.5 Flow Controllers

4.2.5.1 Mass Flow Controller

A mass flow controller maintains a specified mass flow rate independent of upstream and downstream conditions. The equation used to compute the mass flow rate is

$$\dot{m} = \max(\dot{m}_0 * g(t), 0.0)$$

where \dot{m}_0 is a constant value and $g(t)$ is a function of time. Both \dot{m}_0 and $g(t)$ can be set individually by the property *mass_flow_coeff* and the method *set_time_function*, respectively. The property *mass_flow_rate* combines the two into a single interface.

Since flow is only allowed in one direction, if $\dot{m}_0 * g(t) < 0$ the mass flow rate will be zero. Unlike a real mass flow controller, a *MassFlowController* object will maintain the flow even if the downstream pressure is greater than the upstream pressure. This allows the implementation of loops, in which reactor exhaust gas is fed back into the reactor through an inlet. However, this capability does not account for the work required.

4.2.5.2 Pressure Controller

A pressure controller is designed to be used in conjunction with another ‘master’ flow controller, typically a mass flow controller. The master flow controller is installed on the inlet of the reactor, and the corresponding pressure controller is installed on the outlet of the reactor. The pressure controller mass flow rate is equal to the master mass flow rate plus a small correction for the pressure difference from the change in state:

$$\dot{m} = \dot{m}_{master} + K_v(P_1 - P_2)$$

The constructor class for this device requires passing the upstream and downstream reactor objects to the respective keyword arguments, and the master *MassFlowController*

instance it is to be linked. The pressure differential proportionality constant, K_p , is set to 1.0 by default but can be set to 0.0 to maintain mass balance within the reactor.

4.2.6 Reactor Network

ReactorNet objects are used to simultaneously advance the state of one or more coupled reactors. A list of *Reactor* instances must be passed to the constructor to build a *ReactorNet* object. Reactor networks are used to configure the ODE integrator limits, absolute and relative error tolerances allowed for the integration, and provides methods for initializing and advancing the integrator. The state of the reactor network instance is advanced in time using the class inherited *advance* method. The thermodynamic state is advanced from the current time towards the time passed to the method, stepping through as many integration steps as necessary to stay within the integrator limits.

4.3 Radiation Chemistry Model

A solution object instance is created for the initial air mixture and the reactant gas mixture. The initial gas mixture must be defined first since it is used to define the reactant gas mixture. A dictionary is defined with 'N2':0.80, 'O2':0.20 passed as the key:value pairs. This dictionary is passed to a function which uses g-values to calculate the number of each fragmentary, excited, and/or ionized species created per eV per second.

The solution objects for this model are built by passing a CTI formatted mechanism file to the *Solution* constructor argument *source*. The kinetics model is set to gas kinetics by passing '*GasKinetics*' to the *kinetics* argument. Transport model initialization is skipped by passing *None* to the *transport_model* keyword argument. Once the solution object is created, temperature, pressure, and molar fraction of each species composing the initial gas mixture are defined by setting the *TPX* property. The dry air

solution object's *equilibrate* method is called holding internal energy and volume constant to bring the initial gas mixture to a stable equilibrium.

Object	Argument	Value
Solution	<i>source</i>	CTI file
	<i>thermo</i>	'IdealGas'
	<i>kinetics</i>	'GasKinetics'
	<i>transport_model</i>	None
Solution.TPX	<i>T</i>	298 K
	<i>P</i>	1 atm
	<i>X</i>	{O2: 0.21, N2: 0.79}

Table 4.2 *Model Initialization Input Values*

Input arguments passed when building the Solution object. The inherited TPX method sets the state variables for the solution's temperature, pressure, and the molar fraction of the initial species.

The number of each excited or fragmentary species can be calculated directly from the molar fraction of nitrogen and oxygen molecules present in the initial gas mix. During model initialization, the molar fraction of each radiolysis product is calculated from the molar fraction of each component in the initial air mixture multiplied by its g-value. The g-values implemented by WB¹ are implemented in all model variations presented to make a direct comparison between the two computational approaches; however, additional excited species can be included.

$$N_2^+ = G(N_2^+) \cdot \frac{\text{moles}_{N_2}}{\text{moles}_T}, \quad O_2^+ = G(O_2^+) \cdot \frac{\text{moles}_{O_2}}{\text{moles}_T}$$

$$N^+ = G(N^+) \cdot \frac{\text{moles}_{N_2}}{\text{moles}_T}, \quad O^+ = G(O^+) \cdot \frac{\text{moles}_{O_2}}{\text{moles}_T}$$

$$N = G(N) \cdot \frac{\text{moles}_{N_2}}{\text{moles}_T}, \quad O = G(O) \cdot \frac{\text{moles}_{O_2}}{\text{moles}_T}$$

The mass flow rate for the reactant gas is calculated using the number of molecules of each excited or fragmentary species created per unit energy absorbed. The creation rates for all induced species are used to define the molar fractions of the reactant gas *Solution* instance after normalization. Temperature and pressure variables are the same as those set for the air gas *Solution* object. The molar mass of each species is used to define the reactant gas mixture in terms of its molar fractions per eV absorbed. The total energy deposition rate into a volume can be calculated from the specified dose rate being modelled multiplied by the total mass. Since these values and ratios remain constant, the mass flow rate of the reactant gas into the reactor scales directly with the specified energy deposition rate ($eV \cdot g^{-1} \cdot s^{-1}$).

$$Mass\ Flow\ Rate\ (kg/s) = E \cdot M \sum_k \frac{N_k}{N_A} M_k$$

where $E \equiv$ the energy deposition rate ($eV \cdot g^{-1} \cdot s^{-1}$)

$M \equiv$ the total mass within the volume (g)

$N_k \equiv$ the number k particles produced per eV

$N_A \equiv$ Avogadro's number

$M_k \equiv$ the molar mass for species k ($kg \cdot L^{-1}$)

Two instances of the *Reservoir* class are created. One holds the reactant gas mixture to be injected into the reactor by a mass flow controller. Another serves as a container to hold the excess gas vented by the downstream pressure controller to ensure the total mass within the reactor remains fixed.

An energy deposition rate list of increasing orders of magnitude is defined so that a range of deposition rates can be simulated simultaneously. An iterative loop is used to

build and configure a reactor object for each deposition rate in the specified range. The *IdealGasReactor* class was chosen for this model because the volume of the reactor remains fixed while the internal pressure and temperature of the reactor are allowed to change. The solution object created for the initial air mixture is passed to the *contents* argument of the *IdealGasReactor* class constructor, and a volume equal to the chosen energy deposition voxel size is passed to the *volume* argument. Flow device instances are implemented to remove excess mass from the reactor at the same rate the reactant gas is introduced.

A *MassFlowController* object is created to inject the reactant gas into the reactor at a mass flow rate proportional to the user specified energy deposition rate. The upstream container is the reactant reservoir, and the downstream container is the newly created reactor. A *PressureController* object is also created specifying the reactor as the upstream container and the junk reservoir as the downstream container. The previously created *MassFlowController* object is passed to the *master* keyword. The pressure controller parameter, K_v , is set to zero so that the mass flow rate into the reactor is equal to the mass flow rate out of the reactor. The composition of the mass removed from the reactor is equal to the evolving molar fractions inside the reactor. The characteristics of these flow devices is what enables Cantera to simulate radiolysis in this model. Radiolysis fragments can be introduced at the same rate their parent molecules are removed maintaining mass balance within the reactor.

An instance of the *ReactorNetwork* class is created by passing the *IdealGasReactor* object within a Python list to the constructor. The integrator is initialized by calling the inherited method *initialize*, and a programmatic loop is

constructed. With each iteration of the loop, the *advance* method is called for the next time step, and the reactor temperature and the molar fraction of every species of interest are written to file. Figure 4.5 offers a visual representation of the computational model structure that is advanced through time.

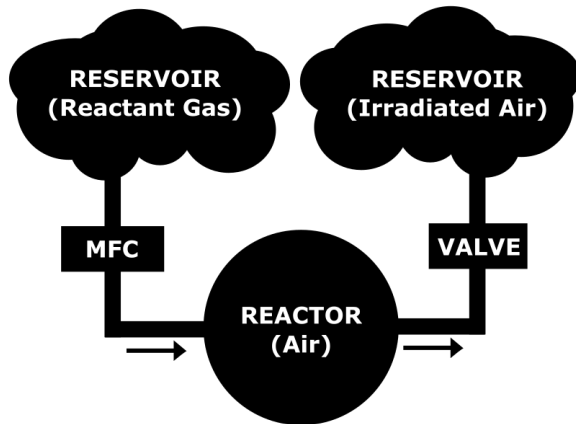


Figure 4.5 *Visual Representation of the Cantera Model Structure*

The mass flow rate out of the reactor is equal to the mass flow rate in, determined by the modelled dose rate. During mass influx, the excess mass to be removed is determined as a fraction of all species within the reactor and directed by the pressure controller into a junk reservoir.

CHAPTER V – MODEL RESULTS

Solutions for three Cantera based kinetics models are reported. First, each model is used to calculate the chemical effects of a single pulse of radiation for validation purposes. Next, solutions for continuous and intermittent exposure are calculated and compared against experiment; solutions for the Moss et al. humid model are also shown for reference.

The validity of the Cantera based approach was tested in comparison to an early pulse radiation model by WB¹. Ionic and neutral yields from the Cantera based model are compared to those from the WB model implementing identical conditions, mechanisms, and rates. Reaction rates for those mechanisms are then updated to the latest available, and the effected yields of each species are compared. Finally, all mechanisms and rates that could be found within the atmospheric chemistry literature are implemented in the posited model to compare with results of the aforementioned model variations.

Species concentrations calculated by the Cantera based model in the continuous radiation scheme are compared to the continuous model for humid air by Moss et al.²⁴ Ozone concentrations were also compared to laboratory experiments conducted by Gautrau²⁸ measuring radiation-induced ozone during continuous exposure to a ²¹⁰Po alpha source. The process of varying mechanisms and associated rates was identical to those used in the pulsed radiation computation. Model results were calculated at incremental dose rates to compare the time evolution and saturation yields against experimental ozone results.

Table 4.1 gives the experimentally determined G-values cited by WB¹ and implemented by all model variations expressed here. As was previously discussed, full

consideration for more detailed calculation of predicted g-values has been considered and deemed to be beyond the scope of this project as it is presented here. Additionally, initial modelling results found that the slight differences in g-values implemented had much less impact on results than differences in reaction rates. This choice also provides consistency across all comparisons to the WB model.

5.1 Pulse Radiation Scheme

There are a few differences between the computational approach implemented by WB and that of the Cantera models. WB used the FORTRAN based WR16 program to integrate ODEs in variable step sizes determined by the program to avoid divergence. The radiation pulse was modelled by a step function utilizing 2 ns steps with energy input values for each step defined by a preceding experiment. Only the total dose, peak intensity, and pulse length were published, making an exact reproduction of the pulse difficult. Computational error is reported to be less than 4% proportionate to species data and reaction rate accuracies. It should be noted, validation experiments conducted by WB could not make Febetron measurements for O_3 outside of the range $1-30 \times 10^{25} \text{ eV} \cdot \text{g}^{-1} \cdot \text{s}^{-1}$ in their experiments. All experimental attempts to measure NO_2 concentration at all dose rates were unsuccessful; it is assumed all yields were below the detection limit of the analytical technique used. A limiting yield of $G(NO_2) \leq 0.15$ was cited.

The ODE solver used in the Cantera models determine step sizes in much the same way as the original WR16 program. Step sizes are variable, determined by the solver internally to maintain a maximum absolute error tolerance of 10^{-15} and relative error tolerance of 10^{-9} . The absolute error tolerance is the threshold below which the

value of the i -th solution component is unimportant. It applies to the individual components of the solution vector and determines accuracy when the solution approaches zero. The relative error tolerance is a measure of the error relative to the size of each solution component. It controls the number of correct digits in all solution components except those smaller than the absolute tolerance. For the default, the calculated value of each component is within 1 billionth of the actual value. When a solution appears to be inaccurate, the relative error tolerance should be reduced and the computed solution used to determine an appropriate value for the absolute error tolerance. In addition, NASA's 9-parameter heat capacity data is used to account for thermodynamically induced changes within the evolving gas mixture by minimizing the Gibbs free energy.

Using WB's description, a Gaussian function was chosen to represent the radiation pulse. The ratio of the total dose ($eV \cdot g^{-1}$) to the maximum intensity ($eV \cdot g^{-1} \cdot s^{-1}$) is equal to the exponential factor of the 30 ns centered Gaussian integrated from 0 to 60 ns.

$$\int_0^{60ns} \exp\left(-\frac{(t - 30ns)^2}{2 (FWHM)^2}\right) dt = \frac{Total Dose}{A}$$

The Full Width Half Max (FWHM) was approximated to 8.7224×10^{-9} seconds by varying its value using WolframAlpha⁵⁹ until the solution converged to the total dose by maximum intensity ratio. Despite having the same amplitude, total dose, and coincidental rising edges, the trailing tail of the WB pulse does not correlate well with the Gaussian pulse used here. Either the pulse shape shown in the original WB figure or the total dose reported is inaccurate.

5.1.1 WB Figure 4 Comparison

The Cantera based approach was first tested against the WB model by reproducing the conditions used to create their figure 4, reproduced in Figure 3.1 of this paper. The model simulates a 60 ns long Gaussian pulse as described above with a maximum intensity equivalent to the published WB rate of $6.2 \times 10^{26} \text{ eV} \cdot \text{L}^{-1} \cdot \text{s}^{-1}$ (scaled by the air density at 830 Torr, $4.8 \times 10^{26} \text{ eV} \cdot \text{g}^{-1} \cdot \text{s}^{-1}$) and total dose of $1.06 \times 10^{19} \text{ eV} \cdot \text{g}^{-1}$. Molar concentrations are tracked over a three-millisecond time evolution, the same duration as the WB model, with state variables set to 830 Torr and 298 K. Figure 5.1 through Figure 5.5 show solutions from models under these conditions. All solutions were offset by -6 ns to overlap the Gaussian pulse with the original WB pulse.

The mechanisms and rates published in WB¹ were used to produce solutions shown in Figure 5.1 and Figure 5.2 (See APPENDIX A for the reaction rates used by the mechanisms proposed by WB). The solution for the closest Cantera approximation to the WB model is shown in Figure 5.1. Unlike the original WB result in Figure 3.1, the peak for the N_2^+ ion is not visible on this scale. The reproduction model results in 11% less O_2^+ , 20% more O_2^- , and 200% less N_2^+ ions. O and N numbers decay much more slowly with 6% more O , and 8% less N at their peaks. The Cantera model also results in 15% less O_3 compared to the published WB figure. While WB claim a calculated value of $G(O_3) = 10.3$ using the mechanisms and rates published, the figure they included shows ozone concentration peaks near $26.8 \times 10^{-7} \text{ moles} \cdot \text{L}^{-1}$ correlating with a g-value $G(O_3) = 11.9$. In addition, WB list a series of conditions to maximize O_3 yields and the effected

g-value, $G(O_3) = 12.1$. This is very close to the value shown in the included figure. The Cantera based reproduction peaks near $22.5 \times 10^{-7} \text{ moles} \cdot L^{-1}$ and correlates with a g-value of $G(O_3) = 10.0$, which is within the computational error of the WB calculation for the value of $G(O_3) = 10.3$ claimed in the text. It is likely the WB figure is the result of one of these model variations to maximize O_3 and not the result produced by the mechanisms and/or rates as implied. Figure 5.2 shows model results after turning off reactions involving N_4^+ ions and has a much more significant N_2^+ peak but 38% less than WB; however, the peak for O and N atoms are much more comparable while O_3 production is only slightly lower at $G(O_3) = 9.9$.

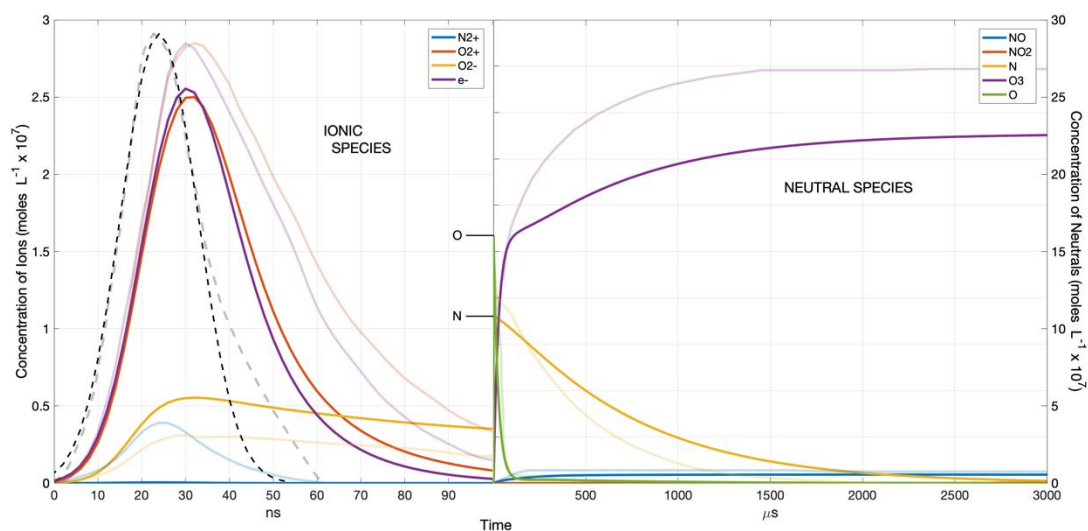


Figure 5.1 *WB Reproduction: Neutral and Ionic Species*

Molar concentrations for neutral and ionic species calculated by the Cantera-based radiation chemistry model reproducing conditions and mechanisms implemented by WB¹. Ozone production correlates to a value of $G(O_3) = 10.0$. The Febetron pulse, the dashed black line, does not correlate with the axis units but has a peak intensity of $6.2 \times 10^{26} \text{ eV} \cdot L^{-1} \cdot s^{-1}$. Original WB results are plotted with transparency for easy comparison.

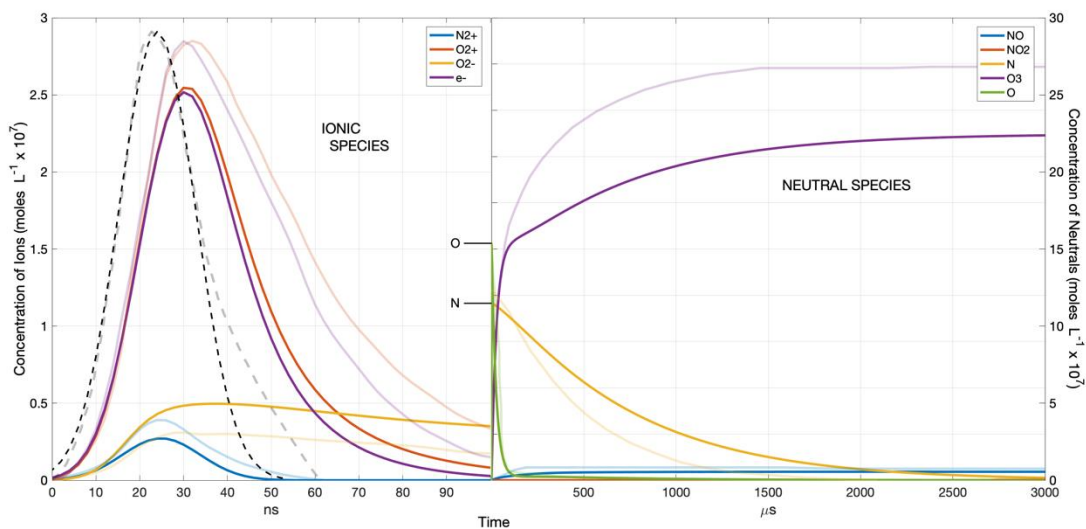


Figure 5.2 *WB Reproduction – No N_4^+ Ions: Neutral and Ionic Species*

Mechanisms and rates are identical to Figure 5.1 except for those associated with the production and destruction of N_4^+ ions, reactions 3 and 4 respectively. Ozone production correlates to a value of $G(O_3) = 9.9$. Original WB solution shown with transparency.

Figure 5.3 shows the evolution of ionic and neutral species for a model utilizing WB mechanisms with updated reaction rates. Figure 5.4 shows the solution of a model identical to that of Figure 5.3 except reactions 11 and 12 (see APPENDIX A) were not replaced by the generalized three-body reaction recommended by Anicich⁵³ and demonstrates this one mechanism is primarily responsible for the difference in calculated ion yields when compared to the WB reproduction model in Figure 5.1. The neutrals solutions in Figure 5.3 and Figure 5.4 are nearly identical despite the evident differences between the ionic solutions. The ion yields published by WB were only calculated, not verified by experiment. The neutral concentrations experimentally found by WB for model validation also agree with this implementation using updated rates. O_3 production correlates to a value of $G(O_3) = 9.9$.

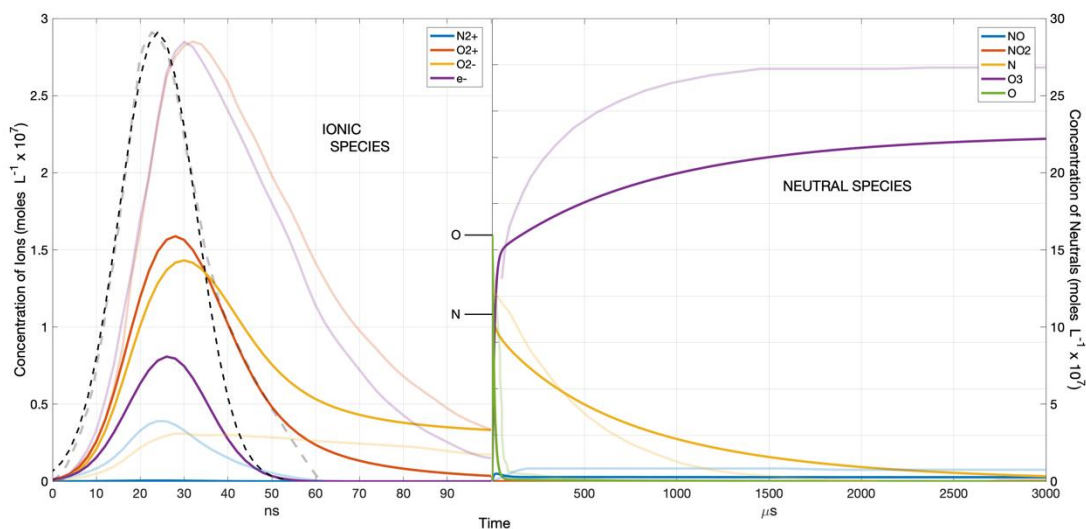


Figure 5.3 WB Reproduction – Updated Rates: Neutral and Ionic Species

Molar concentrations for neutral and ionic species calculated by the radiation chemistry model reproducing conditions and mechanisms implemented by WB¹. Reaction rates published by WB were updated to the latest accepted values. Ozone production correlates to a value of $G(O_3) = 9.9$. Original WB solution shown with transparency.

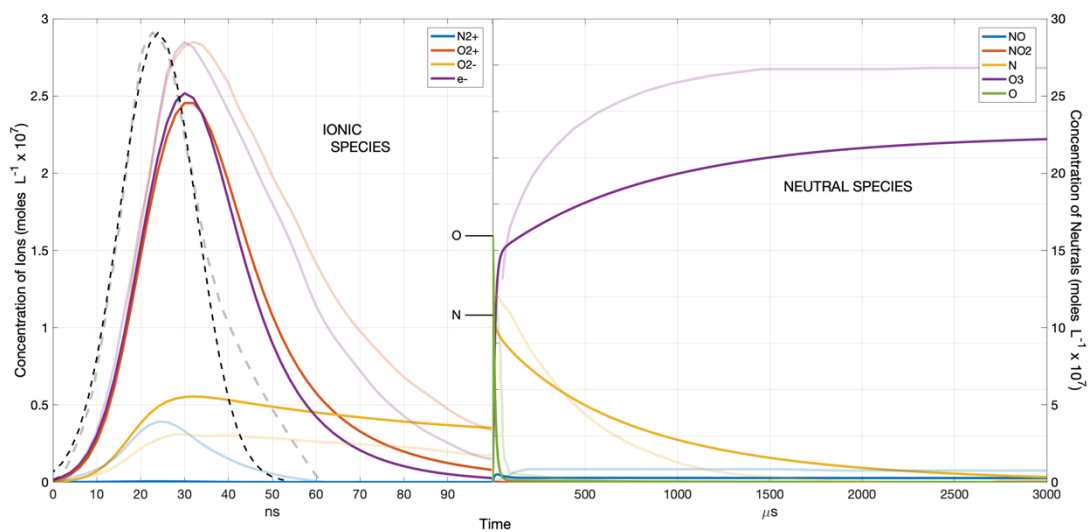


Figure 5.4 WB Reproduction – Updated Rates, WB 11 & 12: Neutral and Ionic Species

Mechanisms and rates are identical to Figure 5.3 except the primary sources of O_2^- i.e., the explicit three-body reactions 11 and 12, are not replaced by the single generalized three-body reaction. Ozone production correlates to a value of $G(O_3) = 9.9$. Original WB solution shown with transparency.

Figure 5.5 shows the molar concentrations for neutral and ionic species calculated by the posited radiation chemistry model (see APPENDIX B). The ionic yields differ for the updated rate model only slightly, with the peak of O_2^+ being reduced about as much as O_2^- increased. The tail for O_2^- decays much faster while electron yields remain unchanged, coincident with the pulse. For neutrals, the peaks for O and N are nearly identical with the previous model. The decay rate for O is very close while N is slightly slower. The largest difference in neutrals between the two models is the O_3 yield. The posited model allows O_3 to grow slightly faster than the updated rate WB reproduction and produces the closest O_3 result to the original WB model. O_3 production correlates to a value of $G(O_3) = 10.9$.

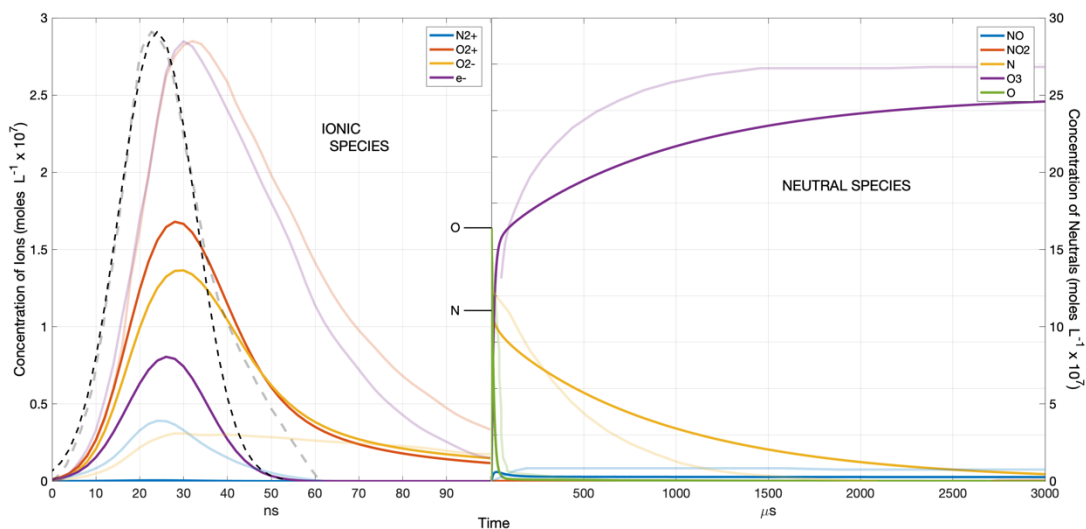


Figure 5.5 *Pulse – Posited Model: Neutral and Ionic Species*

Molar concentrations for neutral and ionic species calculated by the radiation chemistry model reproducing conditions implemented by WB¹. The posited model utilizes 104 mechanisms and reaction rates related to atmospheric chemistry from various sources. Ozone production correlates to a value of $G(O_3) = 10.9$. Original WB results are plotted with transparency.

5.1.2 WB Figure 5 Comparison

The Cantera based approach was tested against the WB model by reproducing the conditions used to create their figure 5 reproduced in Figure 3.2 of this paper. The models simulated a 60 ns wide Gaussian pulse with a peak intensity from 10^{23} – $10^{30} \text{ eV} \cdot \text{g}^{-1} \cdot \text{s}^{-1}$. Molar concentrations are tracked over a three-millisecond time evolution, the same duration of the WB model, with state variables set to 700 Torr and 298 K. Figure 5.6 and Figure 5.7 show the maximum O_3 and NO_2 yields produced under these conditions by each dose rate for all three model variations.

There are two main regions in the O_3 figure: above and below the peak near $5 \times 10^{25} \text{ eV} \cdot \text{g}^{-1} \cdot \text{s}^{-1}$. Calculated g-values for O_3 in the low dose region remains above 10 while the original WB model trends down to $G(O_3) = 7.4$. Similarly, there is an additional turning point at $10^{28} \text{ eV} \cdot \text{g}^{-1} \cdot \text{s}^{-1}$ not present in the original WB figure. For the model using updated rates, the g-values at the peak are nearly identical. In the low dose rate region, yields appear to diverge from the previous model, approaching 9.7 molecules/100 eV at the low dose extreme. In the high dose range, the bump is no longer present and yields trend down much faster with increased dosage. The solution for the posited model follows the same trends as the updated rates solution. Below $10^{28} \text{ eV} \cdot \text{g}^{-1} \cdot \text{s}^{-1}$, the two solutions begin to diverge. Yields for the posited model reach a much higher peak than any of the other model variations, including the original WB model. At the low dose extreme, the solution trends toward the updated rates model yields.

For NO_2 there is no correlation with the original WB model at lower dose rates. It is not obvious why the differences are so pronounced. Since NO_2 measurements were

not successfully conducted by WB, the focus of this work is on computed O_3 concentrations. The WB solution does approach the lower yields of the Cantera-based solutions in the high dose region above $10^{27} \text{ eV} \cdot \text{g}^{-1} \cdot \text{s}^{-1}$. However, no real correlation can be claimed. For the updated rates model, maximum NO_2 yields occur at a dose rate an order of magnitude lower than the Cantera-based reproduction model. The maximum yield for the posited model peaks at dose rates a bit higher than the updated rate model and reaches a slightly higher value. While closer in value, there is no real correlation between the original WB model and the three model variations presented. Recall, the dose rate range for O_3 measurements made by WB was limited to $1\text{--}30 \times 10^{25} \text{ eV} \cdot \text{g}^{-1} \cdot \text{s}^{-1}$, and NO_2 concentrations for all dose rates were below the detection limit of the analytical technique utilized.

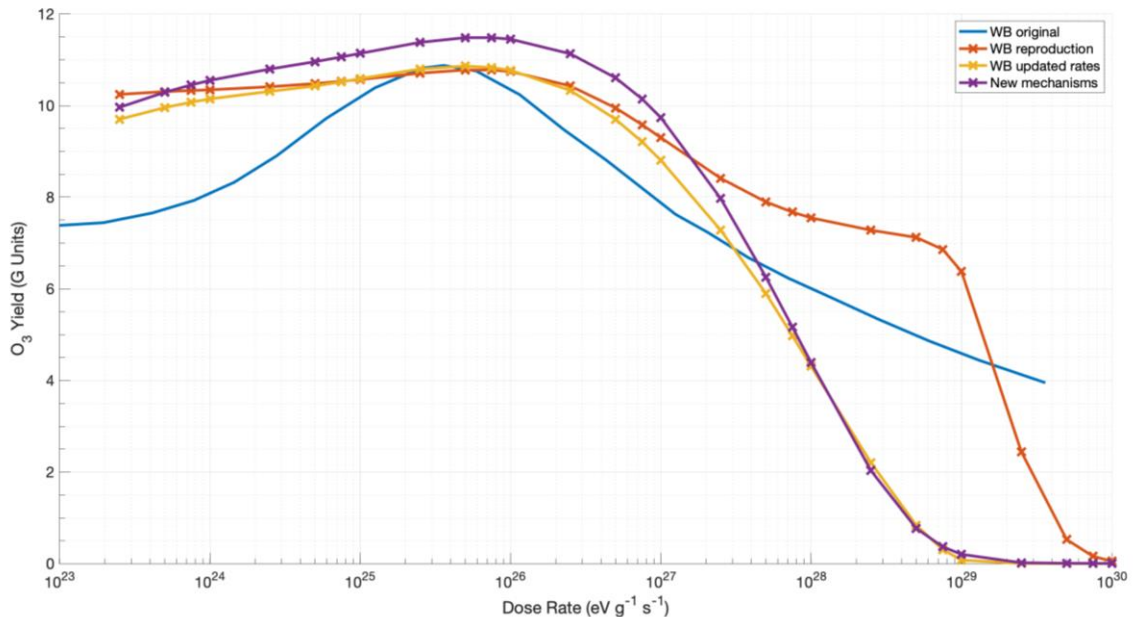


Figure 5.6 *Pulse – O_3 Yields vs. Dose Rate at 700 Torr*

Calculated yields of ozone produced by single pulse irradiations of 80/20 air at 700 Torr.

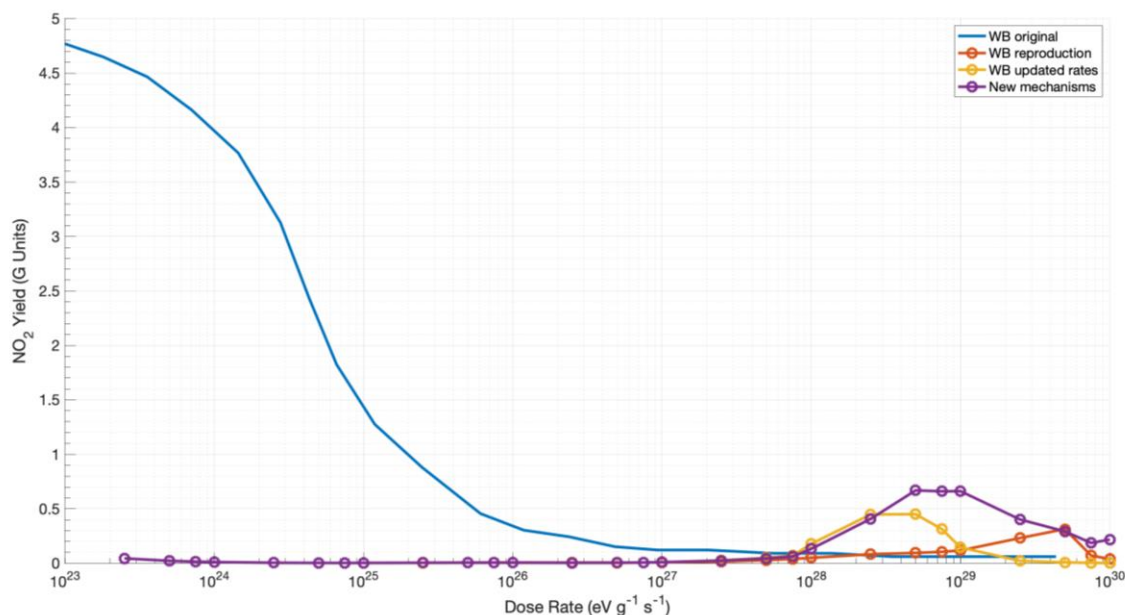


Figure 5.7 *Pulse – NO₂ Yields vs. Dose Rate at 700 Torr*

Calculated yields of nitrogen dioxide produced by single pulse irradiations of 80/20 air at 700 Torr.

5.2 Gautrau Modelled Source

Gautrau²⁸ conducted spectroscopy-based ozone measurements directly over two 5 mCi ²¹⁰Po alpha emitters within a dry atmosphere of 80% nitrogen / 20% oxygen. In one experiment, the source was alternately shielded or exposed every ten minutes completing five cycles. To compare Gautrau’s experimental results to those of a continuous radiation Cantera model, the dose rate distribution above the two sources used must be determined. The dose rate along the optical axis at different heights above the sources was produced from energy deposition data of the GEANT4 simulation provided by Gautrau.⁴⁵ The voxel data used to create Figure 4.3 was duplicated, spatially offset, and summed with the first to match the geometry of the two sources used by Gautrau²⁸. As shown in Figure 4.3, the highest dose rates occur within the gold foil in which the polonium atoms are

embedded. For a sufficiently thin sheet, only half of all energy will leave the foil. Figure 5.8 and Figure 5.9 show a vertical slice along the center of the resulting two-source energy distribution in the space above the foil. The second figure is the same as the previous but with the height and dose rate axes swapped. Figure 5.10 shows the calculated average dose rate vs distance above the foil for the portion of the region that includes affected voxels and for the full length of the optical cavity. From Gautrau²⁸, the distance from the foil to the bottom of the laser beam was approximately 15 mm.

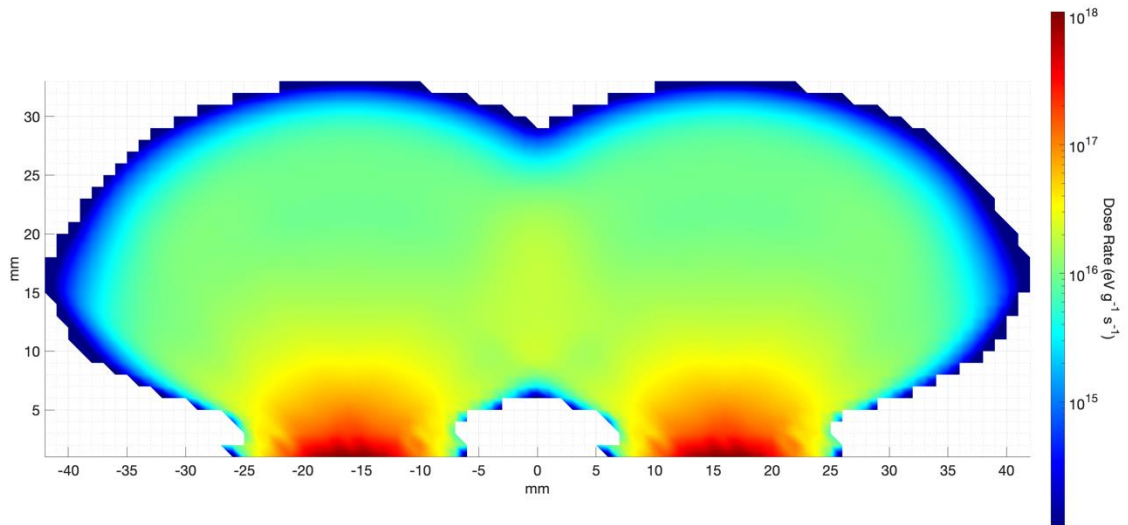


Figure 5.8 *Gautrau: Modelled Dose Rate Distribution*

Visual representation of the dose rate ($eV \cdot g^{-1} \cdot s^{-1}$) for each 1 mm^3 voxel of space above the ^{210}Po impregnated gold foils of two antistatic devices used in experiment by Gautrau²⁸. Energy deposition data was collected by Gautrau⁴⁵ through a yet unpublished GEANT4 energy tracking model which incorporated source geometry to determine the distribution of energy deposited within one atmosphere of $80\%-\text{N}_2 / 20\%-\text{O}_2$ at 298 K.

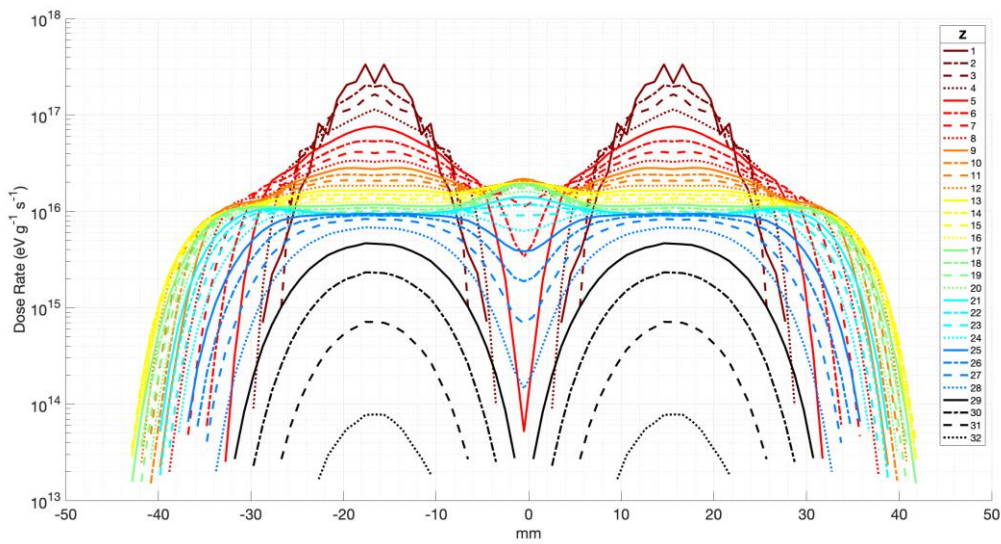


Figure 5.9 *Gautrau: Dose Rate Along Vertical Plane of Beam Path*

The dose rate along the plane of the beam path through the depositional volume. Z values represent the distance, in mm, above the ^{210}Po embedded foil. Gautrau²⁸ gives the beam height of experiment at 15 mm above the foil. This figure is the same as Figure 5.8 with dose rate and z axes swapped.

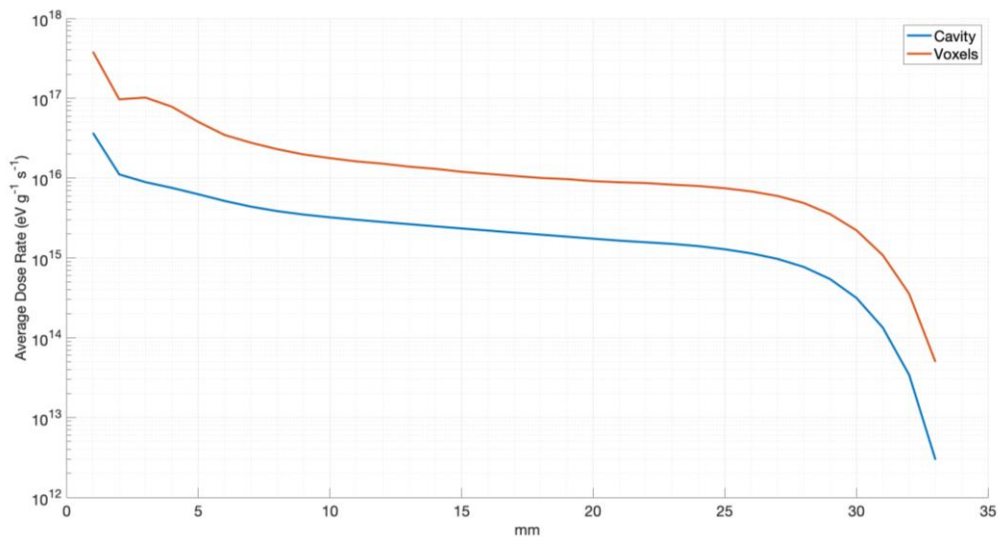


Figure 5.10 *Gautrau: Average Dose Rate v. Distance Above Experimental Sources*

The figure shows the average dose rate along each horizontal line of affected voxels in Figure 5.8 and the average dose rate along the full length of the optical cavity. Refer to Figure 5.9 for length of affected voxels at each height. The horizontal axis represents the distance above the ^{210}Po embedded foil.

5.3 Continuous Exposure Scheme

Figure 5.11 through Figure 5.17 include the corresponding results from the continuous radiation model by Moss et al.²⁴ Figure 3.3 is a reproduction of their results showing the time evolution of chemical species calculated to 10^6 seconds (11.5 days). Although it was a 100% RH model and included reactions for *C* and *H* atoms, recall from Table 3.1 that primary radiation-induced products were reported to be O_3 , 500 ppb; N_2O , 400 ppb; HNO_3 , 300 ppb; HO_2NO_2 , 200 ppb; and NO_2 , 50 ppb at 10^4 seconds (2.77 hours). *NO* yield was not very high at just 2.5 ppb. Moss et al. simulates an assumed dose rate of $3 \times 10^{13} \text{ eV} \cdot \text{g}^{-1} \cdot \text{s}^{-1}$ within humid air at 760 Torr.

No variation of the dry Cantera model predicts O_3 concentration near what Moss et al. predicts for the dose rate published. The highest concentration predicted by any Cantera model is 20 ppb using the extensive mechanism list of the posited model. The inclusion of *C* and *H* atoms introduce many new reactions that directly involve O_3 and will potentially open many secondary, tertiary, etc. pathways that also impact the system. This makes direct comparisons somewhat inappropriate. Nevertheless, the results are shown against the computational solutions to provide added context for the behaviors illustrated.

From Gautrau²⁸, the average dose rate for the entire volume of the 18-inch diameter vacuum chamber, ignoring flanged takeoffs and device extensions, is approximately $1.5 \times 10^{13} \text{ eV} \cdot \text{g}^{-1} \cdot \text{s}^{-1}$ and represents the lower limit of the experiment. As shown in Figure 5.10, the maximum average dose rate along the vertical plane of the optical axis is just above the gold foil at $3.68 \times 10^{16} \text{ eV} \cdot \text{g}^{-1} \cdot \text{s}^{-1}$. At minimum, experimental numbers should fall within the model solutions between dose

rate bounds. At best, numbers would agree most closely with the average dose rate calculated along the CRDS optical cavity at the 15 mm measurement height, $2.33 \times 10^{15} \text{ eV} \cdot \text{g}^{-1} \cdot \text{s}^{-1}$.

Due to the large reservoir of gas not directly impacted by the ionizing radiation, it will most likely be necessary to account for diffusion from hot spots within the chamber when comparing to experimental measurements, but this has not yet been incorporated into the models. Optical measurements made through hot spots near the source are presumed to measure a slower rate of change in the concentration of primary products, such as O_3 , than a non-diffusionary computational solution of the same dose rate.

Figure 5.11 shows the O_3 concentration for the model using WB mechanisms and rates. Experimental results align with computational solutions approximately an order of magnitude above the lower dose limit and an order of magnitude below the average dose rate at measurement beam height.

Figure 5.12 shows the model using the WB mechanisms with updated rates. At the measurement height dose rate, the experimental data is very similar to the evolving computational solution, albeit with a slightly lower concentration. In the first 4 hours, the shape is more comparable to the dip seen in the solution for $10^{14} \text{ eV} \cdot \text{g}^{-1} \cdot \text{s}^{-1}$. Except for this dip, the temporal profiles have comparable forms with experimentally measured values tracing the same shape as the computation.

Figure 5.13 shows results for the posited model using the extensive list of known mechanisms. The time evolution profile at Gautrau's measurement height is very comparable to the previous model; however, O_3 concentrations from the posited model

are much closer to those found through experiment. Like the updated WB based model, the initial dip seen in experiment is absent from the calculated solution. Experiment also falls between adjacent solutions, making it the best fitting result of the three models.

Figure 5.14 shows results from the posited model but with reaction 88 ($NO_2^- + NO_2 \rightarrow NO_3^- + NO$) disabled to limit reaction 91 ($NO_3^- + O_3 \rightarrow NO_2^- + 2 O_2$). Despite Gautrau's concentration measurement aligning with a lower dose computational solution, it is above the lower dose limit of the experiment and demonstrates the impact these ionic reactions have in shaping the initial dip seen in the experimental data.

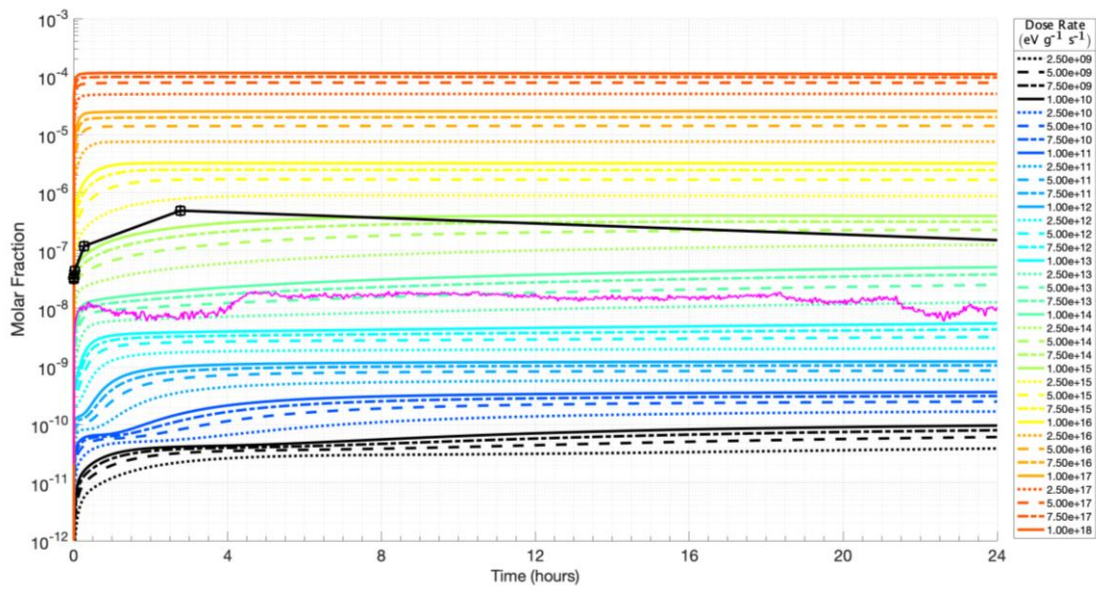


Figure 5.11 *Continuous – WB Mechanisms: O₃ vs. Time vs. Dose Rate*

Ozone vs. time vs. dose rate from model implementing WB mechanisms and rates. Magenta line represents ozone concentration measurements from Gautrau²⁸. Black line with square markers represents ozone results from Moss et al.

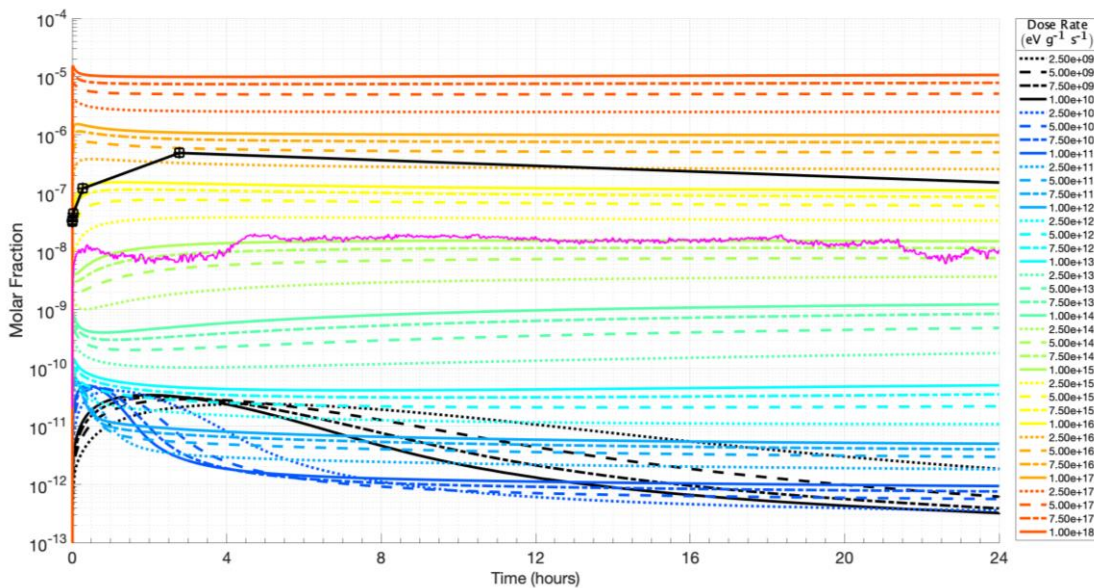


Figure 5.12 *Continuous – WB Mechanisms, Updated Rates: O₃ vs. Time vs. Dose Rate*

Ozone vs. time vs. dose rate from model implementing WB mechanisms using currently accepted rates. Magenta line represents ozone concentration measurements from Gautrau²⁸. Black line with square markers represents ozone results from Moss et al.

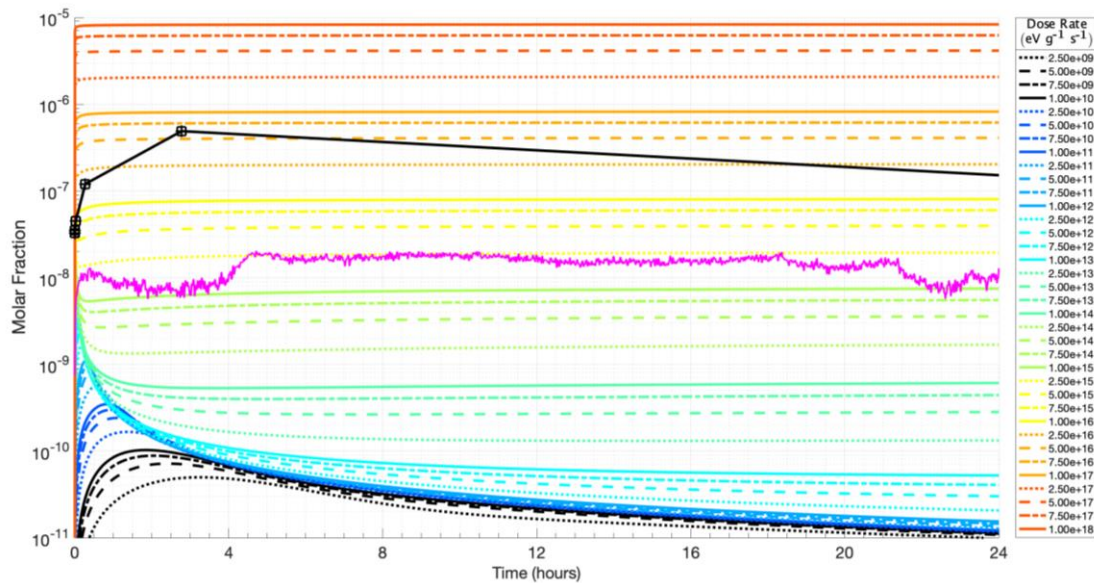


Figure 5.13 *Continuous – Posited Model: O₃ vs. Time vs. Dose Rate*

Ozone vs. time vs. dose rate from model implementing the posited mechanisms and rates. Magenta line represents ozone concentration measurements from Gautrau²⁸. Black line with square markers represents ozone results from Moss et al.

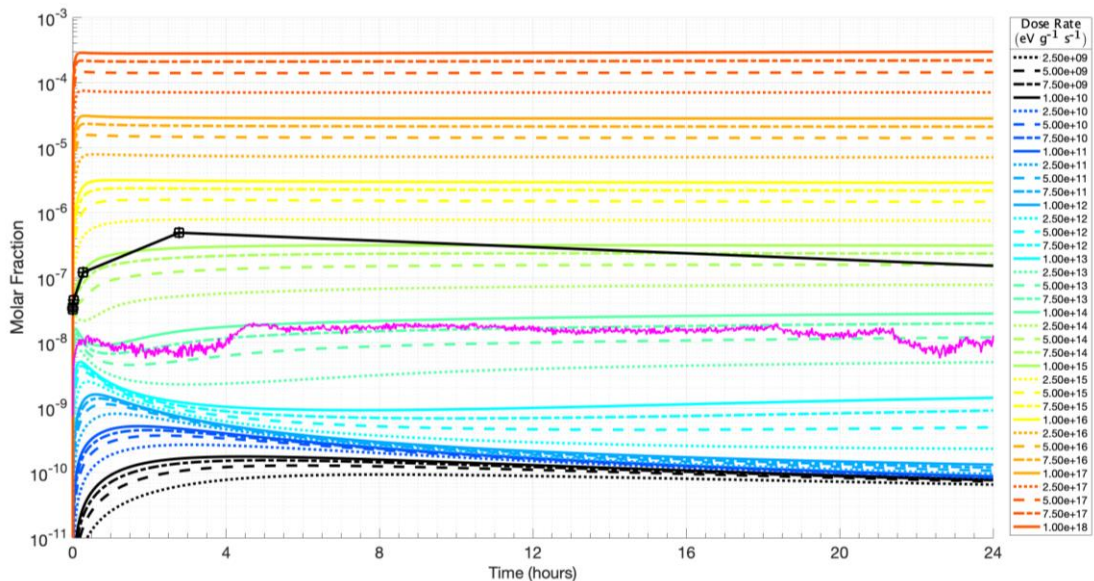


Figure 5.14 *Continuous – Posited Model, Reaction 88 Off: O₃ vs. Time vs. Dose Rate*

Ozone vs. time vs. dose rate from model implementing the posited mechanisms and rates. Reaction 88 disabled to limit reaction 91. Magenta line represents ozone concentration measurements from Gautrau²⁸. Black line with square markers represents ozone results from Moss et al.

Figure 5.15 through Figure 5.17 show computed solutions of the posited model for NO , NO_2 , and N_2O concentrations in the continuous radiation scheme. These concentration profiles are included here to provide a broader understanding of the model's overall results and to give additional context for the complexity and interconnected nature of each concentration's temporal behavior. However, suitable validation comparisons for these species are not readily available currently. While it will serve as the basis for some comparisons here, the computational model presented by Moss et al.²⁴ included 100% RH and therefore is not an ideal benchmark for conclusive model assessment. The O_3 solution by Moss et al. does not correlate well with the dry Cantera models, but solutions for other species correlate better over longer durations.

The NO concentration for the posited dry model reaches the same level as the Moss et al. model but much more quickly. The NO_2 yield increases rapidly at first, but concentrations slowly reduce by more than an order of magnitude over the 24-hour duration. The N_2O solution is the most well behaved of all products and shows a stark stratification of yields versus dose rate. The calculated yields at the dose rate cited is about 10% lower than the Moss et al. solution after 24 hours. Species with molar fractions above 10^{-14} after 24 hours are shown in Table 5.1 for the average absorbed dose rate of the optical cavity at the height of Gautrau's measurement. For comparison, Table 5.2 shows the most abundant species produced at the maximum dose rate simulated, $10^{18} \text{ eV} \cdot \text{g}^{-1} \cdot \text{s}^{-1}$. NO^+ , NO_2^- , and NO_3^- are the most abundant ions and were found to increase with dose rate. This is to be expected since there is no sink for these ions in the model.

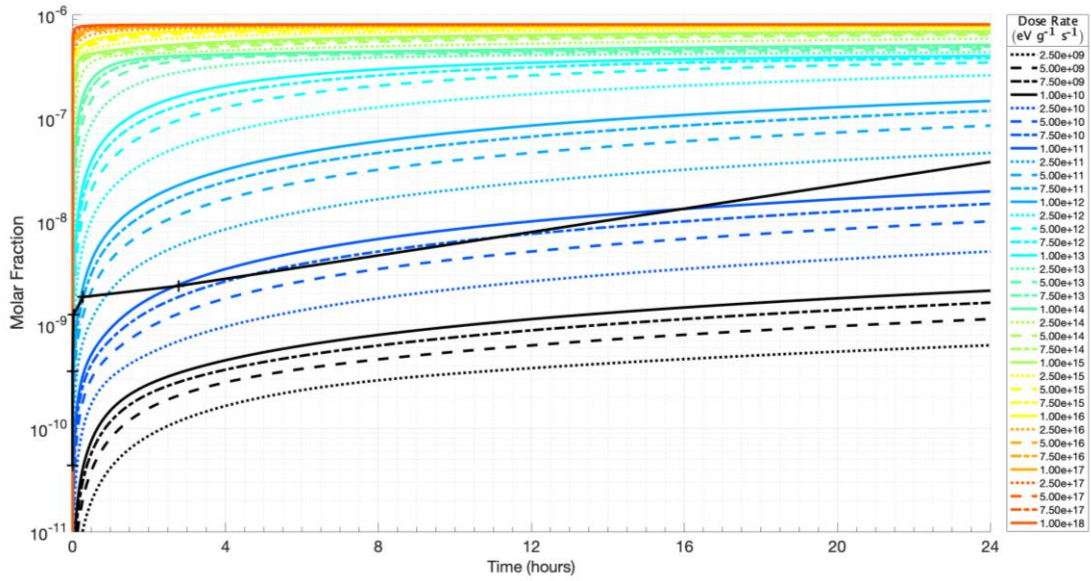


Figure 5.15 *Continuous – Posited Model: NO vs. Time vs. Dose Rate*

NO concentration calculated by the Cantera model implementing the posited mechanisms and rates. Black line with cross markers represents nitric oxide results from the Moss et al. computational model.

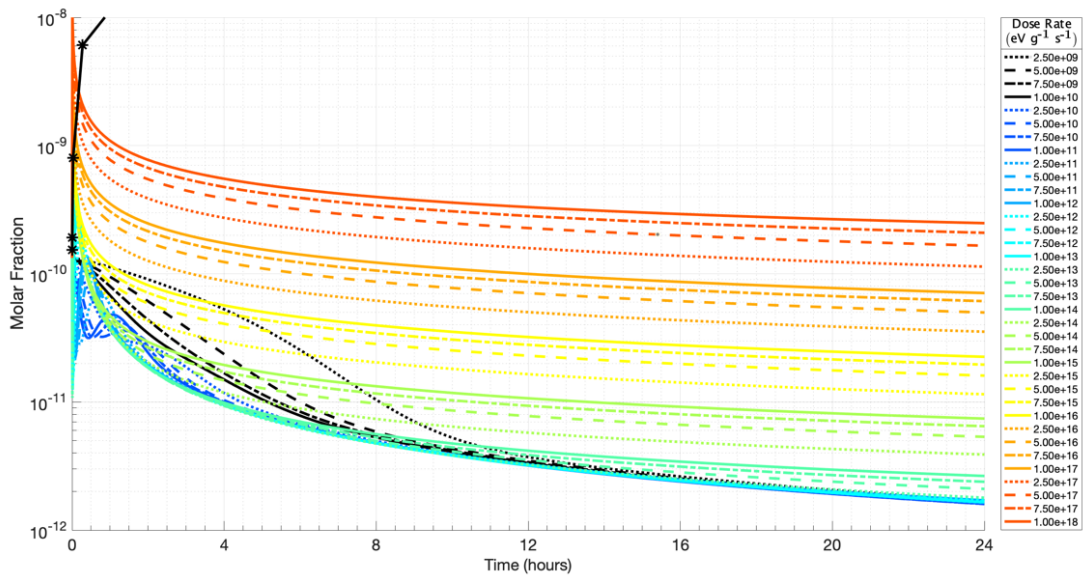


Figure 5.16 *Continuous – Posited Model: NO₂ vs. Time vs. Dose Rate*

NO_2 concentration calculated by the Cantera model implementing the posited mechanisms and rates. Black line with asterisk markers represents nitrogen dioxide results from the Moss et al. computational model and approaches 200 ppb after 24 hours. The scale was limited for clarity in the region displaying the Cantera model results.

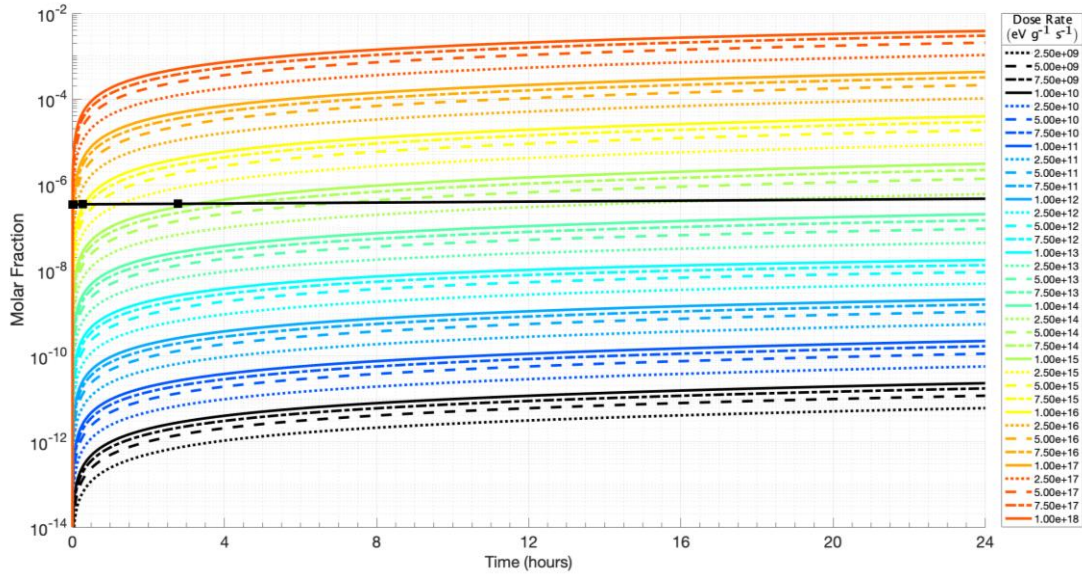


Figure 5.17 *Continuous – Posited Model: N₂O vs. Time vs. Dose Rate*

N₂O concentration calculated by the Cantera model implementing the posited mechanisms and rates. Black line with square markers represents nitrous oxide results from the Moss et al. computational model.

NO ⁺	1.12×10^{-4}	O ₃	7.48×10^{-7}	N	6.11×10^{-12}
NO ₂ ⁻	1.12×10^{-4}	NO	2.05×10^{-8}	NO ₃	3.20×10^{-13}
N ₂ O	1.07×10^{-4}	NO ₃ ⁻	1.09×10^{-9}	O	1.41×10^{-13}
NO ₂	2.88×10^{-6}	NO ₂ ⁺	1.88×10^{-11}	O ₂ ⁺	3.97×10^{-14}

Table 5.1 *Continuous – Posited Model: Top Products at Beam Height*

Table shows the molar fractions of the most abundant species produced by an absorbed dose rate of $2.5 \times 10^{15} \text{ eV} \cdot \text{g}^{-1} \cdot \text{s}^{-1}$.

N ₂ O	5.09×10^{-2}	NO ₂	3.45×10^{-6}	NO ₃ ⁻	1.31×10^{-9}
NO ⁺	2.40×10^{-3}	NO	2.24×10^{-8}	NO ₃	1.27×10^{-10}
NO ₂ ⁻	2.40×10^{-3}	NO ₂ ⁺	7.49×10^{-9}	O	8.02×10^{-11}
O ₃	2.95×10^{-4}	N	2.50×10^{-9}	O ₂ ⁺	2.02×10^{-11}

Table 5.2 *Continuous – Posited Model: Top Products at Max Dose Rate*

Table shows the molar fractions of the most abundant species produced by an absorbed dose rate of $1.0 \times 10^{18} \text{ eV} \cdot \text{g}^{-1} \cdot \text{s}^{-1}$.

5.4 Cycled Exposure Scheme

The cycled exposure experiments by Gautrau²⁸ were simulated with the use of a time dependent function attached to the reactant *MassFlowController* instances. Figure 5.18 through Figure 5.20 show computational solutions for ozone compared against Gautrau using the three mechanism and rate variations outlined previously. The first ten minutes of the experimental data is part of the initial 2-hour shielded measurement CRDS requires for calculating differences from baseline. The erratic behavior is the result of mathematical artifacts indicating the baseline value is near the detection limit of the system. These figures help demonstrate the utility of the built-in functional control Cantera provides over the introduction rate of fragmentary reactant species. All three figures correlate with descriptions of their noncyclical exposure solutions. As with experiment, calculated ozone values immediately return to the last pre-shielded level when the shield is removed indicating some positive level of correlation for all models.

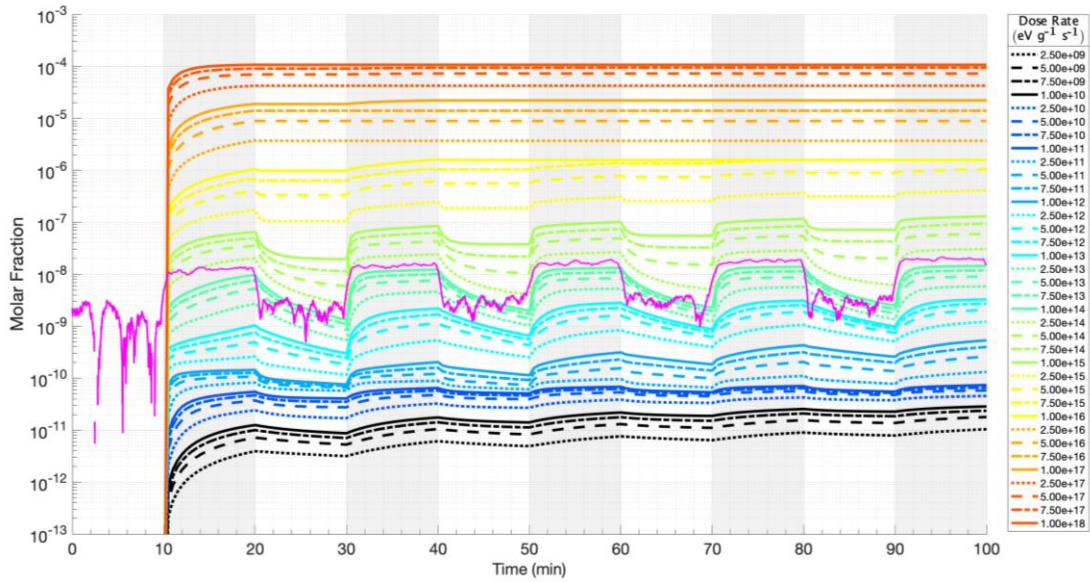


Figure 5.18 *Cycled – WB Mechanisms: O₃ vs. Time vs. Dose Rate*

Ozone concentrations calculated in the cycled exposure scheme. Model implemented WB mechanisms and rates. Shaded areas represent periods of source exposure. Magenta line represents concentrations measured by Gautrau²⁸ with a 50-point moving average.

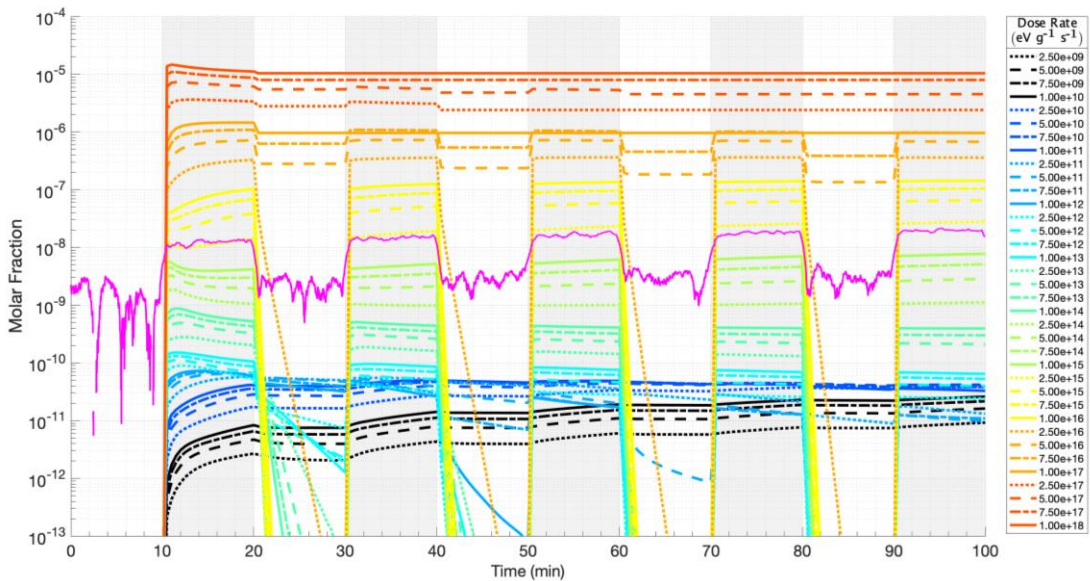


Figure 5.19 *Cycled – WB Mechanisms, Updated Rates: O₃ vs. Time vs. Dose Rate*

Ozone concentrations calculated in the cycled exposure scheme. Model implemented WB mechanisms using updated reaction rates. Shaded areas represent periods of source exposure. Magenta line represents concentrations measured by Gautrau²⁸ with a 50-point moving average applied.

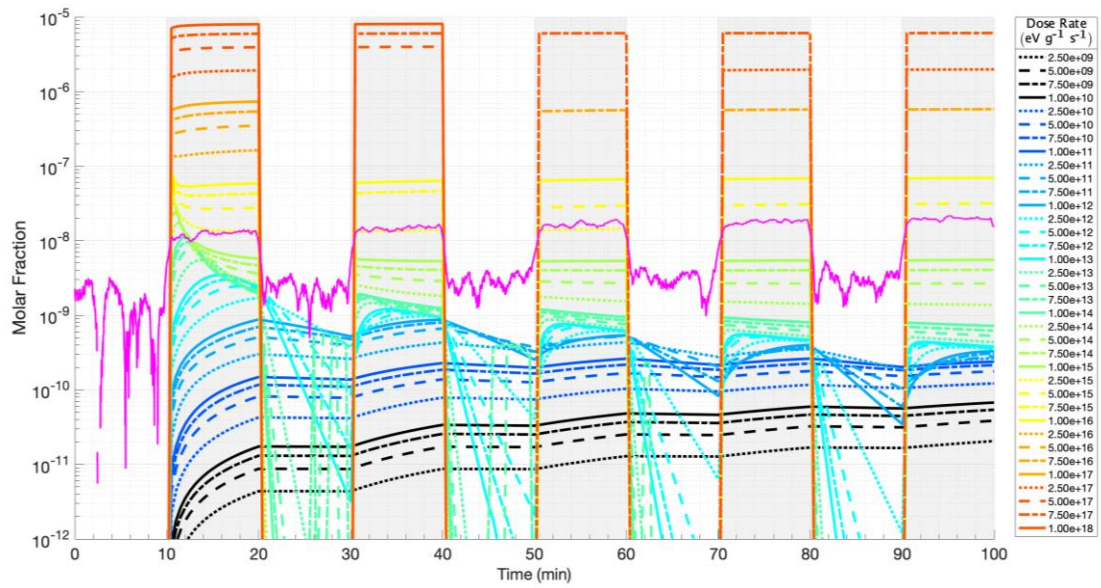


Figure 5.20 *Cycled – Posited Model: O₃ vs. Time vs. Dose Rate*

Ozone concentrations calculated in the cycled exposure scheme. Model implemented all known mechanisms and rates related to atmospheric chemistry. Shaded areas represent periods of source exposure. Magenta line represents concentrations measured by Gautrau²⁸ with a 50-point moving average applied.

CHAPTER VI – DISCUSSION

The Cantera-based pulse model was designed to validate the approach by attempting to reproduce the results of the WB¹ pulse model. Although very similar, the solution produced by the Cantera-based reproduction did not match WB exactly. This may be explained by Cantera's differential solver taking smaller internal steps or the imposed thermodynamic restraint to continuously minimize the Gibbs free energy of the evolving mixture. The amplitude and total dose of the Gaussian pulse used in the Cantera models are identical to the WB description, yet the area under the pulse curve shown by WB appears to be appreciably larger, indicating a larger total dose than described. If the WB pulse is an accurate representation of the pulse used in their model, it is possible the method used to increment the dose rate at each step is responsible for this difference; the total dose may be the lower sum i.e., the sum of inscribed rectangles 2 ns wide. It may also be the case that the total dose or amplitude reported in WB is inaccurate or imprecise.

The charge transfer reaction between N_2^+ and O_2 is very rapid and may occur more rapidly in the Cantera based solutions due to smaller computational steps explaining the much lower N_2^+ peak. Experiments by WB¹ show O_3 yields for air above 400 Torr to be $G(O_3) = 10.3 \pm 0.5$, and yields increase with O_2 partial pressures. Their kinetics model calculated a yield of $G(O_3) = 10.3$ under the same conditions and claim a computational error of less than 4%. The Cantera-based reproduction of the WB model calculated a g-value of $G(O_3) = 10.0$, within the margin of the computational error and the standard deviation of the value measured. This result is a sufficient validation of the Cantera-based approach, so rates were updated to the latest accepted to explore the

change in yields. Implementing WB mechanisms with updated rates produced very similar neutral species yields with an ozone yield of $G(O_3) = 9.9$. To explore the possibility of a new pulse radiation chemistry model, an extensive list of N and O compounds was put together containing all known reactions and their currently accepted rates. The posited model produced a much higher ozone yield at $G(O_3) = 10.9$, slightly greater than one standard deviation above the value WB measured but in reasonable agreement with experiment.

In the continuous radiation scheme, since reactors cannot diffuse heat or gas through the boundary, solutions have the potential to quickly diverge from experimental results with time. Diffusion rate coefficients represent the rate at which the surface area of the bounding volume increases with time. For some chemical species, the area of the bounding spherical surface increases at rates up to 700% per second meaning the density of each diffuse species within the volume is reduced proportionately to that expansion rate.

The solutions for these models in the continuous and cycled radiation schemes were produced by holding the temperature constant to control divergence. Applying the original WB mechanisms and rates in a continuous exposure scheme produced O_3 yields correlating with dose rates much lower than the experiment. The dose rate from Gautrau's experiment correlated with calculated yields near 1 ppm. WB¹ assert the creation of other ionic species by N_2^+ and O_2^+ reactions are not important in pulse radiation models since they are much slower than charge transfer reactions due to relative abundances and hence were omitted from their mechanism list. The model implementing updated rates produced O_3 yields much closer to those measured, correlating with a dose

rate solution 2.5 times lower than the dose rate of the experiment. Although somewhat low, it's interesting that the solution of this model in the cycled exposure scheme fits the measured O_3 concentration at the average dose rate for the experiment. The posited model implementing the extensive list of mechanisms calculated yields in very good agreement with both experiments at the proper dose rates.

The literature asserts most ionic reactions in O_2 and N_2 mixtures result in the creation of NO^+ . In the posited model using all known atmospheric mechanisms, NO^+ is produced by fourteen reactions (46, 48, 50, 53, 56, 58, 61, 62, 63, 65, 67, 68, 69, 71) but only destroyed by the dissociative recombination reaction (78). WB¹ suggests the predominant ion neutralization process under continuous low dose rate irradiation will probably be the reaction $NO^+ + NO_2^- \rightarrow products$ and in all probability will lead to no net yield of O_3 or NO_2 . No reactions of this form could be found in the current literature, so experimental work will be required to test their proposed mechanism. NO_2^- has five known production pathways (91, 97, 98, 99, 101) and four destruction pathways (88, 90, 100, 102); all are driven by negative ions.

If reaction rates and typical abundances proportional to dose rate are taken into account, the NO_2^- destruction mechanisms defined in the posited model, in order of efficiency, are reactions with O_2 , O_3 , N_2O_5 , and NO_2 ; all of which yield NO_3^- plus O , O_2 , NO_2 , and NO respectively. Due to its abundance, reaction with O_2 is the primary sink for NO_2^- and drives reaction 102 which destroys O_3 to produce NO_3^- . The only means of consuming NO_3^- is by reaction with O_3 (91) which yields NO_2^- and O_2 . Reaction 88 between NO_2^- and NO_2 will initially drive NO concentrations higher since N_2O_5 numbers have not had enough time to increase and allow reaction 90 to become more dominant.

This all results in a huge reduction in O_3 relative to the nitrogen oxides if not restrained in the model. To mitigate this effect, reactions 100 and 102 had to be omitted from the posited model to produce reasonable solutions; however, this created a large reservoir of NO^+ , NO_2^- , and NO_3^- ions without a defined neutralization pathway. Charge neutralization pathways involving NO^+ and NO_2^- ions are assumed but not well known since rates are highly dependent on initial ion concentrations. Confidence in the calculated solution for continuous exposure models is substantially reduced as dose rate increases and the concentrations of these ions balloon.

If O_3 , NO , and NO_2 concentration measurements are to be used to validate a non-diffusionary continuous radiation model, at least one experiment should utilize a vessel whose radius is close to the range of the ^{210}Po alpha particle to eliminate the exchange of gases with the reservoir of gas in the indirectly affected volume. The accuracy for continuous exposure models should increase with a more complete and thorough handling of the mechanisms involved, such as specifying each reaction more precisely by quantum state. Other papers by WB^{19,20} attempted to do just that, defining reaction rates for several excited states of nitrogen and oxygen based species, but pursuing a comprehensive inclusion of the concept was beyond the scope of this project in its current phase.

CHAPTER VII – CONCLUSIONS

The work in this paper demonstrates that radiation chemistry models can be created using a community-managed open-source kinetics toolkit like Cantera.⁴⁸ This approach enables independent atmospheric chemistry modelers to accelerate the computational development process. The primary source code and three mechanism files, one for each model, are included in APPENDIX D to provide a kickstart to that effort.

A preliminary investigation into the significance of omitting diffusion showed accounting for its effects is vital for producing an accurate kinetics model for continuous radiation and negligible for pulsed radiation models. WB's decision to use production cross sections for 100 eV collisions is a bit arbitrary, despite its justification. Konovalov³³ has shown most secondaries generated by cascades carry much lower energies in numbers growing much more numerous with time. For N_2/O_2 mixtures, differences in the activation energies for electronically excited molecular states skew energy absorption rates in the low-energy regime toward oxygen resulting in an increase in the prevalence of electronically excited oxygen relative to nitrogen. In short, mixture dependent G-values derived from experiment are useful in validating model outputs but require a series of well-designed experiments that isolate each suspected mechanism to be of use in determining model inputs. A more accurate g-value for each fragmentary, excited, and/or ionized species should be calculable by Monte Carlo through the application of electron energy degradation spectra and electron impact species production cross sections.

7.1 Future Work Toward Model Improvement

Cantera can be utilized as presented here or features relevant to radiation chemistry can be added by modifying its source code. A class representing a radioactive

source would be convenient with attributes like decay particle energy and radioactivity and should include methods for calculating dose rate vs. distance from source. A class defining a partitioned and indexed volume would be useful with initial attributes such as spatial coordinates and dose rate. It should also include built-in methods to instantiate a reactor for each voxel and to calculate diffusion rate differentials between neighboring voxels. Spherically symmetric diffusion reduces the calculation to one dimension which could be solved at much larger step sizes. Users can submit pull requests to the GitHub Cantera project⁶⁰ if they want to share their functional changes with the community.

Mixture dependent electron degradation spectra should also be calculable which would more accurately determine the fragmented and excited species induced by radiation within the medium. This distribution has been calculated by Konovalov³³ for 0.78–N₂ / 0.22–O₂ mixtures with energy balance calculations by both he and WB²⁰. Cantera's *ThermoPhase* class has an *electron_energy_distribution* property which can be set by the *set_discretized_electron_energy_distribution* class method. This enables the user to specify an electron energy distribution unique to the mixture. A more comprehensive kinetics model should attempt to make use of this property. The approach used here to inject fragmentary and excited species into each reactor may need to be modified depending on how this property affects the computation; therefore, a more thorough understanding of the *ThermoPhase* class is required.

7.1.1 Possible Diffusion Approach

To refine the approach described in the work to include diffusion, a few things must be considered. First, transport data for each chemical species is required to instantiate the *transport_model*. Transport properties are described by Lennard–Jones

parameters and can be found for most species in the GRI-Mech 3.0 reaction mechanism available from Berkeley.⁶¹ GRI-Mech 3.0 is widely used for modelling natural gas combustion and was designed for use at pressures where the ideal gas law holds. It contains 325 reactions involving 53 chemical species comprised of the elements *H*, *C*, *O*, *N*, and *Ar*. It does not include transport properties for more complex molecules such as *NO*₃, *N*₂*O*₅, acids, etc., so it cannot be applied directly to the specific mechanism file implemented in this research without additional resources. When initialized, the transport model can calculate diffusion coefficients for a given *Solution* object, but it does not have a built-in function to simulate diffusion within a single reactor over time. It may be possible to implement diffusion by modification of extant *FlowDevice* classes so that the fraction of each diffusive species leaving the reactor volume can be calculated. This would allow one to model a diffusive, symmetric volume by reducing it to one radial dimension and thereby limiting the increase in computation time. Since concentration differentials between neighboring reactors drive the impact of diffusion, the computational approach must be modified to account for this. The following approach is suggested as a potential solution.

The thermodynamic state of the voxel closest to the emission source would be calculated first, recording the number of each diffusive species which would leave the volume over the time step. During the next computational step, the species fractions which exited the upstream reactor would be injected into the downstream reactor, second closest to the source, through an additional flow device metered at a correlative rate. For a cubic voxel, the fraction of each diffused species to be injected downstream would be reduced by six to correlate with a single boundary face. In the same way, another flow

device would inject the appropriate fraction of each diffusively lost species from each downstream reactor into the neighboring upstream reactor. This computational procedure would continue, with each successive reactor being one time step behind the previous one i.e., the first reactor would be calculating step three while the second one is on step two and the third is on step one. In this way, the entire system can be stepped through time simultaneously. Parallelization may also decrease computation time if each step of the first reactor spawns a new process for calculating the downstream reactors. Methods in the *transport_model* would calculate diffusion rates at the start of each new process. To implement parallelization, it may be necessary to keep the reactors decoupled from one another by creating a separate reservoir for each species and only linking reactors to reservoirs. The number of MFCs would remain the same, but introduction rates for each species specific MFC would be calculated from the difference in the neighboring upstream and downstream reactors.

7.2 Final Thoughts

Efforts to improve the accuracy of the Cantera based model as suggested here will be pursued and presented in future publications. This work serves to demonstrate the utility of an open-source chemical kinetics toolkit in computing the radiation induced chemical effects within atmospheric gas mixtures and to report the current obstacles faced pursuant to that end. This work also shows that by measuring number densities for key chemical species in a methodical way and applying the results to a robust radiation chemistry model, it may yet be possible to construct a method to determine the presence and effective energy transfer rate of an unshielded radioactive source based on induced chemical product distributions.

APPENDIX A – Willis and Boyd Reaction List

Table A.1 *Ion-Molecule Reactions for Irradiated N₂-O₂ Mixtures*

	Reaction	WB ¹ Rate Constant (cm ³ molec ⁻¹ s ⁻¹)	Updated Rate Constant (cm ³ molec ⁻¹ s ⁻¹)	Reference
1	$N_2^+ + O_2 \rightarrow N_2 + O_2^+$	1.5×10^{-10}	5×10^{-11}	53
2	$O_2^+ + N_2 \rightarrow NO^+ + NO$	$< 2 \times 10^{-16}$	1×10^{-15}	53
3	$N_2^+ + 2N_2 \rightarrow N_4^+ + N_2$	$* 1 \times 10^{-28}$		
4	$N_4^+ + O_2 \rightarrow O_2^+ + 2N_2$	1×10^{-10}		
5	$N_2^+ + NO \rightarrow NO^+ + N_2$	5×10^{-10}		
6	$O_2^+ + NO \rightarrow NO^+ + O_2$	8×10^{-10}	4.6×10^{-10}	53
7	$NO^+ + e \rightarrow N + O$	4×10^{-7}	4.1×10^{-7}	54
8	$O_2^+ + e \rightarrow O + O$	2×10^{-7}	2.2×10^{-7}	54
8a	$O_2^+ + O_2^- \rightarrow O + O + O_2$	2×10^{-6}		
9	$N_2^+ + e \rightarrow N + N$	1×10^{-7}	2.9×10^{-7}	54
10	$N_2^+ + O_2^- \rightarrow N + N + O_2$	2×10^{-6}		
11	$e + 2O_2 \rightarrow O_2^- + O_2$	$* 1.9 \times 10^{-30}$	$* 2.5 \times 10^{-30}$	54
12	$e + O_2 + N_2 \rightarrow O_2^- + N_2$	$* 1.0 \times 10^{-31}$	$* 2.5 \times 10^{-30}$	54
13	$e + NO_2 + N_2 \rightarrow NO_2^- + N_2$	4×10^{-11}	7×10^{-10}	54
14	$e + NO + M \rightarrow NO^- + M$	$* 1.3 \times 10^{-31}$		
15	$O_2^- + O_3 \rightarrow O_3^- + O_2$	3.5×10^{-10}	6×10^{-10}	56
16	$O_3^- + NO \rightarrow NO_2^- + O_2$	8×10^{-10}	8×10^{-10}	54
17	$O_3^- + NO_2 \rightarrow NO_2^- + O_3$	7×10^{-10}	7×10^{-10}	54
18	$NO_2^- + O_3 \rightarrow NO_3^- + O_2$	1×10^{-11}	1.2×10^{-11}	54
19	$NO^- + O_2 \rightarrow O_2^- + NO$	9×10^{-10}		

* Rate constant has three-body units (cm⁶ molec⁻² s⁻¹).

Rates were calculated at 298 K for model comparison. Where spaces are empty, the WB¹ rate was used.

Table A.2 *Neutral-Neutral Reactions for Irradiated N₂-O₂ Mixtures*

	Reaction	WB ¹ Rate Constant (cm ³ molec ⁻¹ s ⁻¹)	Updated Rate Constant (cm ³ molec ⁻¹ s ⁻¹)	Reference
20	$N + O + M \rightarrow NO + M$	1×10^{-32}	$* 1.08 \times 10^{-32}$	62
21	$2N + N_2 \rightarrow 2N_2$	9×10^{-33}	$* 1.72 \times 10^{-32}$	63
22	$N + O_2 \rightarrow NO + O$	8.0×10^{-13}	9.6×10^{-17}	64
23	$N + O_3 \rightarrow NO + O_2$	5.7×10^{-13}	1×10^{-16}	64
24	$N + NO \rightarrow N_2 + O$	2.2×10^{-11}	3.11×10^{-11}	64
25	$N + NO_2 \rightarrow N_2O + O$	7.7×10^{-12}	3.01×10^{-12}	64
26	$N + NO_2 \rightarrow 2NO$	5.9×10^{-12}	6.11×10^{-12}	65
27	$N + NO_2 \rightarrow N_2 + O_2$	1.8×10^{-12}	1.85×10^{-12}	65
28	$N + NO_2 \rightarrow N_2 + 2O$	2.3×10^{-12}	2.41×10^{-12}	65
29	$O + 2O_2 \rightarrow O_3 + O_2$	$* 5.9 \times 10^{-34}$	$* 5.58 \times 10^{-34}$	66
30	$2O + O_2 \rightarrow 2O_2$	$* 2.0 \times 10^{-33}$	$* 2.7 \times 10^{-33}$	67
31	$O + O_3 \rightarrow 2O_2$	1.0×10^{-14}	8.3×10^{-15}	66
32	$O + NO + O_2 \rightarrow NO_2 + O_2$	$* 8.1 \times 10^{-32}$	$* 1.00 \times 10^{-31}$	66
33	$O + NO + N_2 \rightarrow NO_2 + N_2$	$* 1.1 \times 10^{-31}$	$* 1.00 \times 10^{-31}$	66
34	$O + NO_2 \rightarrow NO + O_2$	1.9×10^{-11}	2.9×10^{-12}	66
35	$O_2 + 2NO \rightarrow 2NO_2$	$* 1 \times 10^{-33}$	$* 1.9 \times 10^{-38}$	66
36	$O_3 + NO \rightarrow NO_2 + O_2$	3.5×10^{-13}	1.8×10^{-14}	66

* Rate constant has three-body units (cm⁶ molec⁻² s⁻¹)

Rates were calculated at 298 K for model comparison. Where spaces are empty, the WB¹ rate was used.

APPENDIX B – Posited Model Reaction List

Table B.1 Neutral-Neutral Reactions for Irradiated N_2 - O_2 Mixtures

	Reaction	Rate Constant ($\text{cm}^3 \text{ molec}^{-1} \text{ s}^{-1}$)	Reference
1*	$2 O \rightarrow O_2$	2.70×10^{-33}	67
2	$N + NO \rightarrow N_2 + O$	3.11×10^{-11}	64
3	$N + O_2 \rightarrow NO + O$	$4.4 \times 10^{-12} \exp\left(\frac{-26.77}{RT}\right)$	64
4	$N_2O + O \rightarrow 2 NO$	1.66×10^{-16}	68
5*	$NO + O + M \rightarrow NO_2 + M$	$9.19 \times 10^{-28} T^{-1.6}$	66
6	$NO_2 + O \rightarrow NO + O_2$	$5.5 \times 10^{-12} \exp\left(\frac{-1.56}{RT}\right)$	66
7	$NO_3 + O \rightarrow O_2 + NO_2$	1.7×10^{-11}	66
8*	$O + O_2 \rightarrow O_3 + M$	$1.54 \times 10^{-27} T^{-2.6}$	66
9	$NO + O_3 \rightarrow NO_2 + O_2$	$1.4 \times 10^{-12} \exp\left(\frac{-10.89}{RT}\right)$	66
10	$NO + NO_3 \rightarrow 2 NO_2$	$1.8 \times 10^{-11} \exp\left(\frac{0.91}{RT}\right)$	66
11	$N + NO_2 \rightarrow N_2O + O$	3.01×10^{-12}	64
12	$NO_2 + O_3 \rightarrow NO_3 + O_2$	$1.4 \times 10^{-13} \exp\left(\frac{-20.54}{RT}\right)$	66
13	$NO_2 + O \rightarrow NO_3$	$5.85 \times 10^{-12} T^{0.24}$	66
14	$2 NO_2 \rightarrow NO + NO_3$	$1.6 \times 10^{-14} T^{0.73} \exp\left(\frac{-87.3}{RT}\right)$	69
15	$N_2O_5 + M \rightarrow NO_2 + NO_3 + M$	$6.08 \times 10^5 T^{-3.5} \exp\left(\frac{-91.46}{RT}\right)$	66
16	$N_2O_3 + M \rightarrow NO + NO_2 + M$	$6.76 \times 10^{14} T^{-8.7} \exp\left(\frac{-40.57}{RT}\right)$	66
17	$2 O_3 + 2 N \rightarrow O_2 + 2 NO_2$	1.21×10^8	64
18	$O_3 + N \rightarrow O_2 + NO$	1.0×10^{-16}	64
19	$O_3 + O \rightarrow 2 O_2$	$8.0 \times 10^{-12} \exp\left(\frac{-17.13}{RT}\right)$	66
20	$O_3 + NO_3 \rightarrow 2 O_2 + NO_2$	1.0×10^{-17}	70
21	$O_3 + NO_2 \rightarrow 2 O_2 + NO$	1.0×10^{-18}	70
22	$O_3 \rightarrow O_2 + O$	$7.16 \times 10^{-10} \exp\left(\frac{-93.122}{RT}\right)$	71
23	$N_2O_4 \rightarrow ONONO_2$	2.86×10^3	72
24	$N_2O_4 + M \rightarrow 2 NO_2 + M$	$3.37 \times 10^4 T^{-3.8} \exp\left(\frac{-4.16}{RT}\right)$	66
25†	$NO_3 \rightarrow O_2 + NO$	$2.50 \times 10^6 \exp\left(\frac{-50.72}{RT}\right)$	73
26	$NO_2 + NO_3 \rightarrow O_2 + NO + NO_2$	$4.5 \times 10^{-14} \exp\left(\frac{-10.48}{RT}\right)$	74
27*	$NO + NO_2 + M \rightarrow N_2O_3 + M$	$3.67 \times 10^{-15} T^{-7.7}$	66
28*	$NO_2 + NO_3 + M \rightarrow N_2O_5 + M$	$5.16 \times 10^{-20} T^{-4.1}$	66
29	$2 NO_2 \rightarrow O_2 + 2 NO$	$2.71 \times 10^{-12} \exp\left(\frac{-109}{RT}\right)$	69
30*	$2 NO_2 + M \rightarrow N_2O_4 + M$	$3.62 \times 10^{-24} T^{-3.8}$	66
31	$NO_2 + N_3 \rightarrow N_2 + 2 NO$	6.0×10^{-13}	75
32	$NO_2 + N_3 \rightarrow 2 N_2O$	2.0×10^{-13}	75

Table B.1 (continued)

	Reaction	Rate Constant ($\text{cm}^3 \text{ molec}^{-1} \text{ s}^{-1}$)	Reference
33	$\text{NO}_2 + \text{N} \rightarrow \text{N}_2 + \text{O}_2$	1.85×10^{-12}	65
34	$\text{NO}_2 + \text{N} \rightarrow \text{N}_2 + 2 \text{O}$	2.41×10^{-12}	65
35	$\text{NO}_2 + \text{N} \rightarrow 2 \text{NO}$	6.11×10^{-12}	65
36*	$\text{O}_2 + 2 \text{NO} \rightarrow 2 \text{NO}_2$	$3.3 \times 10^{-39} \exp\left(\frac{4.41}{RT}\right)$	66
37	$\text{NO} + \text{O} \rightarrow \text{N} + \text{O}_2$	$3.0 \times 10^{-15} T \exp\left(\frac{-162}{RT}\right)$	69
38*	$\text{O} + \text{N} \rightarrow \text{NO}$	$6.89 \times 10^{-33} \exp\left(\frac{1.12}{RT}\right)$	62
39	$\text{O}_2 \rightarrow 2 \text{O}$	$3.01 \times 10^{-6} T^{-1} \exp\left(\frac{-494}{RT}\right)$	76
40*	$\text{N}_2 + \text{O} \rightarrow \text{N}_2\text{O}$	5.02×10^{-38}	77
41*	$\text{O} + \text{NO}_2 + \text{M} \rightarrow \text{NO}_3 + \text{M}$	$6.75 \times 10^{-28} T^{-1.5}$	66
42	$2 \text{NO}_3 \rightarrow \text{O}_2 + 2 \text{NO}_2$	$8.5 \times 10^{-13} \exp\left(\frac{-20.37}{RT}\right)$	74
43*	$2 \text{NO}_2 + \text{M} \rightarrow \text{N}_2\text{O}_4 + \text{M}$	$3.62 \times 10^{-24} T^{-3.8}$	66

* Rate constant has units $\text{cm}^6 \text{ molec}^{-2} \text{ s}^{-1}$

† Rate constant has units s^{-1}

Activation energies in kJ/mol

Table B.2 *Ion-Molecule Reactions for Irradiated N₂-O₂ Mixtures*

	Reaction	Rate Constant (cm ³ molec ⁻¹ s ⁻¹)	Reference
44	$N^+ + N_2 \rightarrow N + N_2^+$	2.55×10^{-10}	53
45	$N^+ + O_2 \rightarrow O^+ + NO$	4.64×10^{-11}	53
46	$N^+ + O_2 \rightarrow NO^+ + O$	2.32×10^{-10}	53
47	$N^+ + O_2 \rightarrow O_2^+ + N$	3.07×10^{-10}	53
48	$N^+ + NO \rightarrow NO^+ + N$	4.72×10^{-10}	53
49	$N^+ + NO \rightarrow N_2^+ + O$	8.33×10^{-11}	53
50	$N^+ + N_2O \rightarrow NO^+ + N_2$	5.5×10^{-10}	53
51	$N_2^+ + N \rightarrow N^+ + N_2$	1.0×10^{-11}	53
52	$N_2^+ + O \rightarrow O^+ + N_2$	9.8×10^{-12}	53
53	$N_2^+ + O \rightarrow NO^+ + N$	1.3×10^{-10}	53
54	$N_2^+ + O_2 \rightarrow O_2^+ + N_2$	5.0×10^{-11}	53
55	$N_2^+ + N_2O \rightarrow N_2O^+ + N_2$	6.0×10^{-10}	53
56	$O^+ + N_2 \rightarrow NO^+ + N$	1.2×10^{-12}	53
57	$O^+ + O_2 \rightarrow O_2^+ + O$	2.1×10^{-11}	53
58	$O^+ + NO \rightarrow NO^+ + O$	8.0×10^{-13}	53
59	$O^+ + NO_2 \rightarrow NO_2^+ + O$	1.6×10^{-9}	53
60	$O^+ + N_2O \rightarrow N_2O^+ + O$	6.3×10^{-10}	53
61	$O_2^+ + N \rightarrow NO^+ + O$	1.5×10^{-10}	53
62	$O_2^+ + N_2 \rightarrow NO^+ + NO$	1.0×10^{-15}	53
63	$O_2^+ + NO \rightarrow NO^+ + O_2$	4.6×10^{-10}	53
64	$O_2^+ + NO_2 \rightarrow NO_2^+ + O_2$	6.6×10^{-10}	53
65	$NO_2^+ + NO \rightarrow NO^+ + NO_2$	2.75×10^{-10}	53
66	$N_2O^+ + O_2 \rightarrow O_2^+ + N_2O$	2.24×10^{-10}	53
67	$N_2O^+ + O_2 \rightarrow NO^+ + NO_2$	4.59×10^{-11}	53
68	$N_2O^+ + NO \rightarrow NO^+ + N_2O$	2.3×10^{-10}	53
69	$N_2O^+ + NO_2 \rightarrow NO^+ + N_2 + O_2$	4.29×10^{-10}	53
70	$N_2O^+ + NO_2 \rightarrow NO_2^+ + N_2O$	2.21×10^{-34}	53
71	$N_2O^+ + N_2O \rightarrow NO^+ + N_2 + NO$	1.2×10^{-11}	53
72	$O^+ + e \rightarrow O$	3.0×10^{-12}	54
73	$O_2^+ + e \rightarrow 2 O$	2.2×10^{-7}	54
74	$O_2^+ + O_2^- \rightarrow 2 O + O_2$	2×10^{-6}	78
75	$N^+ + e \rightarrow N$	3.0×10^{-12}	54
76	$N_2^+ + e \rightarrow 2 N$	2.9×10^{-7}	53
77	$N_2^+ + O_2^- \rightarrow 2 N + O_2$	2.0×10^{-6}	78
78	$NO^+ + e \rightarrow N + O$	4.1×10^{-7}	53
79	$e + O_3 \rightarrow O^- + O_2$	9.0×10^{-12}	79

Table B.2 (continued)

	Reaction	Rate Constant ($\text{cm}^3 \text{ molec}^{-1} \text{ s}^{-1}$)	Reference
80	$O^- + O \rightarrow O_2 + e$	1.9×10^{-10}	56
81	$O^- + 2 O_3 \rightarrow O_3^- + 2 O_2$	8.0×10^{-10}	56
82	$O_2^- + O \rightarrow O^- + O_2$	1.5×10^{-10}	56
83	$O_2^- + O \rightarrow O_3 + e$	1.5×10^{-10}	56
84*	$O_2^- + 2 O_2 \rightarrow O_4^- + O_2$	3.0×10^{-31}	80
85	$O_2^- + O_3 \rightarrow O_3^- + O_2$	6.0×10^{-10}	56
86	$O_3^- + O \rightarrow O_2^- + O_2$	2.5×10^{-10}	56
87	$O_4^- + O \rightarrow O_3^- + O_2$	4.0×10^{-10}	81
88	$NO_2^- + NO_2 \rightarrow NO_3^- + NO$	2.0×10^{-13}	82
89	$O_2^+ + N_2O_5 \rightarrow NO_2^+ + NO_3 + O_2$	8.8×10^{-10}	83
90	$NO_2^- + N_2O_5 \rightarrow NO_3^- + 2 NO_2$	7.0×10^{-10}	83
91	$NO_3^- + O_3 \rightarrow NO_2^- + 2 O_2$	1.0×10^{-13}	84
92*	$e + O_2 + M \rightarrow O_2^- + M$	2.5×10^{-30}	53
92a*	$e + O_2 + N_2 \rightarrow O_2^- + N_2$	1.0×10^{-31}	85
92b*	$e + 2 O_2 \rightarrow O_2^- + O_2$	$4.2 \times 10^{-27} T^{-1} \exp\left(\frac{-600}{T}\right)$	86
93	$e + O_2 \rightarrow O^- + O$	4.8×10^{-14}	53
94	$e + O_3 \rightarrow O_3^-$	1.0×10^{-13}	53
95	$e + O_3 + O_2 \rightarrow O_3^- + O_2$	1.0×10^{-13}	53
96*	$O^- + O_2 + M \rightarrow O_3^- + M$	1.1×10^{-30}	53
97	$O_2^- + NO_2 \rightarrow NO_2^- + O_2$	7.0×10^{-10}	53
98	$O_2^- + N_2O \rightarrow NO_2^- + NO$	2.0×10^{-14}	53
99	$O_3^- + NO \rightarrow NO_2^- + O_2$	8.0×10^{-10}	53
100	$NO_2^- + O_2 \rightarrow NO_3^- + O$	1.0×10^{-11}	53
101	$O_3^- + NO_2 \rightarrow NO_2^- + O_3$	7.0×10^{-10}	53
102	$NO_2^- + O_3 \rightarrow NO_3^- + O_2$	1.2×10^{-10}	53
103*	$N_2^+ + 2 N_2 \rightarrow N_4^+ + N_2$	1.0×10^{-28}	87
104	$N_4^+ + O_2 \rightarrow 2 N_2 + O_2^+$	1.0×10^{-10}	88

* Rate constant has three-body units ($\text{cm}^6 \text{ molec}^{-2} \text{ s}^{-1}$).

APPENDIX C – Permissions



This is a License Agreement between Patrick Ables ("User") and Copyright Clearance Center, Inc. ("CCC") on behalf of the Rightsholder identified in the order details below. The license consists of the order details, the Marketplace Permissions General Terms and Conditions below, and any Rightsholder Terms and Conditions which are included below.

All payments must be made in full to CCC in accordance with the Marketplace Permissions General Terms and Conditions below.

Order Date	10-Apr-2023	Type of Use	Republish in a thesis/dissertation
Order License ID	1343545-1	Publisher	Canadian Science Publishing
ISSN	0008-4042	Portion	Chart/graph/table/figure

LICENSED CONTENT

Publication Title	Canadian journal of chemistry	Publication Type	Journal
Article Title	Radiolysis of air and nitrogen?oxygen mixtures with intense electron pulses: determination of a mechanism by comparison of measured and computed yields	Start Page	1515
		End Page	1525
		Issue	10
		Volume	48
Date	01/01/1951		
Country	Canada		
Rightsholder	Canadian Science Publishing		

REQUEST DETAILS

Portion Type	Chart/graph/table/figure	Distribution	Worldwide
Number of Charts / Graphs / Tables / Figures Requested	2	Translation	Original language of publication
Format (select all that apply)	Electronic	Copies for the Disabled?	No
Who Will Republish the Content?	Academic institution	Minor Editing Privileges?	No
Duration of Use	Life of current edition	Incidental Promotional Use?	No
Lifetime Unit Quantity	Up to 44,999	Currency	USD
Rights Requested	Main product		

NEW WORK DETAILS

Title	A COMPUTATIONAL KINETICS MODEL TO QUANTIFY RADIATION INDUCED CHEMICAL PRODUCTS OF ATMOSPHERIC GAS MIXTURES	Institution Name	University of Southern Mississippi
Instructor Name	Patrick Ables	Expected Presentation Date	2023-06-21

ADDITIONAL DETAILS

Order Reference Number	N/A	The Requesting Person/Organization to Appear on the License	Patrick Ables
-------------------------------	-----	--	---------------

REQUESTED CONTENT DETAILS

Title, Description or Numeric Reference of the Portion(s)	Figs 4,5	Title of the Article/Chapter the Portion Is From	Radiolysis of air and nitrogen?oxygen mixtures with intense electron pulses: determination of a mechanism by comparison of measured and computed yields
Editor of Portion(s)	Willis, C.; Boyd, A. W.; Young, M. J.	Author of Portion(s)	Willis, C.; Boyd, A. W.; Young, M. J.
Volume of Serial or Monograph	48	Issue, if Republishing an Article From a Serial	10
Page or Page Range of Portion	1515-1525	Publication Date of Portion	1970-05-14

Marketplace Permissions General Terms and Conditions

The following terms and conditions ("General Terms"), together with any applicable Publisher Terms and Conditions, govern User's use of Works pursuant to the Licenses granted by Copyright Clearance Center, Inc. ("CCC") on behalf of the applicable Rightsholders of such Works through CCC's applicable Marketplace transactional licensing services (each, a "Service").

1) **Definitions.** For purposes of these General Terms, the following definitions apply:

"License" is the licensed use the User obtains via the Marketplace platform in a particular licensing transaction, as set forth in the Order Confirmation.

"Order Confirmation" is the confirmation CCC provides to the User at the conclusion of each Marketplace transaction. "Order Confirmation Terms" are additional terms set forth on specific Order Confirmations not set forth in the General Terms that can include terms applicable to a particular CCC transactional licensing service and/or any Rightsholder-specific terms.

"Rightsholder(s)" are the holders of copyright rights in the Works for which a User obtains licenses via the Marketplace platform, which are displayed on specific Order Confirmations.

"Terms" means the terms and conditions set forth in these General Terms and any additional Order Confirmation Terms collectively.

This is a License Agreement between Patrick Ables ("User") and Copyright Clearance Center, Inc. ("CCC") on behalf of the Rightsholder identified in the order details below. The license consists of the order details, the Marketplace Permissions General Terms and Conditions below, and any Rightsholder Terms and Conditions which are included below.

All payments must be made in full to CCC in accordance with the Marketplace Permissions General Terms and Conditions below.

Order Date	10-Apr-2023	Type of Use	Republish in a thesis/dissertation
Order License ID	1343544-1	Publisher Portion	ELSEVIER BV Chart/graph/table/figure
ISSN	0168-9002		

LICENSED CONTENT

Publication Title	Nuclear instruments & methods in physics research. Section A, Accelerators, spectrometers, detectors and associated equipment	Publication Type	Journal
Article Title	Remote sensing of radiation	Start Page	832
Date	01/01/1983	End Page	836
Language	English, French, German	Issue	1-3
Country	Netherlands	Volume	422
Rightsholder	Elsevier Science & Technology Journals		

REQUEST DETAILS

Portion Type	Chart/graph/table/figure	Distribution	Worldwide
Number of Charts / Graphs / Tables / Figures Requested	1	Translation	Original language of publication
Format (select all that apply)	Electronic	Copies for the Disabled?	No
Who Will Republish the Content?	Academic institution	Minor Editing Privileges?	No
Duration of Use	Life of current edition	Incidental Promotional Use?	No
Lifetime Unit Quantity	Up to 44,999	Currency	USD
Rights Requested	Main product		

NEW WORK DETAILS

Title	A COMPUTATIONAL KINETICS MODEL TO QUANTIFY RADIATION INDUCED CHEMICAL PRODUCTS OF ATMOSPHERIC GAS MIXTURES	Institution Name	University of Southern Mississippi
Instructor Name	Patrick Ables	Expected Presentation Date	2023-06-21

ADDITIONAL DETAILS

Order Reference Number	N/A	The Requesting Person/Organization to Appear on the License	Patrick Ables
-------------------------------	-----	--	---------------

REQUESTED CONTENT DETAILS

Title, Description or Numeric Reference of the Portion(s)	Fig 1	Title of the Article/Chapter the Portion Is From	Remote sensing of radiation
Editor of Portion(s)	Moss, C.E.; Goeller, R.M.; Milligan, D.F.; Valencia, J.E.; Zinn, J.	Author of Portion(s)	Moss, C.E.; Goeller, R.M.; Milligan, D.F.; Valencia, J.E.; Zinn, J.
Volume of Serial or Monograph	422	Issue, if Republishing an Article From a Serial	1-3
Page or Page Range of Portion	832-836	Publication Date of Portion	1999-02-10

RIGHTSHOLDER TERMS AND CONDITIONS

Elsevier publishes Open Access articles in both its Open Access journals and via its Open Access articles option in subscription journals, for which an author selects a user license permitting certain types of reuse without permission. Before proceeding please check if the article is Open Access on <http://www.sciencedirect.com> and refer to the user license for the individual article. Any reuse not included in the user license terms will require permission. You must always fully and appropriately credit the author and source. If any part of the material to be used (for example, figures) has appeared in the Elsevier publication for which you are seeking permission, with credit or acknowledgement to another source it is the responsibility of the user to ensure their reuse complies with the terms and conditions determined by the rights holder. Please contact permissions@elsevier.com with any queries.

Marketplace Permissions General Terms and Conditions

The following terms and conditions ("General Terms"), together with any applicable Publisher Terms and Conditions, govern User's use of Works pursuant to the Licenses granted by Copyright Clearance Center, Inc. ("CCC") on behalf of the applicable Rightsholders of such Works through CCC's applicable Marketplace transactional licensing services (each, a "Service").

1) **Definitions.** For purposes of these General Terms, the following definitions apply:

"License" is the licensed use the User obtains via the Marketplace platform in a particular licensing transaction, as set forth in the Order Confirmation.

"Order Confirmation" is the confirmation CCC provides to the User at the conclusion of each Marketplace transaction. "Order Confirmation Terms" are additional terms set forth on specific Order Confirmations not set forth in the General Terms that can include terms applicable to a particular CCC transactional licensing service and/or any Rightsholder-

"User" or "you" is the person or entity making the use granted under the relevant License. Where the person accepting the Terms on behalf of a User is a freelancer or other third party who the User authorized to accept the General Terms on the User's behalf, such person shall be deemed jointly a User for purposes of such Terms.

"Work(s)" are the copyright protected works described in relevant Order Confirmations.

2) **Description of Service.** CCC's Marketplace enables Users to obtain Licenses to use one or more Works in accordance with all relevant Terms. CCC grants Licenses as an agent on behalf of the copyright rightsholder identified in the relevant Order Confirmation.

3) **Applicability of Terms.** The Terms govern User's use of Works in connection with the relevant License. In the event of any conflict between General Terms and Order Confirmation Terms, the latter shall govern. User acknowledges that Rightsholders have complete discretion whether to grant any permission, and whether to place any limitations on any grant, and that CCC has no right to supersede or to modify any such discretionary act by a Rightsholder.

4) **Representations; Acceptance.** By using the Service, User represents and warrants that User has been duly authorized by the User to accept, and hereby does accept, all Terms.

5) **Scope of License; Limitations and Obligations.** All Works and all rights therein, including copyright rights, remain the sole and exclusive property of the Rightsholder. The License provides only those rights expressly set forth in the terms and conveys no other rights in any Works

6) **General Payment Terms.** User may pay at time of checkout by credit card or choose to be invoiced. If the User chooses to be invoiced, the User shall: (i) remit payments in the manner identified on specific invoices, (ii) unless otherwise specifically stated in an Order Confirmation or separate written agreement, Users shall remit payments upon receipt of the relevant invoice from CCC, either by delivery or notification of availability of the invoice via the Marketplace platform, and (iii) if the User does not pay the invoice within 30 days of receipt, the User may incur a service charge of 1.5% per month or the maximum rate allowed by applicable law, whichever is less. While User may exercise the rights in the License immediately upon receiving the Order Confirmation, the License is automatically revoked and is null and void, as if it had never been issued, if CCC does not receive complete payment on a timely basis.

7) **General Limits on Use.** Unless otherwise provided in the Order Confirmation, any grant of rights to User (i) involves only the rights set forth in the Terms and does not include subsequent or additional uses, (ii) is non-exclusive and non-transferable, and (iii) is subject to any and all limitations and restrictions (such as, but not limited to, limitations on duration of use or circulation) included in the Terms. Upon completion of the licensed use as set forth in the Order Confirmation, User shall either secure a new permission for further use of the Work(s) or immediately cease any new use of the Work(s) and shall render inaccessible (such as by deleting or by removing or severing links or other locators) any further copies of the Work. User may only make alterations to the Work if and as expressly set forth in the Order Confirmation. No Work may be used in any way that is unlawful, including without limitation if such use would violate applicable sanctions laws or regulations, would be defamatory, violate the rights of third parties (including such third parties' rights of copyright, privacy, publicity, or other tangible or intangible property), or is otherwise illegal, sexually explicit, or obscene. In addition, User may not conjoin a Work with any other material that may result in damage to the reputation of the Rightsholder. Any unlawful use will render any licenses hereunder null and void. User agrees to inform CCC if it becomes aware of any infringement of any rights in a Work and to cooperate with any reasonable request of CCC or the Rightsholder in connection therewith.

8) **Third Party Materials.** In the event that the material for which a License is sought includes third party materials (such as photographs, illustrations, graphs, inserts and similar materials) that are identified in such material as having been used by permission (or a similar indicator), User is responsible for identifying, and seeking separate licenses (under this Service, if available, or otherwise) for any of such third party materials; without a separate license, User may not use such third party materials via the License.

9) **Copyright Notice.** Use of proper copyright notice for a Work is required as a condition of any License granted under the Service. Unless otherwise provided in the Order Confirmation, a proper copyright notice will read substantially as follows: "Used with permission of [Rightsholder's name], from [Work's title, author, volume, edition number and year of copyright]; permission conveyed through Copyright Clearance Center, Inc." Such notice must be provided in a reasonably legible font size and must be placed either on a cover page or in another location that any person, upon gaining access to the material which is the subject of a permission, shall see, or in the case of republication Licenses, immediately adjacent

to the Work as used (for example, as part of a by-line or footnote) or in the place where substantially all other credits or notices for the new work containing the republished Work are located. Failure to include the required notice results in loss to the Rightsholder and CCC, and the User shall be liable to pay liquidated damages for each such failure equal to twice the use fee specified in the Order Confirmation, in addition to the use fee itself and any other fees and charges specified.

10) **Indemnity.** User hereby indemnifies and agrees to defend the Rightsholder and CCC, and their respective employees and directors, against all claims, liability, damages, costs, and expenses, including legal fees and expenses, arising out of any use of a Work beyond the scope of the rights granted herein and in the Order Confirmation, or any use of a Work which has been altered in any unauthorized way by User, including claims of defamation or infringement of rights of copyright, publicity, privacy, or other tangible or intangible property.

11) **Limitation of Liability.** UNDER NO CIRCUMSTANCES WILL CCC OR THE RIGHTSHOLDER BE LIABLE FOR ANY DIRECT, INDIRECT, CONSEQUENTIAL, OR INCIDENTAL DAMAGES (INCLUDING WITHOUT LIMITATION DAMAGES FOR LOSS OF BUSINESS PROFITS OR INFORMATION, OR FOR BUSINESS INTERRUPTION) ARISING OUT OF THE USE OR INABILITY TO USE A WORK, EVEN IF ONE OR BOTH OF THEM HAS BEEN ADVISED OF THE POSSIBILITY OF SUCH DAMAGES. In any event, the total liability of the Rightsholder and CCC (including their respective employees and directors) shall not exceed the total amount actually paid by User for the relevant License. User assumes full liability for the actions and omissions of its principals, employees, agents, affiliates, successors, and assigns.

12) **Limited Warranties.** THE WORK(S) AND RIGHT(S) ARE PROVIDED "AS IS." CCC HAS THE RIGHT TO GRANT TO USER THE RIGHTS GRANTED IN THE ORDER CONFIRMATION DOCUMENT. CCC AND THE RIGHTSHOLDER DISCLAIM ALL OTHER WARRANTIES RELATING TO THE WORK(S) AND RIGHT(S), EITHER EXPRESS OR IMPLIED, INCLUDING WITHOUT LIMITATION IMPLIED WARRANTIES OF MERCHANTABILITY OR FITNESS FOR A PARTICULAR PURPOSE. ADDITIONAL RIGHTS MAY BE REQUIRED TO USE ILLUSTRATIONS, GRAPHS, PHOTOGRAPHS, ABSTRACTS, INSERTS, OR OTHER PORTIONS OF THE WORK (AS OPPOSED TO THE ENTIRE WORK) IN A MANNER CONTEMPLATED BY USER; USER UNDERSTANDS AND AGREES THAT NEITHER CCC NOR THE RIGHTSHOLDER MAY HAVE SUCH ADDITIONAL RIGHTS TO GRANT.

13) **Effect of Breach.** Any failure by User to pay any amount when due, or any use by User of a Work beyond the scope of the License set forth in the Order Confirmation and/or the Terms, shall be a material breach of such License. Any breach not cured within 10 days of written notice thereof shall result in immediate termination of such License without further notice. Any unauthorized (but licensable) use of a Work that is terminated immediately upon notice thereof may be liquidated by payment of the Rightsholder's ordinary license price therefor; any unauthorized (and unlicensable) use that is not terminated immediately for any reason (including, for example, because materials containing the Work cannot reasonably be recalled) will be subject to all remedies available at law or in equity, but in no event to a payment of less than three times the Rightsholder's ordinary license price for the most closely analogous licensable use plus Rightsholder's and/or CCC's costs and expenses incurred in collecting such payment.

14) **Additional Terms for Specific Products and Services.** If a User is making one of the uses described in this Section 14, the additional terms and conditions apply:

a) **Print Uses of Academic Course Content and Materials (photocopies for academic coursepacks or classroom handouts).** For photocopies for academic coursepacks or classroom handouts the following additional terms apply:

i) The copies and anthologies created under this License may be made and assembled by faculty members individually or at their request by on-campus bookstores or copy centers, or by off-campus copy shops and other similar entities.

ii) No License granted shall in any way: (i) include any right by User to create a substantively non-identical copy of the Work or to edit or in any other way modify the Work (except by means of deleting material immediately preceding or following the entire portion of the Work copied) (ii) permit "publishing ventures" where any particular anthology would be systematically marketed at multiple institutions.

iii) Subject to any Publisher Terms (and notwithstanding any apparent contradiction in the Order Confirmation arising from data provided by User), any use authorized under the academic pay-per-use service is limited as follows:

A) any License granted shall apply to only one class (bearing a unique identifier as assigned by the institution, and thereby including all sections or other subparts of the class) at one institution;

B) use is limited to not more than 25% of the text of a book or of the items in a published collection of essays, poems or articles;

C) use is limited to no more than the greater of (a) 25% of the text of an issue of a journal or other periodical or (b) two articles from such an issue;

D) no User may sell or distribute any particular anthology, whether photocopied or electronic, at more than one institution of learning;

E) in the case of a photocopy permission, no materials may be entered into electronic memory by User except in order to produce an identical copy of a Work before or during the academic term (or analogous period) as to which any particular permission is granted. In the event that User shall choose to retain materials that are the subject of a photocopy permission in electronic memory for purposes of producing identical copies more than one day after such retention (but still within the scope of any permission granted), User must notify CCC of such fact in the applicable permission request and such retention shall constitute one copy actually sold for purposes of calculating permission fees due; and

F) any permission granted shall expire at the end of the class. No permission granted shall in any way include any right by User to create a substantively non-identical copy of the Work or to edit or in any other way modify the Work (except by means of deleting material immediately preceding or following the entire portion of the Work copied).

iv) Books and Records; Right to Audit. As to each permission granted under the academic pay-per-use Service, User shall maintain for at least four full calendar years books and records sufficient for CCC to determine the numbers of copies made by User under such permission. CCC and any representatives it may designate shall have the right to audit such books and records at any time during User's ordinary business hours, upon two days' prior notice. If any such audit shall determine that User shall have underpaid for, or underreported, any photocopies sold or by three percent (3%) or more, then User shall bear all the costs of any such audit; otherwise, CCC shall bear the costs of any such audit. Any amount determined by such audit to have been underpaid by User shall immediately be paid to CCC by User, together with interest thereon at the rate of 10% per annum from the date such amount was originally due. The provisions of this paragraph shall survive the termination of this License for any reason.

b) *Digital Pay-Per-Uses of Academic Course Content and Materials (e-coursepacks, electronic reserves, learning management systems, academic institution intranets).* For uses in e-coursepacks, posts in electronic reserves, posts in learning management systems, or posts on academic institution intranets, the following additional terms apply:

i) The pay-per-uses subject to this Section 14(b) include:

A) **Posting e-reserves, course management systems, e-coursepacks for text-based content**, which grants authorizations to import requested material in electronic format, and allows electronic access to this material to members of a designated college or university class, under the direction of an instructor designated by the college or university, accessible only under appropriate electronic controls (e.g., password);

B) **Posting e-reserves, course management systems, e-coursepacks for material consisting of photographs or other still images not embedded in text**, which grants not only the authorizations described in Section 14(b)(i)(A) above, but also the following authorization: to include the requested material in course materials for use consistent with Section 14(b)(i)(A) above, including any necessary resizing, reformatting or modification of the resolution of such requested material (provided that such modification does not alter the underlying editorial content or meaning of the requested material, and provided that the resulting modified content is used solely within the scope of, and in a manner consistent with, the particular authorization described in the Order Confirmation and the Terms), but not including any other form of manipulation, alteration or editing of the requested material;

C) **Posting e-reserves, course management systems, e-coursepacks or other academic distribution for audiovisual content**, which grants not only the authorizations described in Section 14(b)(i)(A) above, but also the following authorizations: (i) to include the requested material in course materials for use consistent with Section 14(b)(i)(A) above; (ii) to display and perform the requested material to such members of such class in the physical classroom or remotely by means of streaming media or other video formats; and (iii) to "clip" or

reformat the requested material for purposes of time or content management or ease of delivery, provided that such "clipping" or reformatting does not alter the underlying editorial content or meaning of the requested material and that the resulting material is used solely within the scope of, and in a manner consistent with, the particular authorization described in the Order Confirmation and the Terms. Unless expressly set forth in the relevant Order Confirmation, the License does not authorize any other form of manipulation, alteration or editing of the requested material.

ii) Unless expressly set forth in the relevant Order Confirmation, no License granted shall in any way: (i) include any right by User to create a substantively non-identical copy of the Work or to edit or in any other way modify the Work (except by means of deleting material immediately preceding or following the entire portion of the Work copied or, in the case of Works subject to Sections 14(b)(1)(B) or (C) above, as described in such Sections) (ii) permit "publishing ventures" where any particular course materials would be systematically marketed at multiple institutions.

iii) Subject to any further limitations determined in the Rightsholder Terms (and notwithstanding any apparent contradiction in the Order Confirmation arising from data provided by User), any use authorized under the electronic course content pay-per-use service is limited as follows:

A) any License granted shall apply to only one class (bearing a unique identifier as assigned by the institution, and thereby including all sections or other subparts of the class) at one institution;

B) use is limited to not more than 25% of the text of a book or of the items in a published collection of essays, poems or articles;

C) use is limited to not more than the greater of (a) 25% of the text of an issue of a journal or other periodical or (b) two articles from such an issue;

D) no User may sell or distribute any particular materials, whether photocopied or electronic, at more than one institution of learning;

E) electronic access to material which is the subject of an electronic-use permission must be limited by means of electronic password, student identification or other control permitting access solely to students and instructors in the class;

F) User must ensure (through use of an electronic cover page or other appropriate means) that any person, upon gaining electronic access to the material, which is the subject of a permission, shall see:

- a proper copyright notice, identifying the Rightsholder in whose name CCC has granted permission,
- a statement to the effect that such copy was made pursuant to permission,
- a statement identifying the class to which the material applies and notifying the reader that the material has been made available electronically solely for use in the class, and
- a statement to the effect that the material may not be further distributed to any person outside the class, whether by copying or by transmission and whether electronically or in paper form, and User must also ensure that such cover page or other means will print out in the event that the person accessing the material chooses to print out the material or any part thereof.

G) any permission granted shall expire at the end of the class and, absent some other form of authorization, User is thereupon required to delete the applicable material from any electronic storage or to block electronic access to the applicable material.

iv) Uses of separate portions of a Work, even if they are to be included in the same course material or the same university or college class, require separate permissions under the electronic course content pay-per-use Service. Unless otherwise provided in the Order Confirmation, any grant of rights to User is limited to use completed no later than the end of the academic term (or analogous period) as to which any particular permission is granted.

v) Books and Records; Right to Audit. As to each permission granted under the electronic course content Service,

User shall maintain for at least four full calendar years books and records sufficient for CCC to determine the numbers of copies made by User under such permission. CCC and any representatives it may designate shall have the right to audit such books and records at any time during User's ordinary business hours, upon two days' prior notice. If any such audit shall determine that User shall have underpaid for, or underreported, any electronic copies used by three percent (3%) or more, then User shall bear all the costs of any such audit; otherwise, CCC shall bear the costs of any such audit. Any amount determined by such audit to have been underpaid by User shall immediately be paid to CCC by User, together with interest thereon at the rate of 10% per annum from the date such amount was originally due. The provisions of this paragraph shall survive the termination of this license for any reason.

c) *Pay-Per-Use Permissions for Certain Reproductions (Academic photocopies for library reserves and interlibrary loan reporting) (Non-academic internal/external business uses and commercial document delivery)*. The License expressly excludes the uses listed in Section (c)(i)-(v) below (which must be subject to separate license from the applicable Rightsholder) for: academic photocopies for library reserves and interlibrary loan reporting; and non-academic internal/external business uses and commercial document delivery.

- i) electronic storage of any reproduction (whether in plain-text, PDF, or any other format) other than on a transitory basis;
- ii) the input of Works or reproductions thereof into any computerized database;
- iii) reproduction of an entire Work (cover-to-cover copying) except where the Work is a single article;
- iv) reproduction for resale to anyone other than a specific customer of User;
- v) republication in any different form. Please obtain authorizations for these uses through other CCC services or directly from the rightsholder.

Any license granted is further limited as set forth in any restrictions included in the Order Confirmation and/or in these Terms.

d) *Electronic Reproductions in Online Environments (Non-Academic-email, intranet, internet and extranet)*. For "electronic reproductions", which generally includes e-mail use (including instant messaging or other electronic transmission to a defined group of recipients) or posting on an intranet, extranet or Intranet site (including any display or performance incidental thereto), the following additional terms apply:

- i) Unless otherwise set forth in the Order Confirmation, the License is limited to use completed within 30 days for any use on the Internet, 60 days for any use on an intranet or extranet and one year for any other use, all as measured from the "republication date" as identified in the Order Confirmation, if any, and otherwise from the date of the Order Confirmation.
- ii) User may not make or permit any alterations to the Work, unless expressly set forth in the Order Confirmation (after request by User and approval by Rightsholder); provided, however, that a Work consisting of photographs or other still images not embedded in text may, if necessary, be resized, reformatted or have its resolution modified without additional express permission, and a Work consisting of audiovisual content may, if necessary, be "clipped" or reformatted for purposes of time or content management or ease of delivery (provided that any such resizing, reformatting, resolution modification or "clipping" does not alter the underlying editorial content or meaning of the Work used, and that the resulting material is used solely within the scope of, and in a manner consistent with, the particular License described in the Order Confirmation and the Terms.

15) **Miscellaneous.**

a) User acknowledges that CCC may, from time to time, make changes or additions to the Service or to the Terms, and that Rightsholder may make changes or additions to the Rightsholder Terms. Such updated Terms will replace the prior terms and conditions in the order workflow and shall be effective as to any subsequent Licenses but shall not apply to Licenses already granted and paid for under a prior set of terms.

b) Use of User-related information collected through the Service is governed by CCC's privacy policy, available online at www.copyright.com/about/privacy-policy/.

c) The License is personal to User. Therefore, User may not assign or transfer to any other person (whether a natural person or an organization of any kind) the License or any rights granted thereunder; provided, however, that, where applicable, User may assign such License in its entirety on written notice to CCC in the event of a transfer of all or substantially all of User's rights in any new material which includes the Work(s) licensed under this Service.

d) No amendment or waiver of any Terms is binding unless set forth in writing and signed by the appropriate parties, including, where applicable, the Rightsholder. The Rightsholder and CCC hereby object to any terms contained in any writing prepared by or on behalf of the User or its principals, employees, agents or affiliates and purporting to govern or otherwise relate to the License described in the Order Confirmation, which terms are in any way inconsistent with any Terms set forth in the Order Confirmation, and/or in CCC's standard operating procedures, whether such writing is prepared prior to, simultaneously with or subsequent to the Order Confirmation, and whether such writing appears on a copy of the Order Confirmation or in a separate instrument.

e) The License described in the Order Confirmation shall be governed by and construed under the law of the State of New York, USA, without regard to the principles thereof of conflicts of law. Any case, controversy, suit, action, or proceeding arising out of, in connection with, or related to such License shall be brought, at CCC's sole discretion, in any federal or state court located in the County of New York, State of New York, USA, or in any federal or state court whose geographical jurisdiction covers the location of the Rightsholder set forth in the Order Confirmation. The parties expressly submit to the personal jurisdiction and venue of each such federal or state court.

Last updated October 2022

Wednesday, June 21, 2023 at 00:14:09 Central Daylight Time

Subject: Re: Permission to publish data
Date: Tuesday, June 20, 2023 at 10:57:51 AM Central Daylight Time
From: Sidney Gautrau
To: Patrick Ables

You have my permission.
Sidney

Get [Outlook for iOS](#)

From: Patrick Ables <Patrick.Ables@usm.edu>
Sent: Monday, June 19, 2023 11:49:04 PM
To: Sidney Gautrau <Sidney.Gautrau@usm.edu>
Subject: Permission to publish data

Sidney,
I would like your permission to publish figures showing the energy deposition data from your yet unpublished GEANT4 model of the Polonium-210 source used in your experiment. The data presented in these figures provide the height dependent dose rate values necessary to make comparisons between your measurements and the calculated solutions of the computational kinetics model.

Sincerely,
Patrick Ables

Page 1 of 1

APPENDIX D – Source Code

D.1 user_set_parameters.py

```
Create a subdirectory named Cantera_Simulation to place file into
#####
                        SET INPUT/OUTPUT FILE NAMES
#####
# Set name of CTI file
CTI = "CTIfile Willis.cti"
#CTI = "CTIfile Willis_update.cti"
#CTI = "WorkingThermo.v6.cti"

# Add tag to output file label autogenerated at end of this script
tag = ""

# Set the location of the CTI file.
ctiFile = "./ThermoFiles/" + CTI

# Set location of output files
concData = "./OutputFiles/ConcData/{0}/".format(CTI.replace('.cti',''))

#####
                        MAIN USER CHOSEN SIMULATION PARAMETERS TO SET
#####

## Omit reactions involving these specie (list of strings or None)
#omit = [ "O4", "N3", "N2O3+", "N2O3-", "O4-", "NO-", "NO3+", "N2O-",
#        "O3+", "N2-", "N3-", "O4+", "N3+", "N-" ]
omit = []

# Figure in Willis and Boyd to replicate 4,5 or None
figure = 4

# Cycle radiation shield
#cycleShield = True
cycleShield = False

# Print thermo report after each run
printreport = True

# abundance threshold for inclusion on thermo report
threshold = 1e-14 # molar fraction
```

```

# Hold reactor temperature constant with 'off'
energyEquation = 'on'

## Reactor setup
volume = 1e-9 # m3
vol_label = '1mm3'

## Set pressure
if figure == 5:
    pressure = 700.0/760.0 # WB pressure
    press_label = '700Torr'
elif figure == 4:
    pressure = 830.0/760.0 # WB pressure
    press_label = '830Torr'
else:
    pressure = 1 # WB pressure
    press_label = '760Torr'

## Set temperature
temp = 298 # Kelvin
temp_label = '298K'

# Simulation Times (seconds)
timeBegin = 0.0

if figure in [4,5]:
    timeEnd = 3e-3
    time_label = '3ms'
elif cycleShield:
    timeEnd = 3600.0*5/3 # 100 mins
    time_label = '100min'
else:
    timeEnd = 3600.0 *24 # 24 hours
    time_label = '24hr'

# Pulse radiation option
pulse = False # use gaussian pulse, see source specifics below
if figure in [4,5]: pulse = True

# Time interval (seconds) source is exposed if cycled.
# Start each cycle with source open or closed
if cycleShield:
    interval = 10*60
    init_cover_pos = 'closed'
else:

```

```

interval = timeEnd
init_cover_pos = 'open'

# Break up time interval into steps or explicitly define dt. Select 'steps' OR 'dt'.
if pulse:
    option = 'dt'
else:
    option = 'steps'

# Define number of steps OR explicitly define the recording time interval.
steps = int(timeEnd/30) # Record every 30 seconds
dt = 2.e-9 # Willis and Boyd

# Scale down error tolerances if solution diverges
# defaults: absolute = 1e-15, relative = 1e-9
err_tol_scaler = 1e0

# Initial contents of the reactors
# Certified gas mix has 5ppm H2O
air = { 'O2' : 0.2,
        'N2' : 0.8
        }

# Species concentrations to monitor and save.
if figure == 4:
    ## WB plot figure 4
    spe = ('N2+', 'O2+', 'O2-', 'e-', 'NO', 'NO2', 'N', 'O3', 'O')
elif figure == 5:
    ## WB plot figure 5
    spe = ('NO2', 'O3')
else:
    spe = ('N2+', 'O2+', 'O2-', 'e-', 'NO', 'NO2', 'N', 'O3', 'O', 'N2O')

#####
                        Radiation Specifics
#####

if figure == 4:
    #total_dose is 1.06e19 # eV/g
    energyRange = [6.2e26] # in pulse peak units eV/L/s from figure 4
elif figure == 5:
    # Figure 5 range eV/g/s

```

```

    energyRange = range(24,31)
else:
    # 10^x range for continuous (hardcoded to give 4 quarters per magnitude)
    energyRange = range(10,19)

pulse_length = 6.e-8 # Febetron 60ns pulse width

#####
                        G-Value Specifics
#####

# Creation rate per 100eV for each reactant for simulating effect of radiation
# should be gValues for pure gases.
gValues = {
    'N2+': 2.9, #WB1970
    'N+': 0.14, # WB1970 from Dondes
    'N': 6.0, #WB1970
    'O2+': 3.3, #WB1970
    'O': 6.1, #WB1970
    'O+': 0.1,#WB1970 #0.59, #WB1976
}

#####
                        autocreate label for trial output file
#####
label = '_' + join([time_label, vol_label, press_label, temp_label])
if energyEquation == 'off': label += '_eOFF'
if cycleShield: label += '_cycle'
if tag: label += '_' + tag
if figure == 5: label = 'Figure5_' + label
elif figure == 4: label = 'Figure4_' + label
if pulse: concData = concData + 'Pulse/' + label + '/'
else: concData = concData + 'Continuous/' + label + '/'

```

D.2 functionContainer.py

Place into Cantera_Simulation subdirectory

```
from Cantera_Simulation import user_set_parameters as p
import cantera as ct
import numpy as np
import sys, timeit

# Used for the square wave function which introduces free radicals
# into the reactor that are created in the presence of radiation
if p.init_cover_pos=='closed':
    opened = False
else: opened = True

def squareWave( time ):
    ## check even or odd, returns 1 or 0
    b = (time//p.interval) % 2 # time in seconds
    if opened: return int(not b)
    else: return b

def normalize( data ):

    normDict = { }

    if type(data) is str:

        total = 0.0
        tempList = data.split(',')
        l = len(tempList)

        for i in range( l ):
            tempList[i] = tempList[i].split(':')
            total += float( tempList[i][1].strip() )

        for i in range( l ):
            normDict[ tempList[i][0].strip() ] = tempList[i][1] / total

    elif type(data) is dict:

        total = sum(list(data.values()), 0.0 )
        normDict = { k : v / total for k, v in data.items() }

    return normDict
```

```

def getReactants( initialMix ):

    # The names of the compounds listed below should match those used in Cantera
    # (100 eV)^-1
    gVals = p.gValues
    reactants = {}

    if 'N2' in initialMix:
        reactants['N2+'] = gVals['N2+'] * initialMix['N2']
        reactants['N+'] = gVals['N+'] * initialMix['N2']
        reactants['N'] = gVals['N'] * initialMix['N2']

    if 'O2' in initialMix:
        reactants['O2+'] = gVals['O2+'] * initialMix['O2']
        reactants['O'] = gVals['O'] * initialMix['O2']
        reactants['O+'] = gVals['O+'] * initialMix['O2']

    reactants['e-'] = ( ((gVals['O2+'] + gVals['O+'])*initialMix['O2'] if 'O2' in initialMix
else 0.0)
        + ((gVals['N2+'] + gVals['N+'])*initialMix['N2'] if 'N2' in initialMix else
0.0) )

    # gValue is molecules per 100eV units, reduce to per eV units
    reactants = {key: reactants[key] / 1e2
        for key in reactants.keys()}

    return reactants # scaled gValues in molecules/eV

def buildNetwork( air, ctiFile, eRange=None ):
#####
                SETUP REACTOR NETWORK
#####
    ## Read ctiFile
    with open(p.ctiFile) as f: cti_def = f.read()

    # Build Solution object from components
    airGas = ct.Solution( source=cti_def, kinetics='GasKinetics', transport_model=None )
    airGas.TPX = p.temp, ct.one_atm*p.pressure, p.air
    airGas.equilibrate('UV')

```

```

# Get reactants from air mix
reactants = getReactants( air )

## Get array of species names
species_names = airGas.species_names

## molar_mass units kg/kmol, g/mol
molar_mass = {k:v for k,v in zip(species_names,airGas.molecular_weights)}

# Setup reactant and electron gas mixes
reactantGas = ct.Solution(source=cti_def, kinetics='GasKinetics',
transport_model=None)
reactantGas.TPX = p.temp, ct.one_atm*p.pressure, normalize(reactants)

# Create reservoirs for the reactants, air, and mass removed
res_Air = ct.Reservoir(airGas)
res_React = ct.Reservoir(reactantGas)
res_Out = ct.Reservoir(airGas)

# Build reactor object/dictionary, elements of each key match at index
r = {
    'reactors' : [],
    'energyDep' : [],
    'mfc' : [],
    'mfcOut' : []
}

tempDict = {}
reactant_mass = {}
NA = 6.022e23

## Get mass of each species to inject (kg/eV)
for k, v in reactants.items():
    # molar mass in g/mol
    reactant_mass[k] = np.float64(v/NA * molar_mass[k]) / 1e3

# total of all masses in kg / eV
reactant_mass = sum( list(reactant_mass.values()), 0.0 )

sys.stdout.write('Loading voxel data...\n')
sys.stdout.flush()
start_time = timeit.default_timer()

## Get density of air mixture (kg/m3)

```

```

airdensity = airGas.density_mass

## Get mass of air mixture (kg)
airmass = airdensity * p.volume

if p.pulse and len(p.energyRange)==1:
    eV_arr = [eRange]
else:
    # Build dose rate array by magnitude
    eV_arr = []
    farr = [10.0** eRange]
    for x in farr:
        for y in [0.25,0.5,0.75,1]:
            eV_arr.append(x*y)

## Iterate depositional absorption rates (eV/g/s)
for i,dep_rate in enumerate(eV_arr):

    ## Create reactor
    reactor = ct.IdealGasConstPressureReactor( contents = airGas, volume = p.volume,
energy=p.energyEquation )
    # r = ct.ConstPressureReactor( contents = airGas, volume = p.volume,
energy=p.energyEquation )
    # r = ct.Reactor( contents = airGas, volume = p.volume, energy=p.energyEquation
    )
    # r = ct.IdealGasReactor( contents = airGas, volume = p.volume,
energy=p.energyEquation )

    r['reactors'].append( reactor )

if p.pulse:
    ## MFR is determined by gaussian function
    ## with maximum amplitude A
    if p.figure == 4:
        ## Convert (eV/L/s) to (eV/g/s)
        A = dep_rate / airdensity
    elif p.figure == 5:
        A = dep_rate
    else:
        A = 0
        print('Error: Pulse but no figure specified')

exp_sum = 2.18511e-8
dep_rate= A

```

```

## Get total eV
total_eV = exp_sum * A * (airmass * 1e3)
print('Dose (eV/g): {:.3E}'.format(A*exp_sum))
print('A (eV/g/s): {:.3E}'.format(A))

## Calculate total energy deposition rate (eV/s)
energyi = dep_rate * (airmass * 1e3)

## Energy Absorption rate (eV/g/s)
r['energyDep'].append( dep_rate )

## Reactant mass flow rate in kg/s
## eV * kg/eV
mfr = energyi * reactant_mass

# Attach MFC from Reactant reservoir to reactor
r['mfc'].append( ct.MassFlowController(
    res_React, r['reactors'][-1]
))

## Set mass flow rate coeff and time function separately
r['mfc'][-1].mass_flow_coeff = mfr # kg/s

if p.pulse:
    a = 1
    b = p.pulse_length/2.0 # center point 30ns
    ## WolframAlpha was used to find the best c value which made
    ## the definite integral of the gaussian function approximately
    ## the same as the Total/Amplitude ratio calculated from WBs
    ## description of the pulse.
    c = 8.7224e-9 # fwhm
    r['mfc'][-1].set_time_function(
        lambda t: np.exp(-((t - b)**2)/(2.0*c**2))
    )
else:
    ## Continuous radiation
    r['mfc'][-1].set_time_function( squareWave )

# Attach MFC from reactor to junk out reservoir
r['mfcOut'].append( ct.PressureController(
    r['reactors'][-1], res_Out, master = r['mfc'][-1], K = 0.0
))

## Get total moles

```

```

totMoles = airGas.density_mole * p.volume * 1e3
print("Total Moles of Gas: {}".format(totMoles))
if p.pulse: print("Total Pulse Energy Deposited: {:.5E}".format(total_eV))
print('Max Energy Absorption Rate (eV/g/s): {:.3E}'.format(dep_rate))
print("Max Total Energy Depo Rate (eV/s): {:.3E}".format(energyi))
print("Airmass start(kg): {}".format(airmass))
print('Max Reactant mass flow rate (kg/s): {:.3E}\n'.format(mfr))

## Create list of dictionaries to keep up with time evolution
## of concentrations for all reactors created
tempDict = [{key:np.empty((p.steps+1,1),dtype=np.float64) for key in p.spe} for x in
range(i+1)]

return (r, tempDict)

```

D.3 simRad.py

```
import sys
import cantera as ct
import numpy as np
import pandas as pd
import time as timer
import os
# contains user set parameters for simulation
from Cantera_Simulation import user_set_parameters as p
# contains functions for calculating gVals, reactants, building reactors
from Cantera_Simulation import functionContainer as container

## Each reactor is stepped through time independently. A group of reactors
## nested in a reactor object is built and returned by buildNetwork. The
## entire script reinitializes each loop if a list of dose rates is specified.

#####
LOCALS FOR SIMULATION SETUP
#####

# For calculating script run time after loop
start_time = timer.time()

if p.pulse:
    num_reactors = 1
    pulse_dum = True
else:
    num_reactors = len( p.energyRange )*4 # hardcoded in buildNetwork
    pulse_dum = False

# Iterate over all energies and collect results
for ii, ener in enumerate(p.energyRange):
    # Total duration to simulate
    totTime = (p.timeEnd - p.timeBegin)

    # Calculates unknown parameters from those given
    if p.option=='steps':
        p.dt = totTime/p.steps
    else:
        p.steps = int( round( (totTime)/p.dt ) )

# Calculate total number of open/close or close/open intervals during the simulation
numint = int( round( totTime/p.interval ) )
nrange = int( round( p.steps/numint ) )
```

```

steps = p.steps + 1 # To include time = 0.0

# Numpy array to store time, temperature, and species concentration
data = np.zeros( ( steps, len(p.spe) + 2 ), dtype = np.float64 )

#####
BUILD REACTOR NETWORK
#####

# buildNetwork returns reactArr object and tempDict
#   reactArr = array of all reactor objects to include in sim
#   tempDict = normalized molar fraction after summing all reactors
(reactArr, tempDict) = container.buildNetwork( p.air, p.ctiFile, eRange=ener )

# Insert reactors into network to run one at a time
for k,jj in enumerate(reactArr['reactors']):
    sim = ct.ReactorNet( [jj] )
    rtol = sim.rtol
    atol = sim.atol
    sim.rtol = rtol*p.err_tol_scaler # change untested
    sim.atol = atol*p.err_tol_scaler # change untested

# Time variable to update during sim
time = p.timeBegin

# Set initial time for Cantera's DE solver
sim.set_initial_time(time)

# Print initial state of the system
print( "\nStarting SIM with for E={:.3E}...\n".format(reactArr['energyDep'][k]))

##### SIMULATION LOOP #####

# Start sim loop
for n in range(steps):

    ## If pulse, turn off reactant flow
    if pulse_dum and time >= p.pulse_length:
        pulse_dum = False
        reactArr['mfc'][k].mass_flow_coeff = 0.0
        reactArr['mfc'][k].set_time_function(0)

```

```

try:
    ## Advance the state of the reactor network in time from
    ## the previous time towards new time (sec). Integrator
    ## takes as many internal timesteps as necessary to reach t.
    sim.advance(time)#, apply_limit=False)

except Exception as err:
    print(err,'\n\n\n')
    print("Reactor Network State at Error")
    print(sim.get_state())
    exit()

data[n,0] = time #time in seconds
data[n,1] = reactArr['reactors'][k].T

## Store current concentrations
for key, value in reactArr['reactors'][k].thermo.mole_fraction_dict().items():
    if key in p.spe:
        tempDict[k][key][n] = np.float64(value)

time += p.dt
if n%1000 == 0:
    sys.stdout.write('.')
    sys.stdout.flush()

##### SAVE SIMULATION #####

## Make sure save path exists
try: os.makedirs(p.concData)
except FileExistsError: pass

## Write each reactor to file with eV as name
d = tempDict[k]

## Copy dictionary entries to data array # artifact from early implementation
for j,key in enumerate(p.spe):
    if key in d:
        data[:,j+2] = d.get(key).squeeze() # Squeeze numpy array to 1D

## Write time evolution of specie concentrations to file
## Set filename to energy absorption rate (eV/g/s)
energy = reactArr['energyDep'][k]
estr = '%1.5e' % energy
f = p.concData + estr + '.csv'

```

```

df =
pd.DataFrame(data=data[:,1:],index=data[:,0],columns=["T(K)"].extend(p.spe),dtype=np.f
loat64)
df.to_csv(f,float_format='%.5e')

## Print report for each dose rate
if p.printreport:
    print( jj.thermo.report(threshold=p.threshold) )

##### PRINT STATEMENTS #####
seconds = int( timer.time() - start_time )
minutes, seconds = divmod(seconds, 60)
hours, minutes = divmod(minutes, 60)

periods = [('hours', hours), ('minutes', minutes), ('seconds', seconds)]
time_string = ', '.join('%s %s' % (value, name)
                        for name, value in periods
                        if value)

print ( "\n\n%s reactors simulated %s minute time evolution" % (num_reactors, round(
(p.timeEnd - p.timeBegin) / 60, 2) ) )
print ( "--- EXECUTION TIME: %s ---\n\n" % time_string )

```

D.4 Data for Building CTI Files

D.4.1 Species Data

```
#units(length = "cm", time = "s", quantity = "mol", act_energy = "cal/mol")
##default_units(length = "m", mass = "kg", quantity = "kmol", time = "s", energy = "J",
act_energy = "K", pressure = "Pa")
```

```
ideal_gas(name = "air",
elements = " O N E ",
species = "" e- N N+ NO NO+ NO2 NO3 NO3- N2 N2+ N4+ N2O N2O+
N2O3 N2O4 N2O5 N3 O O+ O2 O2+ O3 N- NO2- N2- O- O2- ONONO2 O4
O4- O4+ O3+ O3- N3+ N3- NO- NO2+ N2O- NO3+ N2O3+ N2O3- """,
reactions = "all",
initial_state = state(temperature = 298.0,
pressure = OneAtm,
mole_fractions = 'O2:0.22, N2:0.78') )
```

```
#-----
# Species data
#-----
```

```
species(name='e-',
atoms='E:1',
thermo=(NASA9([298.15, 1000.00],
[ 0.000000000E+00, 0.000000000E+00, 2.500000000E+00,
0.000000000E+00, 0.000000000E+00, 0.000000000E+00,
0.000000000E+00, -7.453750000E+02, -1.172081224E+01]),
NASA9([1000.00, 6000.00],
[ 0.000000000E+00, 0.000000000E+00, 2.500000000E+00,
0.000000000E+00, 0.000000000E+00, 0.000000000E+00,
0.000000000E+00, -7.453750000E+02, -1.172081224E+01]),
NASA9([6000.00, 20000.00],
[ 0.000000000E+00, 0.000000000E+00, 2.500000000E+00,
0.000000000E+00, 0.000000000E+00, 0.000000000E+00,
0.000000000E+00, -7.453750000E+02, -1.172081224E+01])),
note='Ref-Species. Chase,1998 3/82. [g12/98]')
```

```
species(name='N',
atoms='N:1',
thermo=(NASA9([200.00, 1000.00],
```

```

[ 0.000000000E+00, 0.000000000E+00, 2.500000000E+00,
  0.000000000E+00, 0.000000000E+00, 0.000000000E+00,
  0.000000000E+00, 5.610463780E+04, 4.193905036E+00]),
NASA9([1000.00, 6000.00],
[ 8.876501380E+04, -1.071231500E+02, 2.362188287E+00,
  2.916720081E-04, -1.729515100E-07, 4.012657880E-11,
  -2.677227571E-15, 5.697351330E+04, 4.865231506E+00]),
NASA9([6000.00, 20000.00],
[ 5.475181050E+08, -3.107574980E+05, 6.916782740E+01,
  -6.847988130E-03, 3.827572400E-07, -1.098367709E-11,
  1.277986024E-16, 2.550585618E+06, -5.848769753E+02])),
note='Hf:Cox,1989. Moore,1975. Gordon,1999. [g 5/97]')

```

```

species(name= 'N+',
atoms='E:-1 N:1',
thermo=(NASA9([298.15, 1000.00],
[ 5.237079210E+03, 2.299958315E+00, 2.487488821E+00,
  2.737490756E-05, -3.134447576E-08, 1.850111332E-11,
  -4.447350984E-15, 2.256284738E+05, 5.076830786E+00]),
NASA9([1000.00, 6000.00],
[ 2.904970374E+05, -8.557908610E+02, 3.477389290E+00,
  -5.288267190E-04, 1.352350307E-07, -1.389834122E-11,
  5.046166279E-16, 2.310809984E+05, -1.994146545E+00]),
NASA9([6000.00, 20000.00],
[ 1.646092148E+07, -1.113165218E+04, 4.976986640E+00,
  -2.005393583E-04, 1.022481356E-08, -2.691430863E-13,
  3.539931593E-18, 3.136284696E+05, -1.706646380E+01])),
note='Moore,1975. Gordon,1999. [g 6/97]')

```

```

species(name= 'NO',
atoms='O:1 N:1',
thermo=(NASA9([200.00, 1000.00],
[-1.143916503E+04, 1.536467592E+02, 3.431468730E+00,
  -2.668592368E-03, 8.481399120E-06, -7.685111050E-09,
  2.386797655E-12, 9.098214410E+03, 6.728725490E+00]),
NASA9([1000.00, 6000.00],
[ 2.239018716E+05, -1.289651623E+03, 5.433936030E+00,
  -3.656034900E-04, 9.880966450E-08, -1.416076856E-11,
  9.380184620E-16, 1.750317656E+04, -8.501669090E+00]),
NASA9([6000.00, 20000.00],
[-9.575303540E+08, 5.912434480E+05, -1.384566826E+02,
  1.694339403E-02, -1.007351096E-06, 2.912584076E-11,
  -3.295109350E-16, -4.677501240E+06, 1.242081216E+03])),
note='Gurvich,1978,1989 pt1 p326 pt2 p203. [tpis89]')

```

```

species(name= 'NO+',
  atoms='E:-1 O:1 N:1',
  thermo=(NASA9([298.15, 1000.00],
    [ 1.398106635E+03, -1.590446941E+02, 5.122895400E+00,
      -6.394388620E-03, 1.123918342E-05, -7.988581260E-09,
      2.107383677E-12, 1.187495132E+05, -4.398433810E+00]),
    NASA9([1000.00, 6000.00],
      [ 6.069876900E+05, -2.278395427E+03, 6.080324670E+00,
        -6.066847580E-04, 1.432002611E-07, -1.747990522E-11,
        8.935014060E-16, 1.322709615E+05, -1.519880037E+01]),
      NASA9([6000.00, 20000.00],
        [ 2.676400347E+09, -1.832948690E+06, 5.099249390E+02,
          -7.113819280E-02, 5.317659880E-06, -1.963208212E-10,
          2.805268230E-15, 1.443308939E+07, -4.324044462E+03])),
  note='Cp,S,IP(NO): Gurvich,1989 pt1 p330 pt2 p205. [g 5/99]')

```

```

species(name= 'NO2',
  atoms='O:2 N:1',
  thermo=(NASA9([200.00, 1000.00],
    [-5.642038780E+04, 9.633085720E+02, -2.434510974E+00,
      1.927760886E-02, -1.874559328E-05, 9.145497730E-09,
      -1.777647635E-12, -1.547925037E+03, 4.067851210E+01]),
    NASA9([1000.00, 6000.00],
      [ 7.213001570E+05, -3.832615200E+03, 1.113963285E+01,
        -2.238062246E-03, 6.547723430E-07, -7.611335900E-11,
        3.328361050E-15, 2.502497403E+04, -4.305130040E+01])),
  note='Gurvich,1989 pt1 p332 pt2 p207. [g 4/99]')

```

```

species(name= 'NO3',
  atoms='O:3 N:1',
  thermo=(NASA9([200.00, 1000.00],
    [ 3.405398410E+04, 2.266670652E+02, -3.793081630E+00,
      4.170732700E-02, -5.709913270E-05, 3.834158110E-08,
      -1.021969284E-11, 7.088112200E+03, 4.273091713E+01]),
    NASA9([1000.00, 6000.00],
      [-3.943872710E+05, -8.244263530E+02, 1.061325843E+01,
        -2.448749816E-04, 5.406060320E-08, -6.195466750E-12,
        2.870000149E-16, 8.982011730E+03, -3.444666597E+01])),
  note='Chase,1998 p1607. [j12/64]')

```

```

species(name= 'NO3-',
  atoms='E:1 O:3 N:1',
  thermo=(NASA9([298.15, 1000.00],
    [ 9.204813610E+04, -3.911171150E+02, -2.354356764E-01,

```

```
2.836042108E-02, -3.461324080E-05, 2.081787460E-08,  
-5.021601270E-12, -3.576411500E+04, 2.299942308E+01]),  
NASA9([1000.00, 6000.00],  
[-3.110005758E+05, -1.369087552E+03, 1.101342913E+01,  
-4.036878820E-04, 8.902086470E-08, -1.019733480E-11,  
4.723330790E-16, -3.364321090E+04, -3.878432657E+01])),  
note='Gurvich,1989 pt1 p335 pt2 p209. [tpis89]')
```

```
species(name= 'N2',  
atoms='N:2',  
thermo=(NASA9([200.00, 1000.00],  
[ 2.210371497E+04, -3.818461820E+02, 6.082738360E+00,  
-8.530914410E-03, 1.384646189E-05, -9.625793620E-09,  
2.519705809E-12, 7.108460860E+02, -1.076003744E+01])),  
NASA9([1000.00, 6000.00],  
[ 5.877124060E+05, -2.239249073E+03, 6.066949220E+00,  
-6.139685500E-04, 1.491806679E-07, -1.923105485E-11,  
1.061954386E-15, 1.283210415E+04, -1.586640027E+01])),  
NASA9([6000.00, 20000.00],  
[ 8.310139160E+08, -6.420733540E+05, 2.020264635E+02,  
-3.065092046E-02, 2.486903333E-06, -9.705954110E-11,  
1.437538881E-15, 4.938707040E+06, -1.672099740E+03])),  
note='Ref-Elm. Gurvich,1978 pt1 p280 pt2 p207. [tpis78]')
```

```
species(name= 'N2+',  
atoms='E:-1 N:2',  
thermo=(NASA9([298.15, 1000.00],  
[-3.474047470E+04, 2.696222703E+02, 3.164916370E+00,  
-2.132239781E-03, 6.730476400E-06, -5.637304970E-09,  
1.621756000E-12, 1.790004424E+05, 6.832974166E+00])),  
NASA9([1000.00, 6000.00],  
[-2.845599002E+06, 7.058893030E+03, -2.884886385E+00,  
3.068677059E-03, -4.361652310E-07, 2.102514545E-11,  
5.411996470E-16, 1.340388483E+05, 5.090897022E+01])),  
NASA9([6000.00, 20000.00],  
[-3.712829770E+08, 3.139287234E+05, -9.603518050E+01,  
1.571193286E-02, -1.175065525E-06, 4.144441230E-11,  
-5.621893090E-16, -2.217361867E+06, 8.436270947E+02])),  
note='Gurvich,1989 pt1 p323 pt2 p200. [tpis89]')
```

```
species(name= 'N4+',  
atoms='E:-1 N:4',  
thermo=(NASA9([298.15, 1000.00],  
[ 1.15107802E+00, 2.15570328E-02, -2.10270939E-05,  
8.21140809E-09, -6.49760980E-13, 1.72530097E+05,
```

```

1.81430748E+01]),
NASA([1000.00, 6000.00],
 [ 7.57784346E+00, 2.48052052E-03, -9.71133430E-07,
 1.65738251E-10, -1.03047740E-14, 1.70839793E+05,
 -1.46808901E+01])),
note=u'cationT1/11')

species(name= 'N2O',
atoms='O:1 N:2',
thermo=(NASA9([200.00, 1000.00],
 [ 4.145714880E+04, -6.350150620E+02, 6.028744010E+00,
 6.335115050E-04, 2.503851759E-06, -2.869887956E-09,
 9.201596710E-13, 1.178288623E+04, -1.002149969E+01])),
NASA9([1000.00, 6000.00],
 [ 3.011065230E+05, -2.236748283E+03, 9.021466570E+00,
 -5.707303550E-04, 1.204841455E-07, -1.336140302E-11,
 6.038524250E-16, 2.098055049E+04, -3.049276420E+01])),
note='Nitrous Oxide JANAF Eec. 1964 [J12/64]')

species(name= 'N2O+',
atoms='E:-1 O:1 N:2',
thermo=(NASA9([298.15, 1000.00],
 [-5.624147080E+04, 6.696211610E+02, 8.781456190E-02,
 1.524476027E-02, -1.527290811E-05, 7.827237390E-09,
 -1.646739623E-12, 1.557295192E+05, 2.562354785E+01])),
NASA9([1000.00, 6000.00],
 [-2.983553254E+04, -1.179455967E+03, 8.300186690E+00,
 -2.887267217E-04, 5.705105010E-08, -5.958885120E-12,
 2.835725557E-16, 1.646021769E+05, -2.287356617E+01])),
note='Chase,1998 p1625. [j12/70]')

species(name= 'N2O3',
atoms='O:3 N:2',
thermo=(NASA9([200.00, 1000.00],
 [-9.204444170E+04, 9.295520150E+02, 3.203664810E+00,
 1.356473078E-02, -6.262966070E-06, -1.402915559E-09,
 1.431620930E-12, 3.313622080E+03, 1.844430953E+01])),
NASA9([1000.00, 6000.00],
 [ 7.783881860E+05, -4.483024660E+03, 1.666668024E+01,
 -2.062143878E-03, 5.309541710E-07, -6.190451220E-11,
 2.692956658E-15, 3.360912450E+04, -6.739212388E+01])),
note='Gurvich,1989 pt1 p338 pt2 p211. [g 4/99]')

species(name= 'N2O4',
atoms='O:4 N:2',

```

```

thermo=(NASA9([200.00, 1000.00],
  [-3.804751440E+04, 5.612828890E+02, -2.083648324E-01,
    3.887087820E-02, -4.422412260E-05, 2.498812310E-08,
    -5.679102380E-12, -3.310794730E+03, 2.963924840E+01]),
  NASA9([1000.00, 6000.00],
    [-4.582843760E+05, -1.604749805E+03, 1.674102133E+01,
      -5.091385080E-04, 1.143634670E-07, -1.316288176E-11,
      5.976316620E-16, 4.306900520E+03, -6.569450380E+01])),
note='Gurvich,1989 pt1 p342 pt2 p212. [tpis89]')

species(name= 'N2O5',
  atoms='O:5 N:2',
  thermo=(NASA9([200.00, 1000.00],
    [ 4.007828170E+04, -8.769675120E+02, 1.055932981E+01,
      1.394613859E-02, -8.884346920E-06, 8.500431150E-10,
      7.791550910E-13, 3.038962037E+03, -2.386831860E+01]),
    NASA9([1000.00, 6000.00],
      [-5.325578960E+04, -3.109277389E+03, 2.036088958E+01,
        -9.959901140E-04, 2.401398635E-07, -3.057161911E-11,
        1.495915511E-15, 1.336957281E+04, -8.298623341E+01])),
  note='Gurvich,1989 pt1 p343 pt2 p213. [g 4/99]')

species(name= 'N3',
  atoms='N:3',
  thermo=(NASA9([200.00, 1000.00],
    [ 3.337406790E+04, -2.965683604E+02, 3.314279150E+00,
      6.721685360E-03, -4.181126390E-06, 8.618442360E-10,
      6.883352530E-14, 5.298840620E+04, 5.312776486E+00]),
    NASA9([1000.00, 6000.00],
      [ 2.529264658E+05, -2.362876591E+03, 9.135267130E+00,
        -6.212870850E-04, 1.324094351E-07, -1.478989640E-11,
        6.721230470E-16, 6.412695390E+04, -3.135825973E+01])),
  note='Gurvich,1989 pt1 p325 pt2 p202. [tpis89]')

species(name= 'O',
  atoms='O:1',
  thermo=(NASA9([200.00, 1000.00],
    [-7.953611300E+03, 1.607177787E+02, 1.966226438E+00,
      1.013670310E-03, -1.110415423E-06, 6.517507500E-10,
      -1.584779251E-13, 2.840362437E+04, 8.404241820E+00]),
    NASA9([1000.00, 6000.00],
      [ 2.619020262E+05, -7.298722030E+02, 3.317177270E+00,
        -4.281334360E-04, 1.036104594E-07, -9.438304330E-12,
        2.725038297E-16, 3.392428060E+04, -6.679585350E-01]),
    NASA9([6000.00, 20000.00],
      [ 2.619020262E+05, -7.298722030E+02, 3.317177270E+00,
        -4.281334360E-04, 1.036104594E-07, -9.438304330E-12,
        2.725038297E-16, 3.392428060E+04, -6.679585350E-01])),
  note='Gurvich,1989 pt1 p325 pt2 p202. [tpis89]')

```

[1.779004264E+08, -1.082328257E+05, 2.810778365E+01,
-2.975232262E-03, 1.854997534E-07, -5.796231540E-12,
7.191720164E-17, 8.890942630E+05, -2.181728151E+02]],
note='E0(O2):Brix,1954. Moore,1976. Gordon,1999. [g 5/97]')

species(name= 'O+',
atoms='E:-1 O:1',
thermo=(NASA9([298.15, 1000.00],
[0.000000000E+00, 0.000000000E+00, 2.500000000E+00,
0.000000000E+00, 0.000000000E+00, 0.000000000E+00,
0.000000000E+00, 1.879352842E+05, 4.393376760E+00]),
NASA9([1000.00, 6000.00],
[-2.166513208E+05, 6.665456150E+02, 1.702064364E+00,
4.714992810E-04, -1.427131823E-07, 2.016595903E-11,
-9.107157762E-16, 1.837191966E+05, 1.005690382E+01]),
NASA9([6000.00, 20000.00],
[-2.143835383E+08, 1.469518523E+05, -3.680864540E+01,
5.036164540E-03, -3.087873854E-07, 9.186834870E-12,
-1.074163268E-16, -9.614208960E+05, 3.426193080E+02])),
note='Martin,W.C.,1993. Gordon,1999. [g 8/97]')

species(name= 'O2',
atoms='O:2',
thermo=(NASA9([200.00, 1000.00],
[-3.425563420E+04, 4.847000970E+02, 1.119010961E+00,
4.293889240E-03, -6.836300520E-07, -2.023372700E-09,
1.039040018E-12, -3.391454870E+03, 1.849699470E+01]),
NASA9([1000.00, 6000.00],
[-1.037939022E+06, 2.344830282E+03, 1.819732036E+00,
1.267847582E-03, -2.188067988E-07, 2.053719572E-11,
-8.193467050E-16, -1.689010929E+04, 1.738716506E+01]),
NASA9([6000.00, 20000.00],
[4.975294300E+08, -2.866106874E+05, 6.690352250E+01,
-6.169959020E-03, 3.016396027E-07, -7.421416600E-12,
7.278175770E-17, 2.293554027E+06, -5.530621610E+02])),
note='Ref-Elm. Gurvich,1989 pt1 p94 pt2 p9. [tpis89]')

species(name= 'O2+',
atoms='E:-1 O:2',
thermo=(NASA9([298.15, 1000.00],
[-8.607205450E+04, 1.051875934E+03, -5.432380470E-01,
6.571166540E-03, -3.274263750E-06, 5.940645340E-11,
3.238784790E-13, 1.345544668E+05, 2.902709750E+01]),
NASA9([1000.00, 6000.00],
[7.384654880E+04, -8.459559540E+02, 4.985164160E+00,

```
-1.611010890E-04, 6.427083990E-08, -1.504939874E-11,  
1.578465409E-15, 1.446321044E+05, -5.811230650E+00]),  
NASA9([6000.00, 20000.00],  
[-1.562125524E+09, 1.161406778E+06, -3.302504720E+02,  
4.710937520E-02, -3.354461380E-06, 1.167968599E-10,  
-1.589754791E-15, -8.857866270E+06, 2.852035602E+03])),  
note='Gurvich,1989 pt1 p98 pt2 p11. [tpis89]')
```

```
species(name='O3',  
atoms='O:3',  
thermo=(NASA9([200.00, 1000.00],  
[-1.282314507E+04, 5.898216640E+02, -2.547496763E+00,  
2.690121526E-02, -3.528258340E-05, 2.312290922E-08,  
-6.044893270E-12, 1.348368701E+04, 3.852218580E+01]),  
NASA9([1000.00, 6000.00],  
[-3.869662480E+07, 1.023344994E+05, -8.961551600E+01,  
3.706144970E-02, -4.137638740E-06, -2.725018591E-10,  
5.248188110E-14, -6.517918180E+05, 7.029109520E+02])),  
note='Gurvich,1989 pt1 p101 pt2 p15. [g 8/01]')
```

```
species(name='uN-',  
atoms='E:1 N:1',  
thermo=(NASA9([298.15, 1000.00],  
[ 1.445682471E+03, 7.335205110E+00, 2.476680939E+00,  
4.227869180E-05, -4.426293320E-08, 2.490985431E-11,  
-5.831608090E-15, 5.617625000E+04, 5.145753977E+00]),  
NASA9([1000.00, 6000.00],  
[ 2.404189576E+03, 2.954965336E-01, 2.499789368E+00,  
8.307564970E-08, -1.829942770E-11, 2.100136461E-15,  
-9.754986710E-20, 5.621413890E+04, 5.006484157E+00]),  
NASA9([6000.00, 20000.00],  
[ 1.884379470E+03, 3.905516910E-01, 2.499914043E+00,  
9.818512540E-09, -6.126037340E-13, 1.980010689E-17,  
-2.593295116E-22, 5.621304520E+04, 5.005647607E+00])),  
note='Hotop,1985. Chase,1998 p1602. Gordon,1999. [j12/82]')
```

```
species(name='uNO2-',  
atoms='E:1 O:2 N:1',  
thermo=(NASA9([298.15, 1000.00],  
[-1.282067858E+04, 6.990138180E+02, -2.812596273E+00,  
2.412894252E-02, -2.831606689E-05, 1.670509365E-08,  
-3.983330130E-12, -2.809915579E+04, 4.063271510E+01]),  
NASA9([1000.00, 6000.00],  
[ 1.325710335E+05, -1.557032129E+03, 8.126721920E+00,  
-2.728626780E-04, -4.707541800E-08, 2.826729008E-11,
```

-2.353985481E-15, -1.715795217E+04, -2.228576043E+01))),
note='Gurvich,1989 pt1 p334 pt2 p208. [tpis89]')

species(name=u'N2-',
atoms='E:1 N:2',
thermo=(NASA9([298.15, 1000.00],
[-8.146227110E+04, 9.063600790E+02, -1.520054079E-01,
6.023190840E-03, -2.897138445E-06, -4.129106680E-11,
3.206989770E-13, 1.218808548E+04, 2.638068855E+01]),
NASA9([1000.00, 6000.00],
[2.169637706E+05, -1.275098516E+03, 5.391095700E+00,
-3.198907510E-04, 7.311051350E-08, -8.202017370E-12,
3.740044700E-16, 2.424964308E+04, -9.014934294E+00]),
NASA9([6000.00, 20000.00],
[1.345850786E+06, -1.060565497E+03, 4.732026850E+00,
-5.091450050E-06, 1.628212099E-09, -5.224243560E-14,
6.796651250E-19, 2.394627677E+04, -4.297861544E+00])),
note='Chase,1998 p1623. [j 9/77]')

species(name=u'O-',
atoms='E:1 O:1',
thermo=(NASA9([298.15, 1000.00],
[-5.695857110E+03, 1.099287334E+02, 2.184719661E+00,
5.326359800E-04, -5.298878440E-07, 2.870216236E-10,
-6.524692740E-14, 1.093287498E+04, 6.729863860E+00]),
NASA9([1000.00, 6000.00],
[9.769363180E+03, 7.159604780E+00, 2.494961726E+00,
1.968240938E-06, -4.304174850E-10, 4.912083080E-14,
-2.271600083E-18, 1.149554438E+04, 4.837036440E+00]),
NASA9([6000.00, 20000.00],
[5.662391000E+02, 7.572340320E+00, 2.498352500E+00,
1.862632395E-07, -1.151227211E-11, 3.688814210E-16,
-4.793297600E-21, 1.148426000E+04, 4.813406590E+00])),
note='Gurvich,1989 pt1 p93. Hotop,1985. Gordon,1999. [g 1/97]')

species(name=u'O2-',
atoms='E:1 O:2',
thermo=(NASA9([298.15, 1000.00],
[1.883874344E+04, 1.149551768E+02, 1.518876821E+00,
8.016111380E-03, -9.850571030E-06, 6.044196210E-09,
-1.486439845E-12, -7.101538760E+03, 1.501210380E+01]),
NASA9([1000.00, 6000.00],
[-5.655208050E+04, -2.367815862E+02, 4.675833670E+00,
-2.197245300E-05, 1.711509280E-08, -1.757645062E-12,
8.248172790E-17, -5.960177750E+03, -2.436885556E+00])),

note='Gurvich,1989 pt1 p100 pt2 p13. [g11/99]')

species(name='O4',
atoms='O:4',
thermo=(NASA([200.00, 1000.00],
[1.90385797E+00, 1.65202009E-02, -4.81057050E-06,
-1.22755219E-08, 8.03977166E-12, 4.65897886E+04,
1.41925069E+01]),
NASA([1000.00, 6000.00],
[7.98777248E+00, 2.07473713E-03, -8.15656374E-07,
1.39579414E-10, -8.69452778E-15, 4.49028858E+04,
-1.75119295E+01])),
note='u'cycloT1/11')

species(name='O4+',
atoms='E:-1 O:4',
thermo=(NASA([298.15, 1000.00],
[1.15107802E+00, 2.15570328E-02, -2.10270939E-05,
8.21140809E-09, -6.49760980E-13, 1.72530097E+05,
1.81430748E+01]),
NASA([1000.00, 6000.00],
[7.57784346E+00, 2.48052052E-03, -9.71133430E-07,
1.65738251E-10, -1.03047740E-14, 1.70839793E+05,
-1.46808901E+01])),
note='u'cationT1/11')

species(name='O4-',
atoms='E:1 O:4',
thermo=(NASA([298.15, 1000.00],
[3.76742717E+00, 1.52352066E-02, -1.67050863E-05,
8.99679984E-09, -1.92867534E-12, -1.33342585E+04,
6.42680556E+00]),
NASA([1000.00, 6000.00],
[8.00618937E+00, 2.02027580E-03, -7.86172513E-07,
1.33669567E-10, -8.29026235E-15, -1.44401544E+04,
-1.51237720E+01])),
note='u'cycloanionT1/11')

species(name='O3+',
atoms='E:-1 O:3',
thermo=(NASA([298.15, 1000.00],
[2.09881658E+00, 1.31588046E-02, -1.49792721E-05,
7.85110637E-09, -1.50346077E-12, 1.62012128E+05,
1.35091444E+01]),
NASA([1000.00, 6000.00],

```

[ 5.79866945E+00, 1.23352553E-03, -4.83692178E-07,
  8.26330790E-11, -5.14128292E-15, 1.61085509E+05,
  -5.15613353E+00]),
note=u'T10/09')

species(name=u'O3-',
  atoms='E:1 O:3',
  thermo=(NASA([298.15, 1000.00],
    [ 1.90241113E+00, 1.56105437E-02, -2.09605956E-05,
      1.35889864E-08, -3.46558506E-12, -9.16517169E+03,
      1.51033864E+01]),
    NASA([1000.00, 6000.00],
      [ 5.95188221E+00, 1.08039003E-03, -4.24642763E-07,
        7.26564042E-11, -4.52533445E-15, -1.01080130E+04,
        -4.96701318E+00])),
  note=u'g1/97')

species(name=u'N3+',
  atoms='E:-1 N:3',
  thermo=(NASA([298.15, 1000.00],
    [ 3.67011652E+00, 4.59806506E-03, 1.39108363E-06,
      -5.02694961E-09, 2.21155760E-12, 1.81883765E+05,
      3.94467784E+00]),
    NASA([1000.00, 6000.00],
      [ 5.48199577E+00, 2.01665176E-03, -7.78258436E-07,
        1.31617313E-10, -8.13320494E-15, 1.81240003E+05,
        -6.06985591E+00])),
  note=u'cationT7/11')

species(name=u'N3-',
  atoms='E:1 N:3',
  thermo=(NASA([298.15, 1000.00],
    [ 2.24780799E+00, 9.62809932E-03, -8.68930659E-06,
      4.35991076E-09, -9.90198590E-13, 2.11461886E+04,
      1.02228504E+01]),
    NASA([1000.00, 6000.00],
      [ 4.73550286E+00, 2.67431169E-03, -1.01221572E-06,
        1.69074578E-10, -1.03605229E-14, 2.04280987E+04,
        -2.69430895E+00])),
  note=u'anionT7/11')

species(name=u'N2O3-',
  atoms='E:1 O:3 N:2',
  thermo=(NASA([298.15, 1000.00],
    [ 2.89324483E+00, 3.19808640E-02, -5.05683173E-05,

```

```

        3.86459138E-08, -1.15116280E-11, -1.51573664E+04,
        1.43021997E+01]),
NASA([1000.00, 6000.00],
 [ 1.01755814E+01, 1.89076587E-03, -7.37782071E-07,
  1.18497726E-10, -6.98566653E-15, -1.66739068E+04,
  -2.08612575E+01])),
note=u'ONONO-T9/11')

species(name=u'N2O3+',
atoms='E:-1 O:3 N:2',
thermo=(NASA([298.15, 1000.00],
 [ 7.20942869E+00, 8.16248467E-03, -4.97073757E-06,
  1.63966869E-09, -3.35148057E-13, 1.22231866E+05,
  -4.70591859E+00]),
NASA([1000.00, 6000.00],
 [ 9.25815628E+00, 3.58625676E-03, -1.34956361E-06,
  2.24572549E-10, -1.37255559E-14, 1.21553684E+05,
  -1.57010434E+01])),
note=u'ATcT/A')

species(name=u'NO3+',
atoms='E:-1 O:3 N:1',
thermo=(NASA([298.15, 1000.00],
 [ 3.59690725E+00, 1.02349640E-02, -2.16756198E-06,
  -5.75967671E-09, 3.25185928E-12, 1.53961219E+05,
  7.28796163E+00]),
NASA([1000.00, 6000.00],
 [ 7.35799538E+00, 2.67096283E-03, -1.03781441E-06,
  1.76272387E-10, -1.09243947E-14, 1.52774118E+05,
  -1.28565412E+01])),
note=u'T09/09')

species(name=u'N2O-',
atoms='E:1 O:1 N:2',
thermo=(NASA([298.15, 1000.00],
 [ 2.64781275E+00, 1.02374979E-02, -1.03596841E-05,
  4.81418366E-09, -7.88188960E-13, 1.01242088E+04,
  1.16810435E+01]),
NASA([1000.00, 6000.00],
 [ 5.59139743E+00, 1.42679504E-03, -5.55079528E-07,
  9.43596949E-11, -5.85139723E-15, 9.34126250E+03,
  -3.36642832E+00])),
note=u'O(NN)-cyclT10/11')

species(name=u'NO2+',

```

```

atoms='E:-1 O:2 N:1',
thermo=(NASA([298.15, 1000.00],
  [ 3.56214086E+00, 3.43628731E-03, -1.19400585E-07,
    -1.31592209E-09, 5.01138796E-13, 1.14779715E+05,
    7.19236092E+00]),
  NASA([1000.00, 6000.00],
    [ 4.34739782E+00, 2.51040238E-03, -9.39355569E-07,
      1.54999215E-10, -9.19955387E-15, 1.14465056E+05,
      2.74113794E+00])),
note=u'ATcTA')

```

```

species(name=u'NO-',
atoms='E:1 O:1 N:1',
thermo=(NASA([298.15, 1000.00],
  [ 3.56601901E+00, -1.73810582E-03, 8.25578308E-06,
    -9.10347890E-09, 3.27538426E-12, 8.78530820E+03,
    5.19753973E+00]),
  NASA([1000.00, 6000.00],
    [ 3.68353191E+00, 8.37252448E-04, -3.15197942E-07,
      5.33094078E-11, -3.29420062E-15, 8.60364845E+03,
      3.86332845E+00])),
note=u'anionT4/16')

```

```

species(name=u'ONONO2',
atoms='O:4 N:2',
thermo=(NASA([200.00, 1000.00],
  [ 2.97565571E+00, 2.97669896E-02, -3.21501150E-05,
    1.89019097E-08, -5.02083573E-12, 4.26648639E+03,
    1.32487955E+01]),
  NASA([1000.00, 6000.00],
    [ 1.16087956E+01, 4.35184794E-03, -1.77836774E-06,
      3.10967025E-10, -1.96385003E-14, 1.86449781E+03,
      -3.12108726E+01])),
note=u'T9/11')

```

D.4.2 CTIfile Willis.cti

```
#-----  
# Reaction data for Willis and Boyd (prepend species data)  
#-----  
#k_f(T)=AT^b exp(-E/RT)  
# [A,b,E]  
## Ion-molecule reactions in N2-O2 irradiated mixtures  
  
# Reaction 1  
reaction( "N2+ + O2 => O2+ + N2", [(1.5E-10, 'cm3/molec/s'), 0 ,0])  
  
# Reaction 2  
reaction( "O2+ + N2 => NO+ + NO", [(2.0E-16, 'cm3/molec/s'), 0 ,0])  
  
# Reaction 3 * Turn off brings back N2+ ions  
three_body_reaction( "N2+ + 2 N2 => N4+ + N2", [(1.0E-28, 'cm6/molec2/s'), 0 ,0])  
  
# Reaction 4  
reaction( "N4+ + O2 => O2+ + 2 N2", [(1.0E-10, 'cm3/molec/s'), 0 ,0])  
  
# Reaction 5  
reaction( "N2+ + NO => NO+ + N2", [(5.0E-10, 'cm3/molec/s'), 0 ,0])  
  
# Reaction 6  
reaction( "O2+ + NO => NO+ + O2", [(8.0E-10, 'cm3/molec/s'), 0 ,0])  
  
# Reaction 7  
reaction( "NO+ + e- => N + O", [(4E-7, 'cm3/molec/s'), 0 ,0])  
  
# Reaction 8  
reaction( "O2+ + e- => 2 O", [(2E-7, 'cm3/molec/s'), 0 ,0])  
  
# Reaction 8a  
reaction( "O2+ + O2- => 2 O + O2", [(2E-6, 'cm3/molec/s'), 0 ,0])  
  
# Reaction 9  
reaction( "N2+ + e- => 2 N", [(1E-7, 'cm3/molec/s'), 0 ,0])  
  
# Reaction 10  
reaction( "N2+ + O2- => 2 N + O2", [(2E-6, 'cm3/molec/s'), 0 ,0])  
  
# Reaction 11 *  
three_body_reaction( "e- + 2 O2 => O2- + O2", [(4.2E-27, 'cm6/molec2/s'), -1  
,(600,'K')])
```

```

# Reaction 12 *
three_body_reaction( "e- + O2 + N2 => O2- + N2", [(1.0E-31, 'cm6/molec2/s'), 0 ,0])

# Reaction 13
reaction( "e- + NO2 + N2 => NO2- + N2", [(4E-11, 'cm3/molec/s'), 0 ,0])

# Reaction 14 *
three_body_reaction( "e- + NO + M => NO- + M", [(1.3E-31, 'cm6/molec2/s'), 0 ,0])

# Reaction 15
reaction( "O2- + O3 => O3- + O2", [(3.5E-10, 'cm3/molec/s'), 0 ,0])

# Reaction 16
reaction( "O3- + NO => NO2- + O2", [(8E-10, 'cm3/molec/s'), 0 ,0])

# Reaction 17
reaction( "O3- + NO2 => NO2- + O3", [(7E-10, 'cm3/molec/s'), 0 ,0])

# Reaction 18
reaction( "NO2- + O3 => NO3- + O2", [(1E-11, 'cm3/molec/s'), 0 ,0])

# Reaction 19
reaction( "NO- + O2 => O2- + NO", [(9E-10, 'cm3/molec/s'), 0 ,0])

## neutral-neutral reactions in N2-O2 irradiated mixtures

# Reaction 20
three_body_reaction( "N + O + M => NO + M", [(1.0E-32, 'cm3/molec/s'), 0 ,0])

# Reaction 21
three_body_reaction( "2 N + N2 => 2 N2", [(5.0E-33, 'cm3/molec/s'), 0 ,0]) # above 400
Torr

# Reaction 22
reaction( "N + O2 => NO + O", [(1.4E-11, 'cm3/molec/s'), 0 ,(7.1,'kcal/mol')]) # 1st one

# Reaction 23
reaction( "N + O3 => NO + O2", [(2E-13, 'cm3/molec/s'), 0 ,0]) # used for 830Torr

# Reaction 24
reaction( "N + NO => N2 + O", [(2.2E-11, 'cm3/molec/s'), 0 ,0])

```

```

# Reaction 25
reaction( "N + NO2 => N2O + O", [(7.7E-12, 'cm3/molec/s'), 0 ,0])

# Reaction 26
reaction( "N + NO2 => 2 NO", [(5.9E-12, 'cm3/molec/s'), 0 ,0])

# Reaction 27
reaction( "N + NO2 => N2 + O2", [(1.8E-12, 'cm3/molec/s'), 0 ,0])

# Reaction 28
reaction( "N + NO2 => N2 + 2 O", [(2.3E-12, 'cm3/molec/s'), 0 ,0])

# Reaction 29 *
three_body_reaction( "O + O2 + M => O3 + M", [(2.8E-34, 'cm6/molec2/s'), 0 ,0])

# Reaction 30 *
three_body_reaction( "O + O + O2 => 2 O2", [(2.0E-33, 'cm6/molec2/s'), 0 ,0])

# Reaction 31
reaction( "O + O3 => 2 O2", [(1.0E-14, 'cm3/molec/s'), 0 ,0])

# Reaction 32 *
three_body_reaction( "O + NO + O2 => NO2 + O2", [(8.1E-32, 'cm6/molec2/s'), 0 ,0])

# Reaction 33 *
three_body_reaction( "O + NO + N2 => NO2 + N2", [(1.1E-31, 'cm6/molec2/s'), 0 ,0])

# Reaction 34
reaction( "O + NO2 => NO + O2", [(3.2E-11, 'cm3/molec/s'), 0 ,(0.6,'kcal/mol')])

# Reaction 35 *
reaction( "O2 + 2 NO => 2 NO2", [(1.0E-33, 'cm6/molec2/s'), 0 ,0])

# Reaction 36
reaction( "O3 + NO => NO2 + O2", [(9.5E-13, 'cm3/molec/s'), 0 ,(2.46,'kcal/mol')])

```

D.4.3 CTIfile Willis_update.cti

```
#-----  
# Reaction data for Willis and Boyd, updates rates (prepend species data)  
#-----  
#k_f(T)=AT^b exp(-E/RT)  
# [A,b,E]  
## Ion-molecule reactions in N2-O2 irradiated mixtures  
  
# Reaction 1  
reaction( "N2+ + O2 => O2+ + N2", [(5.00E-11,'cm3/molec/s'), 0 ,0])  
  
# Reaction 2  
reaction( "O2+ + N2 => NO+ + NO", [(1.00E-15,'cm3/molec/s'), 0 ,0])  
  
# Reaction 3 *  
three_body_reaction( "N2+ + 2 N2 => N4+ + N2", [(1.0E-28, 'cm6/molec2/s'), 0 ,0]) #  
Willis/Boyd  
# Not Found  
  
# Reaction 4  
reaction( "N4+ + O2 => O2+ + 2 N2", [(1.0E-10, 'cm3/molec/s'), 0 ,0]) # Willis/Boyd  
# Not Found  
  
# Reaction 5  
reaction( "N2+ + NO => NO+ + N2", [(5.0E-10, 'cm3/molec/s'), 0 ,0]) # Willis/Boyd  
# Not Found  
  
# Reaction 6  
reaction( "O2+ + NO => NO+ + O2", [(4.60E-10,'cm3/molec/s'), 0 ,0])  
  
# Reaction 7  
reaction( "NO+ + e- => N + O", [(4.1E-7,'cm3/molec/s'), 0 ,0])  
  
# Reaction 8  
reaction( "O2+ + e- => 2 O", [(2.2E-7,'cm3/molec/s'), 0 ,0])  
  
# Reaction 8a  
reaction( "O2+ + O2- => 2 O + O2", [(2E-6, 'cm3/molec/s'), 0 ,0]) # Willis/Boyd  
# Not Found  
  
# Reaction 9  
reaction( "N2+ + e- => 2 N", [(2.9E-7,'cm3/molec/s'), 0 ,0])  
  
# Reaction 10
```

```

reaction( "N2+ + O2- => 2 N + O2", [(2E-6, 'cm3/molec/s'), 0 ,0]) # Willis/Boyd
# Not Found

# Reaction 11 *
three_body_reaction( "e- + O2 + M => O2- + M", [(2.5E-30,'cm6/molec2/s'), 0 ,0])

# Reaction 12 *
# Handled by three-body above

# Reaction 13
reaction( "e- + NO2 + N2 => NO2- + N2", [(4E-11, 'cm3/molec/s'), 0 ,0]) # Willis/Boyd
# Not Found

# Reaction 14 *
three_body_reaction( "e- + NO + M => NO- + M", [(1.3E-31, 'cm6/molec2/s'), 0 ,0]) #
Willis/Boyd
# Not Found

# Reaction 15
reaction( "O2- + O3 => O3- + O2", [(6E-10, 'cm3/molec/s'), 0 ,0])

# Reaction 16
reaction( "O3- + NO => NO2- + O2", [(8E-10,'cm3/molec/s'), 0 ,0])

# Reaction 17
reaction( "O3- + NO2 => NO2- + O3", [(7E-10,'cm3/molec/s'), 0 ,0])

# Reaction 18
reaction( "NO2- + O3 => NO3- + O2", [(1.2E-10,'cm3/molec/s'), 0 ,0])

# Reaction 19
reaction( "NO- + O2 => O2- + NO", [(9E-10, 'cm3/molec/s'), 0 ,0]) # Willis/Boyd
# Not Found

## neutral-neutral reactions in N2-O2 irradiated mixtures

# Reaction 20
reaction( "O + N => NO", [(6.89E-33,'cm6/molec2/s'), 0 ,(-1.12,'kJ/mol')])

# Reaction 21
reaction( "2 N + N2 => 2 N2", [(1.72E-32, 'cm6/molec2/s'), 0 ,0]) # Harteck

# Reaction 22

```

```

reaction( "N + O2 => NO + O", [(4.40E-12,'cm3/molec/s'), 0 ,(26.77, 'kJ/mol')],
id='0003')

# Reaction 23
reaction( "O3 + N => O2 + NO", [(1.0E-16,'cm3/molec/s'), 0 ,0])

# Reaction 24
reaction( "N + NO => N2 + O", [(3.11E-11,'cm3/molec/s'), 0 , 0])

# Reaction 25
reaction( "N + NO2 => N2O + O", [(3.01E-12,'cm3/molec/s'), 0 ,(0,'kJ/mole')])

# Reaction 26
reaction( "NO2 + N => 2 NO", [(6.11E-12,'cm3/molec/s'), 0 ,0])

# Reaction 27
reaction( "NO2 + N => N2 + O2", [(1.85E-12,'cm3/molec/s'), 0 ,0])

# Reaction 28
reaction( "NO2 + N => N2 + 2 O", [(2.41E-12,'cm3/molec/s'), 0 ,0])

# Reaction 29 *
three_body_reaction( "O + O2 + M => O3 + M", [(1.54E-27,'cm6/molec2/s'), -2.6 ,0])

# Reaction 30 *
reaction( "2 O => O2", [(2.70E-33,'cm6/molec2/s'), 0 , 0])

# Reaction 31
reaction( "O3 + O => 2 O2", [(8.0E-12,'cm3/molec/s'), 0 ,(17.13,'kJ/mol')])

# Reaction 32 *
three_body_reaction( "NO + O + M => NO2 + M", [(9.19E-28,'cm6/molec2/s'), -1.60
,0])

# Reaction 33 *
#Handled by three-body above

# Reaction 34
reaction( "NO2 + O => NO + O2", [(5.5E-12,'cm3/molec/s'), 0 ,(1.56,'kJ/mol')])

# Reaction 35 *
reaction( "O2 + 2 NO => 2 NO2", [(3.3E-39,'cm6/molec2/s'), 0 ,(-4.41,'kJ/mol')])

# Reaction 36
reaction( "NO + O3 => NO2 + O2", [(1.4E-12,'cm3/molec/s'), 0 ,(10.89,'kJ/mol')])

```

D.4.4 WorkingThermo.v6.cti

```
#-----  
# Reaction data for Posited Model (Prepend species data)  
#-----  
  
## Cantera CTI Format  
## k = AT^(b)exp(-E/RT)  
  
# Reaction 1  
reaction( "2 O => O2", [(2.70E-33,'cm6/molec2/s'), 0 , 0])  
  
# Reaction 2  
reaction( "N + NO => N2 + O", [(3.11E-11,'cm3/molec/s'), 0 , 0])  
  
# Reaction 3  
reaction( "N + O2 => NO + O", [(4.40E-12,'cm3/molec/s'), 0 ,(26.77, 'kJ/mol')])  
  
# Reaction 4  
#reaction( "N2O + O => 2 NO", [(1.66E-16,'cm3/molec/s'), 0 ,(0, 'kJ/mol')])  
# All High Temp Data  
  
# Reaction 5  
three_body_reaction( "NO + O + M => NO2 + M", [(9.19E-28,'cm6/molec2/s'), -1.60  
,0])  
  
# Reaction 6  
reaction( "NO2 + O => NO + O2", [(5.5E-12,'cm3/molec/s'), 0 ,(1.56,'kJ/mole')])  
  
# Reaction 7  
reaction( "NO3 + O => O2 + NO2", [(1.7E-11,'cm3/molec/s'), 0 ,0])  
  
# Reaction 8  
three_body_reaction( "O + O2 + M => O3 + M", [(1.54E-27,'cm6/molec2/s'), -2.6 ,0])  
  
# Reaction 9  
reaction( "NO + O3 => NO2 + O2", [(1.4E-12,'cm3/molec/s'), 0 ,(10.89,'kJ/mole')])  
  
# Reaction 10  
reaction( "NO + NO3 => NO2 + NO2", [(1.3E-11,'cm3/molec/s'), 0 ,(-250,'K')])  
  
# Reaction 11  
reaction( "N + NO2 => N2O + O", [(3.01E-12,'cm3/molec/s'), 0 ,(0,'kJ/mole')])  
  
# Reaction 12
```

```

reaction( "NO2 + O3 => NO3 + O2", [(1.4E-13,'cm3/molec/s'), 0 ,(20.54,'kJ/mole')])

# Reaction 13
#reaction( "NO2 + O => NO3", [(5.85E-12,'cm3/molec/s'), 0.24 ,0])
# Handled by 41

# Reaction 14
reaction( "2 NO2 => NO + NO3", [(1.6E-14,'cm3/molec/s'), 0.73 ,(87.30,'kJ/mole')])

# Reaction 15
three_body_reaction( "N2O5 + M => NO2 + NO3 + M", [(6.08E+5,'cm3/molec/s'), -
3.50 ,(91.46,'kJ/mole')])

# Reaction 16
three_body_reaction( "N2O3 + M => NO + NO2 + M", [(6.76E+14,'cm3/molec/s'), -
8.70 ,(40.57,'kJ/mole')])

# Reaction 17 ## Doesn't exist in NIST
reaction( "2 O3 + 2 N => O2 + 2 NO2", [1.21E+08, 0 ,0])

# Reaction 18
reaction( "O3 + N => O2 + NO", [(1.0E-16,'cm3/molec/s'), 0 ,0])

# Reaction 19
reaction( "O3 + O => 2 O2", [(8.0E-12,'cm3/molec/s'), 0 ,(17.13,'kJ/mole')])

# Reaction 20
reaction( "O3 + NO3 => 2 O2 + NO2", [(1.00E-17,'cm3/molec/s'), 0 ,0])

# Reaction 21
reaction( "O3 + NO2 => 2 O2 + NO", [(1.0E-18,'cm3/molec/s'), 0 ,0])

# Reaction 22
reaction( "O3 => O2 + O", [(7.16E-10,'cm3/molec/s'), 0 ,(93.122,'kJ/mole')])

# Reaction 23
reaction( "N2O4 => ONONO2", [2.86E+3, 0 ,0])

# Reaction 24
three_body_reaction( "N2O4 + M => 2 NO2 + M", [(3.37E+4,'cm3/molec/s'), -3.8
,(4.16,'kJ/mole')])

# Reaction 25
reaction( "NO3 => O2 + NO", [(2.50E+06,'1/s'), 0 ,(50.72,'kJ/mole')])

```

```

# Reaction 26
reaction( "NO2 + NO3 => O2 + NO + NO2", [(4.5E-14,'cm3/molec/s'), 0
,(10.48,'kJ/mole')])

# Reaction 27
three_body_reaction( "NO + NO2 + M => N2O3 + M", [(3.67E-15,'cm6/molec2/s'), -7.7
,0])

# Reaction 28
three_body_reaction( "NO2 + NO3 + M => N2O5 + M", [(5.16E-20,'cm6/molec2/s'), -
4.1 ,0])

# Reaction 29
reaction( "2 NO2 => O2 + 2 NO ", [(2.71E-12,'cm3/molec/s'), 0 ,(109,'kJ/mole')])

# Reaction 30
three_body_reaction( "2 NO2 + M => N2O4 + M", [(3.62E-24, 'cm6/molec2/s'), -3.8 ,0])
# Duplicate of 43

# Reaction 31
reaction( "NO2 + N3 => N2 + 2 NO", [(6.0E-13,'cm3/molec/s'), 0 ,0])

# Reaction 32
reaction( "NO2 + N3 => 2 N2O", [(2.0E-13,'cm3/molec/s'), 0 ,0])

# Reaction 33
reaction( "NO2 + N => N2 + O2", [(1.85E-12,'cm3/molec/s'), 0 ,0])

# Reaction 34
reaction( "NO2 + N => N2 + 2 O", [(2.41E-12,'cm3/molec/s'), 0 ,0])

# Reaction 35
reaction( "NO2 + N => 2 NO", [(6.11E-12,'cm3/molec/s'), 0 ,0])

# Reaction 36
reaction( "O2 + 2 NO => 2 NO2", [(3.3E-39,'cm6/molec2/s'), 0 ,(-4.41,'kJ/mole')])

# Reaction 37
reaction( "NO + O => N + O2", [(3.0E-15,'cm3/molec/s'), 1 ,(162,'kJ/mole')])

# Reaction 38
reaction( "O + N => NO", [(6.89E-33,'cm6/molec2/s'), 0 ,(-1.12,'kJ/mole')])

# Reaction 39
reaction( "O2 => 2 O", [(3.01E-6,'cm3/molec/s'), -1.00 ,(494,'kJ/mole')])

```

```

# Reaction 40
reaction( "N2 + O => N2O", [(5.02E-38,'cm6/molec2/s'), 0 ,0])

# Reaction 41
three_body_reaction( "O + NO2 + M => NO3 + M", [(6.75E-28, 'cm6/molec2/s'), -1.5
,0])

# Reaction 42
reaction( "2 NO3 => O2 + 2 NO2", [(8.5E-13, 'cm3/molec/s'), 0 ,(20.37,'kJ/mole')])

# Reaction 43
#three_body_reaction( "2 NO2 + M => N2O4 + M", [(3.62E-24, 'cm6/molec2/s'), -3.8
,0])
# Duplicate of 30

#-----
# IONIC REACTIONS
#-----

# Reaction 44
reaction( "N+ + N2 => N + N2+", [(2.55E-10,'cm3/molec/s'), 0 ,0])

# Reaction 45
reaction( "N+ + O2 => O+ + NO", [(4.64E-11,'cm3/molec/s'), 0 ,0])

# Reaction 46
reaction( "N+ + O2 => NO+ + O", [(2.32E-10,'cm3/molec/s'), 0 ,0])

# Reaction 47
reaction( "N+ + O2 => O2+ + N", [(3.074E-10,'cm3/molec/s'), 0 ,0])

# Reaction 48
reaction( "N+ + NO => NO+ + N", [(4.7175E-10,'cm3/molec/s'), 0 ,0])

# Reaction 49
reaction( "N+ + NO => N2+ + O", [(8.325E-11,'cm3/molec/s'), 0 ,0])

# Reaction 50
reaction( "N+ + N2O => NO+ + N2", [(5.5E-10,'cm3/molec/s'), 0 ,0])

# Reaction 51
reaction( "N2+ + N => N+ + N2", [(1.0E-11,'cm3/molec/s'), 0 ,0])

```

```

# Reaction 52
reaction( "N2+ + O => O+ + N2", [(9.8E-12,'cm3/molec/s'), 0 ,0])

# Reaction 53
reaction( "N2+ + O => NO+ + N", [(1.3E-10,'cm3/molec/s'), 0 ,0])

# Reaction 54
reaction( "N2+ + O2 => O2+ + N2", [(5.00E-11,'cm3/molec/s'), 0 ,0])

# Reaction 55
reaction( "N2+ + N2O => N2O+ + N2", [(6.00E-10,'cm3/molec/s'), 0 ,0])

# Reaction 56
reaction( "O+ + N2 => NO+ + N ", [(1.20E-12,'cm3/molec/s'), 0 ,0])

# Reaction 57
reaction( "O+ + O2 => O2+ + O", [(2.1E-11,'cm3/molec/s'), 0 ,0])

# Reaction 58
reaction( "O+ + NO => NO+ + O", [(8.00E-13,'cm3/molec/s'), 0 ,0])

# Reaction 59
reaction( "O+ + NO2 => NO2+ + O", [(1.60E-9,'cm3/molec/s'), 0 ,0])

# Reaction 60
reaction( "O+ + N2O => N2O+ + O", [(6.3E-10,'cm3/molec/s'), 0 ,0])

# Reaction 61
reaction( "O2+ + N => NO+ + O ", [(1.50E-10,'cm3/molec/s'), 0 ,0])

# Reaction 62
reaction( "O2+ + N2 => NO+ + NO", [(1.00E-15,'cm3/molec/s'), 0 ,0])

# Reaction 63
reaction( "O2+ + NO => NO+ + O2", [(4.60E-10,'cm3/molec/s'), 0 ,0])

# Reaction 64
reaction( "O2+ + NO2 => NO2+ + O2", [(6.60E-10,'cm3/molec/s'), 0 ,0])

# Reaction 65
reaction( "NO2+ + NO => NO+ + NO2", [(2.75E-10,'cm3/molec/s'), 0 ,0])

# Reaction 66
reaction( "N2O+ + O2 => O2+ + N2O", [(2.241E-10,'cm3/molec/s'), 0 ,0])

```

```

# Reaction 67
reaction( "N2O+ + O2 => NO+ + NO2", [(4.59E-11,'cm3/molec/s'), 0 ,0])

# Reaction 68
reaction( "N2O+ + NO => NO+ + N2O", [(2.30E-10,'cm3/molec/s'), 0 ,0])

# Reaction 69
reaction( "N2O+ + NO2 => NO+ + N2 + O2", [(4.29E-10,'cm3/molec/s'), 0 ,0])

# Reaction 70
reaction( "N2O+ + NO2 => NO2+ + N2O", [(2.21E-34,'cm3/molec/s'), 0 ,0])

# Reaction 71
reaction( "N2O+ + N2O => NO+ + N2 + NO", [(1.20E-11,'cm3/molec/s'), 0 ,0])

# Reaction 72
reaction( "O+ + e- => O", [(3.0E-12,'cm3/molec/s'), 0 ,0])

# Reaction 73
reaction( "O2+ + e- => O + O", [(2.2E-7,'cm3/molec/s'), 0 ,0])

# Reaction 74 8a from WB
reaction( "O2+ + O2- => O + O + O2", [(2E-6,'cm3/molec/s'), 0 ,0])

# Reaction 75
reaction( "N+ + e- => N", [(3.0E-12,'cm3/molec/s'), 0 ,0])

# Reaction 76
reaction( "N2+ + e- => N + N", [(2.9E-7,'cm3/molec/s'), 0 ,0])

# Reaction 77 10 from WB
reaction( "N2+ + O2- => N + N + O2", [(2.0E-6,'cm3/molec/s'), 0 ,0])

# Reaction 78
reaction( "NO+ + e- => N + O", [(5.4E-5,'cm3/molec/s'), -0.85 ,0])

# Reaction 79
reaction( "e- + O3 => O- + O2", [(5.4198E+12,'cm3/mol/s'), 0 ,0])

# Reaction 80
reaction( "O- + O => O2 + e-", [(1.1442E+14,'cm3/mol/s'), 0 ,0])

# Reaction 81
reaction( "O- + 2 O3 => O3- + 2 O2", [(4.8176E+14,'cm3/mol/s'), 0 ,0])

```

```

# Reaction 82
reaction( "O2- + O => O- + O2", [(9.0330E+13,'cm3/mol/s'), 0 ,0])

# Reaction 83
reaction( "O2- + O => O3 + e-", [(9.0330E+13,'cm3/mol/s'), 0 ,0])

# Reaction 84
reaction( "O2- + 2 O2 => O4- + O2", [(1.8066E-07,'cm3/mol/s'), 0 ,0])

# Reaction 85
reaction( "O2- + O3 => O3- + O2", [(3.6132E+14,'cm3/mol/s'), 0 ,0])

# Reaction 86
reaction( "O3- + O => O2- + O2", [(1.5055E+14,'cm3/mol/s'), 0 ,0])

# Reaction 87
reaction( "O4- + O => O3- + O2", [(2.4088E+14,'cm3/mol/s'), 0 ,0])

# Reaction 88
reaction( "NO2- + NO2 => NO3- + NO", [(1.2044E+11,'cm3/mol/s'), 0 ,0])

# Reaction 89
reaction( "O2+ + N2O5 => NO2+ + NO3 + O2", [(4.2154E+14,'cm3/mol/s'), 0 ,0])

# Reaction 90
reaction( "NO2- + N2O5 => NO3- + 2 NO2", [(4.2154E+14,'cm3/mol/s'), 0 ,0])

# Reaction 91
reaction( "NO3- + O3 => NO2- + 2 O2", [(6.0220E+10,'cm3/mol/s'), 0 ,0])

# Reaction 92
three_body_reaction( "e- + O2 + M => O2- + M", [(2.5E-30,'cm6/molec2/s'), 0 ,0])

# Reaction 92a 12 from WB
#three_body_reaction( "e- + O2 + N2 => O2- + N2", [(1.0E-31,'cm6/molec2/s'), 0 ,0])

# Reaction 92b 11 from WB
#three_body_reaction( "e- + 2 O2 => O2- + O2", [(4.2E-27,'cm6/molec2/s'), -1
,(600,'K')])

# Reaction 93
reaction( "e- + O2 => O- + O ", [(4.8E-14,'cm3/molec/s'), 0 ,0])

# Reaction 94

```

```

reaction( "e- + O3 => O3- ", [(1E-13,'cm3/molec/s'), 0 ,0])
# Duplicate of 95

# Reaction 95
#reaction( "e- + O3 + O2 => O3- + O2", [(1E-13,'cm3/molec/s'), 0 ,0])

# Reaction 96
three_body_reaction( "O- + O2 + M => O3- + M", [(1.1E-30,'cm6/molec2/s'), 0 ,0])

# Reaction 97
reaction( "O2- + NO2 => NO2- + O2", [(7E-10,'cm3/molec/s'), 0 ,0])

# Reaction 98
reaction( "O2- + N2O => NO2- + NO", [(2E-14,'cm3/molec/s'), 0 ,0])

# Reaction 99
reaction( "O3- + NO => NO2- + O2", [(8E-10,'cm3/molec/s'), 0 ,0])

# Reaction 100
#reaction( "NO2- + O2 => NO3- + O", [(1E-11,'cm3/molec/s'), 0 ,0])

# Reaction 101
reaction( "O3- + NO2 => NO2- + O3", [(7E-10,'cm3/molec/s'), 0 ,0])

# Reaction 102
#reaction( "NO2- + O3 => NO3- + O2", [(1.2E-10,'cm3/molec/s'), 0 ,0])

# Reaction 103 3 from WB
three_body_reaction( "N2+ + 2 N2 => N4+ + N2", [(1.0E-28,'cm6/molec2/s'), 0 ,0])

# Reaction 104 4 from WB
reaction( "N4+ + O2 => 2 N2 + O2+", [(1.0E-10,'cm3/molec/s'), 0 ,0])

```

REFERENCES

- (1) Willis, C.; Boyd, A. W.; Young, M. J. Radiolysis of Air and Nitrogen-Oxygen Mixtures with Intense Electron Pulses: Determination of a Mechanism by Comparison of Measured and Computed Yields. *Can. J. Chem.* **1970**, *48* (10), 1515–1525.
- (2) Seinfeld, J. H.; Pandis, S. N. *Atmospheric Chemistry and Physics: From Air Pollution to Climate Change*, 2nd ed.; J. Wiley: Hoboken, N.J, 2006.
- (3) Spinks, J. W. T.; Woods, R. J. *An Introduction to Radiation Chemistry*, 3rd ed.; Wiley: New York, 1990.
- (4) *Layers of Earth's Atmosphere*.
<https://www.britannica.com/science/atmosphere/Troposphere#/media/1/41364/99826> (accessed 2023-03-22).
- (5) Annamalai, K.; Puri, I. K. *Combustion Science and Engineering*; CRC series in computational mechanics and applied analysis; CRC Press/Taylor & Francis: Boca Raton, 2007.
- (6) *Composition, Chemistry, and Climate of the Atmosphere*; Singh, H. B., Ed.; Van Nostrand Reinhold: New York, 1995.
- (7) Crutzen, P. J. The Influence of Nitrogen Oxides on the Atmospheric Ozone Content. *Q. J. R. Meteorol. Soc.* **1970**, *96* (408), 320–325.
<https://doi.org/10.1002/qj.49709640815>.
- (8) Johnston, H. Reduction of Stratospheric Ozone by Nitrogen Oxide Catalysts from Supersonic Transport Exhaust. *Science* **1971**, *173* (3996), 517–522.
<https://doi.org/10.1126/science.173.3996.517>.
- (9) Markovic, V. Radiation Chemistry: Little Known Branch of Science. *Int Energy Bull. Int. At. Energy Agency* **1989**, *31* (1), 20–23.
- (10) Olson, C. A.; Spencer, L. V. Energy Spectra of Cascade Electrons and Photons. *J. Res. Natl. Bur. Stand.* **1958**, *60* (2), 85. <https://doi.org/10.6028/jres.060.010>.
- (11) Röntgen, W. C. On a New Kind of Rays. *Science* **1896**, *3* (59), 227–231.
<https://doi.org/10.1126/science.3.59.227>.
- (12) Curie, P.; Curie, M. S. On a New Radioactive Substance Contained in Pitchblende. *Comptes Rendus* **1898**, No. 127, 175–178.
- (13) Burton, M. Radiation Chemistry. *J. Phys. Colloid Chem.* **1947**, *51* (2), 611–625.
<https://doi.org/10.1021/j150452a029>.
- (14) Lind, S. C. Radiation Chemistry: Gases. *Nucleon. US Ceased Publ.* **1961**, *19* (10).
- (15) Harteck, P.; Dondes, S. Radiation Chemistry of the Fixation of Nitrogen. *Science* **1964**, *146* (3640), 30–35. <https://doi.org/10.1126/science.146.3640.30>.
- (16) Schmidt, K. H. *COMPUTER PROGRAM FOR THE KINETIC TREATMENT OF RADIATION-INDUCED SIMULTANEOUS CHEMICAL REACTIONS.*; ANL--7199, 4472414; 1966; p ANL--7199, 4472414. <https://doi.org/10.2172/4472414>.
- (17) Shah, J.; Maxie, E. C. Gamma-Ray Radiosynthesis of Ozone from Air. *Int. J. Appl. Radiat. Isot.* **1966**, *17* (3), 155–159. [https://doi.org/10.1016/0020-708X\(66\)90040-8](https://doi.org/10.1016/0020-708X(66)90040-8).

- (18) Willis, C.; Boyd, A. W.; Armstrong, D. A. Gas Phase Radiolysis of Hydrogen Chloride, Hydrogen Bromide, and Nitrous Oxide with Intense Electron Pulses. *Can. J. Chem.* **1969**, *47* (20), 3783–3791. <https://doi.org/10.1139/v69-631>.
- (19) Willis, C.; Boyd, A. W.; Young, M. J.; Armstrong, D. A. Radiation Chemistry of Gaseous Oxygen: Experimental and Calculated Yields. *Can. J. Chem.* **1970**, *48* (10), 1505–1514. <https://doi.org/10.1139/v70-246>.
- (20) Willis, C.; Boyd, A. W. Excitation in the Radiation Chemistry of Inorganic Gases. *Int. J. Radiat. Phys. Chem.* **1976**, *8* (1–2), 71–111. [https://doi.org/10.1016/0020-7055\(76\)90061-9](https://doi.org/10.1016/0020-7055(76)90061-9).
- (21) Boyd, A. W.; Miller, O. A. The Radiation Chemistry of Nitric Oxide. *Can. J. Chem.* **1978**, *56* (8), 1075–1079. <https://doi.org/10.1139/v78-182>.
- (22) Bichsel, H.; Peirson, D. H.; Boring, J. W.; Green, A.; Inokuti, M.; Hurst, G. 1. Introduction. *Rep. Int. Comm. Radiat. Units Meas.* **1979**, *os-16* (2), 1–3. https://doi.org/10.1093/jicru_os16.2.1.
- (23) Kroh, J.; Ferradini, C. P.; Bensasson, R. V. *Glimpses of Ninety Years of Radiation Chemistry in France. In Early Developments in Radiation Chemistry, Chapter 8*; Royal society of chemistry: London, 1989.
- (24) Moss, C. E.; Goeller, R. M.; Milligan, D. F.; Valencia, J. E.; Zinn, J. Remote Sensing of Radiation. *Nucl. Instrum. Methods Phys. Res. Sect. Accel. Spectrometers Detect. Assoc. Equip.* **1999**, *422* (1–3), 832–836. [https://doi.org/10.1016/S0168-9002\(98\)01120-6](https://doi.org/10.1016/S0168-9002(98)01120-6).
- (25) Sigmund, P. *Particle Penetration and Radiation Effects: General Aspects and Stopping of Swift Point Charges*; Springer series in solid-state sciences; Springer: Berlin ; New York, 2006.
- (26) Reese, T. A System for Measuring Radiation Induced Chemical Products in Atmospheric Gases Using Optical Detection Methods. Master's Thesis, The University of Southern Mississippi, 2010.
- (27) Mozumder, A. Radiation Chemistry: Background, Current Status and Outlook. *J. Phys. Chem. Lett.* **2011**, *2* (23), 2994–2995. <https://doi.org/10.1021/jz2012758>.
- (28) Gautrau, S. Cavity Ringdown Spectroscopy in Nitrogen/Oxygen Mixtures in the Presence of Alpha Radiation, 2016. https://aquila.usm.edu/masters_theses/258.
- (29) Hecht, A. A.; Galo, R.; Fellows, S.; Baldez, P.; Koonath, P. Radiolytic Ozone Yield G(O₃) from ²¹⁰Po Alpha-Particle Radiation in Air. *Radiat. Phys. Chem.* **2021**, *183*, 109387. <https://doi.org/10.1016/j.radphyschem.2021.109387>.
- (30) US EPA, O. *Radiation Basics*. <https://www.epa.gov/radiation/radiation-basics> (accessed 2023-06-16).
- (31) Konovalov, V. P.; Bychkov, V. L. Non-Stationary Electron Degradation Spectrum in Air Mixtures; International Plasma Technology Center; Saint-Petersburg, Russia, 2014.
- (32) Green, A. E. S.; Sawada, T. Ionization Cross Sections and Secondary Electron Distributions. *J. Atmospheric Terr. Phys.* **1972**, *34* (10), 1719–1728. [https://doi.org/10.1016/0021-9169\(72\)90031-1](https://doi.org/10.1016/0021-9169(72)90031-1).
- (33) Konovalov, V. P. Degradation spectra of electrons in nitrogen, oxygen and air. *Zhurnal Tekhnicheskoy Fiz.* **1993**, *63* (3), 23–33.

- (34) Konovalov, V. P.; Son, E. E. Degradation Spectra of Electrons in the Ionosphere. *J. Phys. Conf. Ser.* **2015**, *653*, 012120. <https://doi.org/10.1088/1742-6596/653/1/012120>.
- (35) Tabata, T.; Shirai, T.; Sataka, M.; Kubo, H. Analytic Cross Sections for Electron Impact Collisions with Nitrogen Molecules. *At. Data Nucl. Data Tables* **2006**, *92* (3), 375–406. <https://doi.org/10.1016/j.adt.2006.02.002>.
- (36) Itikawa, Y. Cross Sections for Electron Collisions with Nitrogen Molecules. *J. Phys. Chem. Ref. Data* **2006**, *35* (1), 31–53. <https://doi.org/10.1063/1.1937426>.
- (37) Itikawa, Y. Cross Sections for Electron Collisions with Oxygen Molecules. *J. Phys. Chem. Ref. Data* **2009**, *38* (1), 1–20. <https://doi.org/10.1063/1.3025886>.
- (38) Tian, C.; Vidal, C. R. Electron Impact Ionization of and : Contributions from Different Dissociation Channels of Multiply Ionized Molecules. *J. Phys. B At. Mol. Opt. Phys.* **1998**, *31* (24), 5369–5381. <https://doi.org/10.1088/0953-4075/31/24/018>.
- (39) Thomas, R. H.; Lyman, J. T.; De Castro, T. M. A Measurement of the Average Energy Required to Create an Ion Pair in Nitrogen by High-Energy Ions. *Radiat. Res.* **1980**, *82* (1), 1. <https://doi.org/10.2307/3575232>.
- (40) *NIST: Appendix for ESTAR, PSTAR, and ASTAR.* <https://physics.nist.gov/PhysRefData/Star/Text/appendix.html> (accessed 2023-06-16).
- (41) Stopping-Power & Range Tables for Electrons, Protons, and Helium Ions. *NIST* **2009**.
- (42) Allison, J.; Amako, K.; Apostolakis, J.; Arce, P.; Asai, M.; Aso, T.; Bagli, E.; Bagulya, A.; Banerjee, S.; Barrant, G.; Beck, B. R.; Bogdanov, A. G.; Brandt, D.; Brown, J. M. C.; Burkhardt, H.; Canal, Ph.; Cano-Ott, D.; Chauvie, S.; Cho, K.; Cirrone, G. A. P.; Cooperman, G.; Cortés-Giraldo, M. A.; Cosmo, G.; Cuttone, G.; Depaola, G.; Desorgher, L.; Dong, X.; Dotti, A.; Elvira, V. D.; Folger, G.; Francis, Z.; Galoyan, A.; Garnier, L.; Gayer, M.; Genser, K. L.; Grichine, V. M.; Guatelli, S.; Guèye, P.; Gumplinger, P.; Howard, A. S.; Hřivnáčová, I.; Hwang, S.; Incerti, S.; Ivanchenko, A.; Ivanchenko, V. N.; Jones, F. W.; Jun, S. Y.; Kaitaniemi, P.; Karakatsanis, N.; Karamitros, M.; Kelsey, M.; Kimura, A.; Koi, T.; Kurashige, H.; Lechner, A.; Lee, S. B.; Longo, F.; Maire, M.; Mancusi, D.; Mantero, A.; Mendoza, E.; Morgan, B.; Murakami, K.; Nikitina, T.; Pandola, L.; Paprocki, P.; Perl, J.; Petrović, I.; Pia, M. G.; Pokorski, W.; Quesada, J. M.; Raine, M.; Reis, M. A.; Ribon, A.; Ristić Fira, A.; Romano, F.; Russo, G.; Santin, G.; Sasaki, T.; Sawkey, D.; Shin, J. I.; Strakovsky, I. I.; Tabora, A.; Tanaka, S.; Tomé, B.; Toshito, T.; Tran, H. N.; Truscott, P. R.; Urban, L.; Uzhinsky, V.; Verbeke, J. M.; Verderi, M.; Wendt, B. L.; Wenzel, H.; Wright, D. H.; Wright, D. M.; Yamashita, T.; Yarba, J.; Yoshida, H. Recent Developments in Geant4. *Nucl. Instrum. Methods Phys. Res. Sect. Accel. Spectrometers Detect. Assoc. Equip.* **2016**, *835*, 186–225. <https://doi.org/10.1016/j.nima.2016.06.125>.
- (43) Allison, J.; Amako, K.; Apostolakis, J.; Araujo, H.; Arce Dubois, P.; Asai, M.; Barrant, G.; Capra, R.; Chauvie, S.; Chytráček, R.; Cirrone, G. A. P.; Cooperman, G.; Cosmo, G.; Cuttone, G.; Daquino, G. G.; Donszelmann, M.; Dressel, M.; Folger, G.; Foppiano, F.; Generowicz, J.; Grichine, V.; Guatelli, S.; Gumplinger, P.; Heikkinen, A.; Hrivnacova, I.; Howard, A.; Incerti, S.; Ivanchenko, V.; Johnson, T.;

- Jones, F.; Koi, T.; Kokoulin, R.; Kossov, M.; Kurashige, H.; Lara, V.; Larsson, S.; Lei, F.; Link, O.; Longo, F.; Maire, M.; Mantero, A.; Mascialino, B.; McLaren, I.; Mendez Lorenzo, P.; Minamimoto, K.; Murakami, K.; Nieminen, P.; Pandola, L.; Parlati, S.; Peralta, L.; Perl, J.; Pfeiffer, A.; Pia, M. G.; Ribon, A.; Rodrigues, P.; Russo, G.; Sadilov, S.; Santin, G.; Sasaki, T.; Smith, D.; Starkov, N.; Tanaka, S.; Tcherniaev, E.; Tome, B.; Trindade, A.; Truscott, P.; Urban, L.; Verderi, M.; Walkden, A.; Wellisch, J. P.; Williams, D. C.; Wright, D.; Yoshida, H. Geant4 Developments and Applications. *IEEE Trans. Nucl. Sci.* **2006**, *53* (1), 270–278. <https://doi.org/10.1109/TNS.2006.869826>.
- (44) Agostinelli, S.; Allison, J.; Amako, K.; Apostolakis, J.; Araujo, H.; Arce, P.; Asai, M.; Axen, D.; Banerjee, S.; Barrand, G.; Behner, F.; Bellagamba, L.; Boudreau, J.; Broglia, L.; Brunengo, A.; Burkhardt, H.; Chauvie, S.; Chuma, J.; Chytracek, R.; Cooperman, G.; Cosmo, G.; Degtyarenko, P.; Dell'Acqua, A.; Depaola, G.; Dietrich, D.; Enami, R.; Feliciello, A.; Ferguson, C.; Fesefeldt, H.; Folger, G.; Foppiano, F.; Forti, A.; Garelli, S.; Giani, S.; Giannitrapani, R.; Gibin, D.; Gómez Cadenas, J. J.; González, I.; Gracia Abril, G.; Greeniaus, G.; Greiner, W.; Grichine, V.; Grossheim, A.; Guatelli, S.; Gumplinger, P.; Hamatsu, R.; Hashimoto, K.; Hasui, H.; Heikkinen, A.; Howard, A.; Ivanchenko, V.; Johnson, A.; Jones, F. W.; Kallenbach, J.; Kanaya, N.; Kawabata, M.; Kawabata, Y.; Kawaguti, M.; Kelner, S.; Kent, P.; Kimura, A.; Kodama, T.; Kokoulin, R.; Kossov, M.; Kurashige, H.; Lamanna, E.; Lampén, T.; Lara, V.; Lefebure, V.; Lei, F.; Liendl, M.; Lockman, W.; Longo, F.; Magni, S.; Maire, M.; Medernach, E.; Minamimoto, K.; Mora De Freitas, P.; Morita, Y.; Murakami, K.; Nagamatu, M.; Nartallo, R.; Nieminen, P.; Nishimura, T.; Ohtsubo, K.; Okamura, M.; O'Neale, S.; Oohata, Y.; Paech, K.; Perl, J.; Pfeiffer, A.; Pia, M. G.; Ranjard, F.; Rybin, A.; Sadilov, S.; Di Salvo, E.; Santin, G.; Sasaki, T.; Savvas, N.; Sawada, Y.; Scherer, S.; Sei, S.; Sirotenko, V.; Smith, D.; Starkov, N.; Stoecker, H.; Sulkimo, J.; Takahata, M.; Tanaka, S.; Tcherniaev, E.; Safai Tehrani, E.; Tropeano, M.; Truscott, P.; Uno, H.; Urban, L.; Urban, P.; Verderi, M.; Walkden, A.; Wander, W.; Weber, H.; Wellisch, J. P.; Wenaus, T.; Williams, D. C.; Wright, D.; Yamada, T.; Yoshida, H.; Zschesche, D. Geant4—a Simulation Toolkit. *Nucl. Instrum. Methods Phys. Res. Sect. Accel. Spectrometers Detect. Assoc. Equip.* **2003**, *506* (3), 250–303. [https://doi.org/10.1016/S0168-9002\(03\)01368-8](https://doi.org/10.1016/S0168-9002(03)01368-8).
- (45) Gautrau, S. Personal Correspondence: GEANT4 Energy Deposition Model for a Polonium-210 Radioactive Source in 1 Atmosphere of Dry Air.
- (46) *NIST ASTAR Database Program: Text-only version.* <https://www.physics.nist.gov/PhysRefData/Star/Text/ASTAR-t.html> (accessed 2023-02-01).
- (47) *Ansys Chemkin-Pro | Chemical Kinetics Simulation Software.* <https://www.ansys.com/products/fluids/ansys-chemkin-pro> (accessed 2023-06-15).
- (48) *Cantera.* <https://cantera.org/> (accessed 2023-02-12).
- (49) Harris, C. R.; Millman, K. J.; Van Der Walt, S. J.; Gommers, R.; Virtanen, P.; Cournapeau, D.; Wieser, E.; Taylor, J.; Berg, S.; Smith, N. J.; Kern, R.; Picus, M.; Hoyer, S.; Van Kerkwijk, M. H.; Brett, M.; Haldane, A.; Del Río, J. F.; Wiebe, M.; Peterson, P.; Gérard-Marchant, P.; Sheppard, K.; Reddy, T.; Weckesser, W.;

- Abbasi, H.; Gohlke, C.; Oliphant, T. E. Array Programming with NumPy. *Nature* **2020**, *585* (7825), 357–362. <https://doi.org/10.1038/s41586-020-2649-2>.
- (50) *SUNDIALS / Computing*. <https://computing.llnl.gov/projects/sundials> (accessed 2023-06-15).
- (51) *NASA Thermo Build*. https://cearun.grc.nasa.gov/ThermoBuild/index_ds.html (accessed 2022-11-09).
- (52) Manion, J. A.; Huie, R. E.; Levin, R. D.; Burgess Jr., D. R.; Orkin, V. L.; Tsang, W.; McGivern, W. S.; Hudgens, J. W.; Knyazev, V. D.; Atkinson, D. B.; Chai, E.; Tereza, A. M.; Lin, C.-Y.; Allison, T. C.; Mallard, W. G.; Westley, F.; Herron, J. T.; Hampson, R. F.; Frizzell, D. H. *NIST Chemical Kinetics Database*. <https://kinetics.nist.gov/> (accessed 2021-09-23).
- (53) Anicich, V. G. Evaluated Bimolecular Ion-Molecule Gas Phase Kinetics of Positive Ions for Use in Modeling Planetary Atmospheres, Cometary Comae, and Interstellar Clouds. *J. Phys. Chem. Ref. Data* **1993**, *22* (6), 1469–1569. <https://doi.org/10.1063/1.555940>.
- (54) Boyarchuk, K. A. Estimation of the Concentration of Complex Negative Ions Resulting from Radioactive Contamination of the Troposphere. *Tech. Phys.* **1999**, *44* (3), 334–336. <https://doi.org/10.1134/1.1259334>.
- (55) Torr, D. G.; Torr, M. R. Chemistry of the Thermosphere and Ionosphere. *J. Atmospheric Terr. Phys.* **1979**, *41* (7–8), 797–839. [https://doi.org/10.1016/0021-9169\(79\)90126-0](https://doi.org/10.1016/0021-9169(79)90126-0).
- (56) Ferguson, E. E.; Fehsenfeld, F. C.; Albritton, D. L. Ion Chemistry of the Earth's Atmosphere. In *Gas Phase Ion Chemistry*; Elsevier, 1979; pp 45–82. <https://doi.org/10.1016/B978-0-12-120801-1.50008-9>.
- (57) Shuman, N. S.; Hunton, D. E.; Viggiano, A. A. Ambient and Modified Atmospheric Ion Chemistry: From Top to Bottom. *Chem. Rev.* **2015**, *115* (10), 4542–4570. <https://doi.org/10.1021/cr5003479>.
- (58) Verronen, P. T.; Turunen, E.; Ulich, Th.; Kyrölä, E. Modelling the Effects of the October 1989 Solar Proton Event on Mesospheric Odd Nitrogen Using a Detailed Ion and Neutral Chemistry Model. *Ann. Geophys.* **2002**, *20* (12), 1967–1976. <https://doi.org/10.5194/angeo-20-1967-2002>.
- (59) *Wolfram|Alpha: Making the world's knowledge computable*. <https://www.wolframalpha.com> (accessed 2023-03-22).
- (60) *GitHub - Cantera/cantera: Chemical kinetics, thermodynamics, and transport tool suite*. <https://github.com/Cantera/cantera> (accessed 2023-02-28).
- (61) *GRI-Mech 3.0*. <http://combustion.berkeley.edu/gri-mech/version30/text30.html> (accessed 2023-02-28).
- (62) Campbell, I. M.; Thrush, B. A. The Association of Oxygen Atoms and Their Combination with Nitrogen Atoms. *Proc. R. Soc. Lond. Ser. Math. Phys. Sci.* **1967**, *296* (1445), 222–232. <https://doi.org/10.1098/rspa.1967.0015>.
- (63) Harteck, P.; Reeves, R. R.; Mannella, G. Rate of Recombination of Nitrogen Atoms. *J. Chem. Phys.* **1958**, *29* (3), 608–610. <https://doi.org/10.1063/1.1744546>.
- (64) Atkinson, R.; Baulch, D. L.; Cox, R. A.; Hampson, R. F.; Kerr (Chairman), J. A.; Troe, J. Evaluated Kinetic and Photochemical Data for Atmospheric Chemistry: Supplement III. IUPAC Subcommittee on Gas Kinetic Data Evaluation for

- Atmospheric Chemistry. *J. Phys. Chem. Ref. Data* **1989**, *18* (2), 881–1097.
<https://doi.org/10.1063/1.555832>.
- (65) Phillips, L. F.; Schiff, H. I. Mass-Spectrometric Studies of Atomic Reactions. V. The Reaction of Nitrogen Atoms with NO₂. *J. Chem. Phys.* **1965**, *42* (9), 3171–3174. <https://doi.org/10.1063/1.1696396>.
- (66) Atkinson, R.; Baulch, D. L.; Cox, R. A.; Crowley, J. N.; Hampson, R. F.; Hynes, R. G.; Jenkin, M. E.; Rossi, M. J.; Troe, J. Evaluated Kinetic and Photochemical Data for Atmospheric Chemistry: Volume I - Gas Phase Reactions of O₂, HO₂, NO₂, and SO₂ Species. *Atmospheric Chem. Phys.* **2004**, *4* (6), 1461–1738. <https://doi.org/10.5194/acp-4-1461-2004>.
- (67) Reeves, R. R.; Mannella, G.; Harteck, P. Rate of Recombination of Oxygen Atoms. *J. Chem. Phys.* **1960**, *32* (2), 632–633. <https://doi.org/10.1063/1.1730767>.
- (68) Herron, J. T.; Schiff, H. I. A MASS SPECTROMETRIC STUDY OF NORMAL OXYGEN AND OXYGEN SUBJECTED TO ELECTRICAL DISCHARGE. *Can. J. Chem.* **1958**, *36* (8), 1159–1170. <https://doi.org/10.1139/v58-170>.
- (69) Tsang, W.; Herron, J. T. Chemical Kinetic Data Base for Propellant Combustion I. Reactions Involving NO, NO₂, HNO, HNO₂, HCN and N₂O. *J. Phys. Chem. Ref. Data* **1991**, *20* (4), 609–663. <https://doi.org/10.1063/1.555890>.
- (70) Hjorth, J.; Notholt, J.; Restelli, G. ChemInform Abstract: Spectroscopic Study of the Equilibrium NO₂ + NO₃ + M ⇌ N₂O₅ + M and the Kinetics of the O₃/N₂O₅/NO₃/NO₂/Air System. *ChemInform* **2010**, *23* (15), no-no. <https://doi.org/10.1002/chin.199215022>.
- (71) Heimerl, J.; Coffee, T. The Unimolecular Ozone Decomposition Reaction. *Combust. Flame* **1979**, *35*, 117–123. [https://doi.org/10.1016/0010-2180\(79\)90015-4](https://doi.org/10.1016/0010-2180(79)90015-4).
- (72) Putikam, R.; Lin, M.-C. A Novel Mechanism for the Isomerization of N₂O₄ and Its Implication for the Reaction with H₂O and Acid Rain Formation. *Int. J. Quantum Chem.* **2018**, *118* (12), e25560. <https://doi.org/10.1002/qua.25560>.
- (73) Johnston, H. S.; Cantrell, C. A.; Calvert, J. G. Unimolecular Decomposition of NO₃ to Form NO and O₂ and a Review of N₂O₅/NO₃ Kinetics. *J. Geophys. Res.* **1986**, *91* (D4), 5159. <https://doi.org/10.1029/JD091iD04p05159>.
- (74) DeMore, W. B.; Sander, S. P.; Golden, D. M.; Hampson, R. F.; Kurylo, M. J.; Howard, C. J.; Ravishankara, A. R.; Kolb, C. E.; Molina, M. J. Chemical Kinetics and Photochemical Data for Use in Stratospheric Modeling. **1997**.
- (75) Orlando, J. J.; Tyndall, G. S.; Betterton, E. A.; Lowry, J.; Stegall, S. T. Atmospheric Chemistry of Hydrazoic Acid (HN₃): UV Absorption Spectrum, HO[•] Reaction Rate, and Reactions of the [•]N₃ Radical. *Environ. Sci. Technol.* **2005**, *39* (6), 1632–1640. <https://doi.org/10.1021/es048178z>.
- (76) Tsang, W.; Hampson, R. F. Chemical Kinetic Data Base for Combustion Chemistry. Part I. Methane and Related Compounds. *J. Phys. Chem. Ref. Data* **1986**, *15* (3), 1087–1279. <https://doi.org/10.1063/1.555759>.
- (77) Schofield, K. Evaluated Chemical Kinetic Rate Constants for Various Gas Phase Reactions. *J. Phys. Chem. Ref. Data* **1973**, *2* (1), 25–84. <https://doi.org/10.1063/1.3253112>.

- (78) Ferguson, E. E. Thermal Energy Ion-Molecule Reactions. In *Advances in Electronics and Electron Physics*; Elsevier, 1968; Vol. 24, pp 1–50. [https://doi.org/10.1016/S0065-2539\(08\)60970-1](https://doi.org/10.1016/S0065-2539(08)60970-1).
- (79) Stelman, D.; Moruzzi, J. L.; Phelps, A. V. Low Energy Electron Attachment to Ozone Using Swarm Techniques. *J. Chem. Phys.* **1972**, *56* (8), 4183–4189. <https://doi.org/10.1063/1.1677832>.
- (80) Parkes, D. A. Electron Attachment and Negative Ion-Molecule Reactions in Pure Oxygen. *Trans. Faraday Soc.* **1971**, *67*, 711. <https://doi.org/10.1039/tf9716700711>.
- (81) Fehsenfeld, F. C.; Ferguson, E. E.; Bohme, D. K. Additional Flowing Afterglow Measurements of Negative Ion Reactions of D-Region Interest. *Planet. Space Sci.* **1969**, *17* (10), 1759–1762. [https://doi.org/10.1016/0032-0633\(69\)90052-X](https://doi.org/10.1016/0032-0633(69)90052-X).
- (82) Fehsenfeld, F. C.; Howard, C. J.; Schmeltekopf, A. L. Gas Phase Ion Chemistry of HNO₃. *J. Chem. Phys.* **1975**, *63* (7), 2835. <https://doi.org/10.1063/1.431722>.
- (83) Davidson, J. A.; Viggiano, A. A.; Howard, C. J.; Dotan, I.; Fehsenfeld, F. C.; Albritton, D. L.; Ferguson, E. E. Rate Constants for the Reactions of O₂⁺, NO₂⁺, NO⁺, H₃O⁺, CO₃⁻, NO₂⁻, and Halide Ions with N₂O₅ at 300 K. *J. Chem. Phys.* **1978**, *68* (5), 2085–2087. <https://doi.org/10.1063/1.436032>.
- (84) Fehsenfeld, F. C.; Ferguson, E. E.; Streit, G. E.; Albritton, D. L. Stratospheric Ion Chemistry and the 11-Year Variation in Polar Ozone. *Science* **1976**, *194* (4264), 544–545. <https://doi.org/10.1126/science.194.4264.544>.
- (85) Chanin, L. M.; Phelps, A. V.; Biondi, M. A. Measurements of the Attachment of Low-Energy Electrons to Oxygen Molecules. *Phys. Rev.* **1962**, *128* (1), 219–230. <https://doi.org/10.1103/PhysRev.128.219>.
- (86) Moruzzi, J. L.; Ekin, J. W.; Phelps, A. V. Electron Production by Associative Detachment of O⁻ Ions with NO, CO, and H₂. *J. Chem. Phys.* **1968**, *48* (7), 3070–3076. <https://doi.org/10.1063/1.1669574>.
- (87) Warneck, P. Studies of Ion—Neutral Reactions by a Photoionization Mass-Spectrometer Technique. I. *J. Chem. Phys.* **1967**, *46* (2), 502–512. <https://doi.org/10.1063/1.1840695>.
- (88) Shahin, M. M. Use of Corona Discharges for the Study of Ion—Molecule Reactions. *J. Chem. Phys.* **1967**, *47* (11), 4392–4398. <https://doi.org/10.1063/1.1701643>.